UWB Communication Systems Acquisition at Symbol Rate Sampling for IEEE Standard Channel Models

A Thesis Submitted

to the Faculty of Graduate Studies and Research

in Partial Fulfillment of the Requirements

for the Degree of Master of Science

in the Department of Electrical and Computer Engineering

University of Saskatchewan

Saskatoon, Saskatchewan, Canada

By

Xia Cheng

PERMISSION TO USE

In presenting this thesis in partial fulfillment of the requirement for a Degree of Master of Science from the University of Saskatchewan, the author agrees that the libraries of this University may make it freely available for inspection. The author further agrees that permission for copying of this thesis in any manner, in whole or in part for scholarly purposes may be granted by the professor who supervised this thesis work or, in his absence, by the Head of the Department or the Dean of the College of Graduate Studies and Research at the University of Saskatchewan. Any copying, publication, or use of this thesis, or parts thereof, for financial gain without the author's written permission is strictly prohibited. Proper recognition shall be given to the author and the University of Saskatchewan in any scholarly use which may be made of any material in this thesis.

Request for permission to copy or to make any other use of material in this thesis in whole or part should be addressed to:

Head of the Department of Electrical and Computer Engineering,

57 Campus Drive,

University of Saskatchewan,

Saskatoon, Saskatchewan,

Canada S7N 5A9

ABSTRACT

For ultra-wideband (UWB) communications, acquisition is challenging. The reason is from the ultra short pulse shape and ultra dense multipath interference. Ultra short pulse indicates the acquisition region is very narrow. Sampling is another challenge for UWB design due to the need for ultra high speed analog-to-digital converter.

A sub-optimum and under-sampling scheme using pilot codes as transmitted reference is proposed here for acquisition. The sampling rate for the receiver is at the symbol rate. A new architecture, the reference aided matched filter is studied in this project. The reference aided matched filter method avoids using complex rake receiver to estimate channel parameters and high sampling rate for interpolation. A limited number of matched filters are used as a filter bank to search for the strongest path. Timing offset for acquisition is then estimated and passed to an advanced verification algorithm. For optimum performance of acquisition, the adaptive post detection integration is proposed to solve the problem from dense inter-symbol interference during the acquisition. A low-complex early-late gate tracking loop is one element of the adaptive post detection integration. This tracking scheme assists in improving acquisition accuracy. The proposed scheme is evaluated using Matlab Simulink simulations in term of mean acquisition time, system performance and false alarm. Simulation results show proposed algorithm is very effective in ultra dense multipath channels. This research proves reference-aided acquisition with tracking loop is promising in UWB application.

DEDICATION

To my husband, Ren, Weilin, for his constant supports and encouragement, as well as all my lovely daughter, Qiqi, and my father, Cheng, Shujia.

ACKNOWLEDGEMENTS

First and foremost I would like to appreciate my supervisor Dr. Anh Dinh for his critical comments and suggestions during the research, and for his long-term guidance in the simulations and dedicated help of my thesis even after I joined Vecima Networks company. His continuous supervision helped me to keep this research project on the right track and achieve this final research thesis. I want to say, thank you, Dr. Dinh, from my heart.

I would like to thank my classmate Wan, Qian who helped me with many discussions about UWB techniques. He generously shared his time and knowledge in my work regarding theories as well as protocols of the UWB technologies.

At last I would like to express my deepest thanks to my family, my mother Li, Zhiying, and my sister Cheng, Yun, for their emotional help and support throughout my studies in Canada. I also want to thank my friend, Yang, Qian, who gave me so many warm helps during my hard time.

TABLE OF CONTENTS

LIST OF FIGURES

LIST OF TABLES

ABBREVIATIONS

3G	Third Generation Mobile Communications
A	Amplifier
A/D	Analog-to-digital
APDI	Adaptive Post Detection Integration
AWGN	Additive White Gaussian Noise
BER	Bit Error Rate
BIS	Bit Iteration Search
BPSK	Binary Phase-shift Keying
CDMA	Code Division Multiple Access
DA	Data Aided
DFT	Discrete Fourier Transform
DSSS	Direct Sequence Spread Spectrum
DS-UWB	Direct Sequence Ultra Wide Band
EIRP	Effective Isotropic Radiated Power
FFT	Fast Fourier Transform
GPS	Global Positioning System
IEEE	Institute of Electrical and Electronics Engineers
ISI	Inter Symbol Interference
MAP	Maximum a Posteriori Probability
MAT	Mean Acquisition Time
MF	Matched Filter
ML	Maximum Likelihood
LNA	Low Noise Amplifier
LTI	Linear Time Invariant
NLOS	Non Line of Sight
OFDM	Orthogonal Frequency Division Multiplexing
OOK	On-off Keying
PAM	Pulse Amplitude Modulation
PDF	Probability Density of Function
PDI	Post Detection Integration
PSD	Power Spectral Density

PHY	Physical Layer
PLL	Phase Locked Loop
PN	Pseudo-Noise
PPM	Pulse Position Modulation
PSD	Power Spectral Density
RAMF	Reference Aided Matched Filter
RF	Radio Frequency
RMS	Root Mean Square
SNR	Signal to Noise Ratio
VCO	Voltage Controlled Oscillator

CHAPTER 1 INTRODUCTION

ULTRA-WIDEBAND (UWB) communications is increasingly attracting attention from both research community and industries. As a promising radio technology, UWB meets the demand for both high speed wireless communications and short-range access. UWB is not new; the research history was dated back to 1962, as work of electromagnetic in time-domain through the characteristic impulse response by Ross [1]. In 1998, the Federal Communications Commission (FCC) first proposed UWB transmissions under part 15 rules. In February 2002, the commission issued First Report and Order [2] that permits the market to design and fabricate certain types of products incorporating UWB applications. UWB technology holds great promise for a vast region of new applications that provide significant benefits for public safety, businesses and consumers. Impulse radio is potentially cheaper than millimeter wave wireless communications for the same short-range communication environment. Under appropriate technical standards, UWB devices operate at the same spectrum already occupied by existing radio services, thereby allowing scarce spectrum resources to be used more efficiently.

1.1 Technical Issues of UWB Communication Systems

The initial idea of UWB is based on impulse radio communication systems which employ very sharp pulse trains to carry information bits without mixers,

oscillators and bandpass filters. This idea results in low cost for transceiver design since only a small number of analog components is needed. A simple UWB system scheme is presented in Figure 1.1.

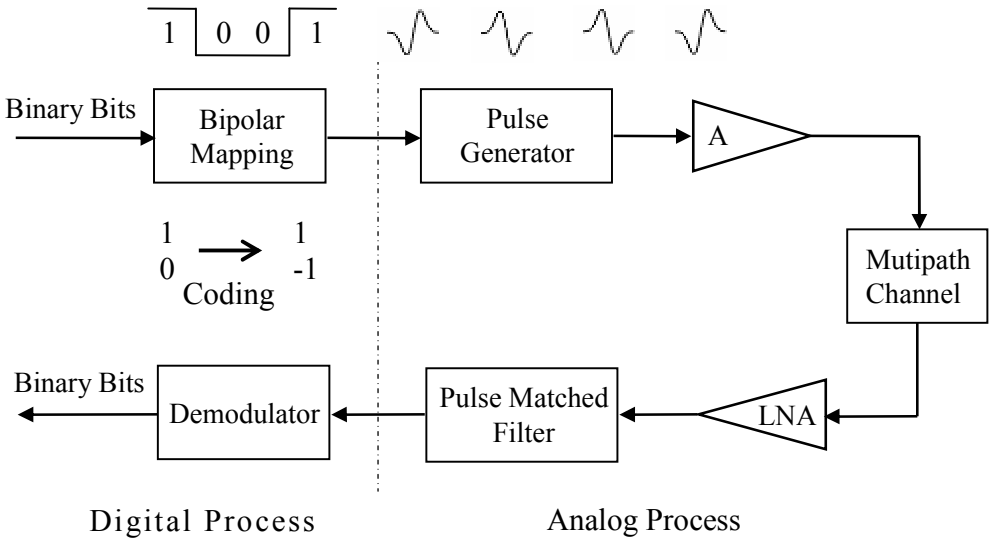

Figure 1.1 A simple UWB transceiver over a multipath channel

There are two main differences between UWB and other narrow band or general wideband systems. First, the bandwidth of UWB systems, as defined by FCC in [2], is greater than 20% of a center frequency or more than 500 MHz. Clearly, this bandwidth is much greater than the bandwidth used by any current technology for communications. Second, UWB is typically implemented in carrierless fashion. Conventional “narrowband” and “wideband” systems use radio frequency (RF) carriers to move the signal from baseband frequency to the actual carrier frequency region. Conversely, UWB implementations can directly modulate an “impulse” that has a very sharp rise and fall time, thus resulting in a waveform that occupies a very wide bandwidth. Figure 1.2 illustrates the effective isotropic

radiated power (EIRP) emission spectrum utilization in UWB and compares with narrow band signals in frequency domain.

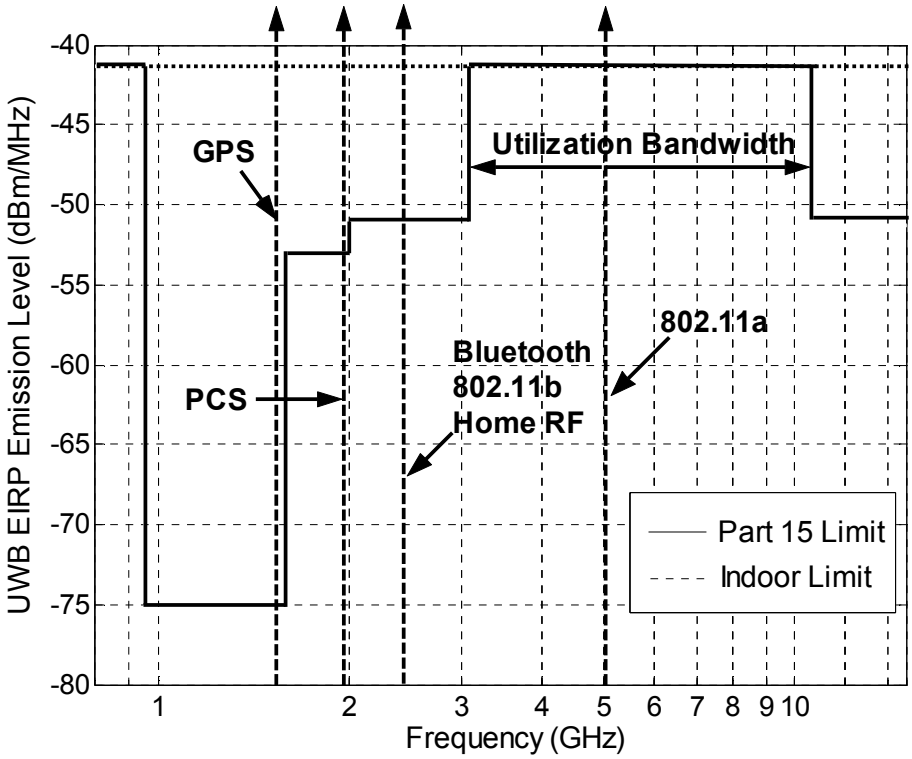

Figure 1.2 UWB spectrum utilization profile [2]

The UWB communications in Figure 1.2 is one of a number of technologies being considered as a potential candidate for short-range wireless broadband applications. This technology combines reduced complexity with low power consumption and high immunity to multipath fading [3].

The most attractive property of UWB is its ultra high speed communications which is up to 120Mbps or more. It is useful to briefly explore capacity of a digital communication link to understand transferring speed of a UWB system.

1.2 Error-free Capacity of a Communication System

Suppose that a communication system is subjected to additive white Gaussian noise (AWGN) which is the only interference of the channel. Based on the work of Claude Shannon in the late 1940s, the maximum rate at which information can be transmitted with high reliability is

$$C = W \log_2(1 + \frac{P}{N_0 W}) = W \log_2[1 + \frac{P/W}{N_0}] \quad (1.1)$$

where

C : channel capacity, bits/s

W : transmission bandwidth, Hz

P : received signal power, W

N_0 : single-side noise power spectral density, W/Hz

Let look at how the equation (1.1) works from an example. If the data are transferred using a bandwidth of $W = 1\,\text{GHz}$, the emission power level P/W = -51.3dBm/MHz and the noise power spectral density, N_0, is used at -41dBm/MHz [2], which is treated as white Gaussian noise. Under such conditions, the channel capacity is at 123Mbps.

1.3 Brief Literature Review and Research Motivation

FCC allowed up to 7.5GHz of spectrum for wireless usage which generated considerable interest in developing UWB communication systems, primarily through standard efforts such as IEEE 802.15.3a. The standard created several new opportunities for innovation and technical advancement. However, as author in [4]

pointed out, UWB faces outstanding design challenges in terms of timing acquisition and energy collecting using a rake structure for the channel equalization [5-6].

UWB has its own characteristics in channel modeling, signal modeling, interference with other bands, and security problems. The challenges drive more exhaustive research and testing [5-7]. One of the critical challenges in UWB realization is its symbol synchronization. Synchronization plays an extremely important role in performance of a communication system. The difficulty of the synchronization is accentuated due to the fact that the waveform bearing information is impulse-like and transmitted at very low power compared with the narrow band signals in the same bandwidth [7,8]. Synchronization consists of two tasks, acquisition and tracking. Acquisition is more difficult to design than tracking. Acquisition realization in UWB systems must be robust to suppress dense multi-path interferences and sufficiently simple to maintain a low cost system.

The topic of acquisition UWB communications has been discussed in literature [6][9,10]. Unfortunately, most of the reports proposed synchronization algorithms assuming a multipath channel which is not the same as the IEEE standard channel models presented in [11]. Channel model is a key to evaluate performance of a UWB communication system. Previous experiences on designing acquisition for wide code-division multiple access (CDMA) and 3G wireless communication systems in dense multipath channels can not be fully relied on for UWB acquisition designs. A new field for wireless communication research is

about to explore an effective method to solve the acquisition challenge to meet the requirements of the IEEE standard both now and in the near future.

There is a considerable amount of literature related to UWB acquisition in the past 5 years. Maravic and Vettli proposed to sample the signal below the Nyquist rate [9]. Annihilating filter method is applied to estimate the unknown time delay of the pulses. The receiver uniformly samples the received signals at one-fifth of the Nyquist rate and averaging the samples over 60 cycles. The corresponding pulse shapes are obtained by a polynomial approximation of the discrete Fourier transform (DFT) coefficients. In this case, an order of polynomial R = 20, with RL+1 equations is needed where L is the number of the multipath. Approximate 200 equations for one coefficient estimation are required if the UWB IEEE standard channel models are used.

Yang and Giannakis assumed the received signals after multipath fading having a duration which is confined in the symbol period [10]. Then inter-symbol interference (ISI) is avoided by such assumption. In reality, ISI can not be avoided if the symbol period is shorter than the delay of the arrived symbols.

Christensen combined adaptive linear minimum mean-square error synchronization and detection for DS-CDMA UWB communications [12]. In the receiver, an anti-aliasing filter processes the received signal before it is uniformly sampled. For example, the number of samples per monocycle is set to 13. Thus around 13GHz sampling rate is required in order to provide good rejection of aliasing at half of the sample rate if the monocycle pulse period is assumed to be

1ns. This requires a very high sampling A/D converter which causes high energy consumption.

Homier and Scholtz applied a similar channel as the UWB IEEE channel model CM4 for acquisition [13]. A fixed-dwell-time parallel/serial mixed search technique was used for fast acquisition. This search is a hybrid bit reversal search. Unfortunately the sampling issue and system performance were not addressed in this publication.

Above all, lower-sampling rate, suppressing ISI and fast acquisition are motivating UWB synchronization research. The research of synchronization using IEEE standard channel models is desired to provide approaches from these requirements. For upcoming practical applications of UWB technology, pervious research results do not satisfy the performance requirement under FCC part 15 rules. This thesis is going to propose effective algorithms for timing acquisition using IEEE UWB standard channel models. The goal of the research is to balance system complexity with low sampling rate and to compress dense ISI for fast acquisition.

1.4 Objectives of the Thesis

This thesis attempts to achieve such objectives for practical applications as follows

- Using under-sampling rate to avoid traditional Nyquist sampling rate. At the same time, the receiver is able to detect the signals with a good performance.

- Proposing a search strategy to achieve fast acquisition, because the ultra narrow pulse shape of the UWB signals means more searchable timing phase than the traditional communication signals in the same condition.
- Devising the sub-optimum symbol timing recovery architecture to suppress ISI and dense multipath for UWB communications using IEEE UWB standard channel models.

1.5 Organization of the Thesis

The remainder of this thesis contains five chapters. Chapter two provides an overview of UWB communications, such as UWB signal models, UWB IEEE channel models, modulation schemes, and sampling issues. Chapter three briefly summarizes timing acquisition approaches adopted by the traditional acquisition. Chapter four is dedicated to propose UWB symbol timing recovery methods such as matched filter (MF) detection, reference aided matched filter (RAMF) acquisition and adaptive post detection integration. Chapter five presents performance evaluation through simulations for the proposed UWB acquisition. Chapter six concludes the research and provides directions for the future exploration in acquisition algorithm.

CHAPTER 2 UWB ACQUISITION BACKGROUND

This chapter presents an overview of UWB communications to provide several important concepts related to acquisition. Section 1 describes a signal model. In section 2, the IEEE standard UWB channel is discussed from a system design point view. Section 3 explains the reason for choosing sampling rate at the symbol frequency.

2.1 UWB Signal Model

A UWB transmitter works by means of sending extremely short duration pulses with a wide range in frequency spectrum, several GHz in bandwidth. UWB signals carry data using a low signal level below the thermal noise floor through a dense multipath channel. There were activities in designing suitable signal waveforms to satisfy the requirements of FCC [14,15]. UWB makes full use of impulse radio benefits to span the energy of a radio signal from near DC to a few GHz. The emission power of spectral density can be lower than the noise floor which makes UWB co-exist with other narrowband or wide band communication systems without interfering with other communication systems [5]. It is necessary to have a standard for UWB signal in order to protect the existing wireless communication systems [5].

2.1.1 Definition of UWB Signals

There is no strict rule for the waveform of UWB signals. Any signal can be used for UWB if it meets the following conditions

1) A fractional bandwidth B_f , measured at the -10dB points

$$B_f = 2\frac{f_H - f_L}{f_H + f_L} > 20\% \tag{2.1}$$

or

2) A total signal BW is greater than 500MHz.

Then UWB signals are those signals having a fractional bandwidth greater than 20%. Table 2.1 presents a bandwidth comparison among three communication systems [16]. For example, the narrow band signal has fractional bandwidth of 0.04% and occupies a bandwidth of 30KHz. Wide CDMA has a fractional bandwidth of 0.8% and a bandwidth of 5MHz. From part 15 rule [2], UWB is allowed to use a maximum bandwidth of 7.5GHz (from 3.1GHz to 10.6GHz).

Table 2.1 Classification of signals based on the bandwidth

Narrow Band	$B_f < 1\%$
Wideband	$1\% < B_f < 20\%$
UWB	$B_f > 20\%$

In addition to spectrum allocation, FCC also specifies that a UWB signal must have a minimum -10dB bandwidth of 500MHz. In many ways, this portion of the ruling has revolutionized the design of UWB communication systems. Instead

of having to use the entire band to transmit information, the spectrum can now be divided into several sub-bands. These bandwidths are approximately 500MHz each. By interleaving symbols across the sub-bands, UWB systems can still maintain the same transmission power as if they are using the entire bandwidth.

2.1.2 Signal Waveform Format

In the view of system design, UWB pulse shape can be chosen for the purpose of simplifying a design. A pulse shape is an important factor affecting overall system performance and design challenge. An applicable pulse shape should be easy to implement and be convenient for theoretical analysis. Generally there are three main waveforms in UWB systems: the Gaussian-like pulse, the monocycle pulse, and the polycycle pulse [17]. The Gaussian monocycle pulse is chosen in this thesis due to its simplicity. The pulse has a waveform described by the Gaussian distribution. The amplitude of the waveform is given by

$$f(t) = Ae^{(-t/\tau)^2} \tag{2.2}$$

where A is the maximum amplitude and τ is the pulse half-duration.

A Gaussian monocycle is a wide-bandwidth signal. Its center frequency and bandwidth depends on the monocycle width. In time domain, the Gaussian monocycle pulse is mathematically similar to the first derivative of the Gaussian function. This research uses an ideally modeled pulse shape propagating in free space, i.e., the first derivative of Gaussian monocycles. A mathematical expression for the monocycles in time domain is given as [18]:

$$f(t) = \frac{t}{\tau} e^{-(\frac{t}{\tau})^2} \tag{2.3}$$

where τ is a parameter which determines the template width of the pulse. In frequency domain, the pulse is transformed into

$$F(\omega) = -j\pi \cdot \sqrt{\pi}\omega\tau^2 \cdot e^{-\pi^2\omega^2\tau^2} \tag{2.4}$$

To normalize (2.3), the normalized pulse shape function $g(t)$ is defined as

$$g(t) = \frac{1}{\sqrt{\frac{3}{4}\tau}} \frac{t}{\tau} e^{-(\frac{t}{\tau})^2} \tag{2.5}$$

The coefficient $\sqrt{\frac{3}{4}\tau}$ ensures the signal shape is normalized as unit energy, in another word

$$\int_{-\infty}^{+\infty} g^2(t)dt = 1 \tag{2.6}$$

Normalized waveform is a simple way to state the signal energy since the received energy in $\sqrt{E_g}g(t)$ is E_g. Figure 2.1 shows a typical waveform of the Gaussian monocycle pulse and its spectrum.

2.1.3 UWB Signal Modulation

Modulation is the process of facilitating the transfer of information over a medium. There are three main ways of modulating classified by the variation of the pulse amplitude, phase, or frequency in accordance with the information being transmitted. Data rate, transceiver complexity, bit error rate (BER) performance,

spectral characteristics of the transmitted signal, and robustness against impairments and interference are related to modulation types.

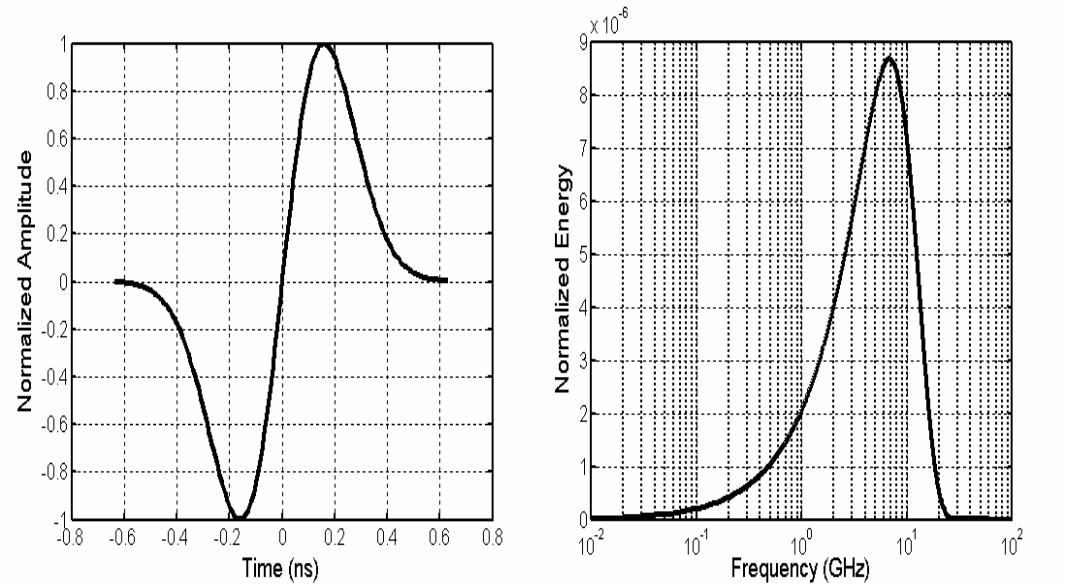

(a) (b)

Figure 2.1 Gaussian monocycle pulse and spectrum: (a) A Gaussian monocycle pulse, (b) Energy spectrum of a Gaussian monocycle pulse

There are several modulations described in [19]. UWB signals can be modulated in different ways such as orthogonal pulse position modulation (PPM), optimum PPM, binary phase-shift keying (BPSK), pulse amplitude modulation (PAM), and on-off keying (OOK) for binary schemes; M-ary PPM and M-ary PAM for M-ary schemes. Among those, BPSK is the best modulation for AWGN channels and Rayleigh fading channels [21]. PPM, OOK, and BPSK are comparable in term of power spectral density (PSD). PSD is one of the design factors required in FCC part 15 rules: the PSD of UWB has to be lower than the Part 15 limit in Figure 1.2. The lower PSD, the better for UWB signals since the interface of UWB to other narrow band systems operated in the same spectrum is

less. PPM has sparse PSD curves in contrast with the other two but it is more sensitive to timing jitter. BPSK is better than on-off keying for PSD at the same condition. BPSK is an optimum modulation to trade off design complexity and PSD [21].

2.2 UWB Channel Model Description

This section describes channel models for UWB communications and responses of an impulse passing through a channel. An accurate model is a prerequisite for designing an efficient communication system which includes maximum achievable data rate, suitable modulation scheme, and algorithm for signal processing.

In general, the received signal is made up of several components: first, the direct component is commensurate with the portion of the wave travel along a line-of-sight (LOS) between the transmit and receive antennae and; second, the components arrive after having been reflected or diffracted on scattering objects that are part of the propagation environment. The latter is the result of a well known effect: multipath propagation. As a consequence, the received signal is made up of multiple replicas of the transmitted signal, all of which exhibit different attenuations, delays and polarizations. Multipath propagation gives rise to two important phenomena: time and location dependent on the received signal strength. Multipath components that arrive at different time instants, which causes a frequency-selective (as opposed to a frequency-flat) transmission channel.

UWB channel model is a dense multipath channel. A great deal of proposals and measurements support this conclusion [22-25]. Different from the narrow band, which used Rayleigh fading channel, UWB channel model is presented by a log-normal fading model. A modified Saveh-Valenzuela (S-V) model is used for power and delay profile as shown in Figure 2.2. To unify the evaluation of UWB design, the IEEE 802.15.3a group developed channel models for UWB communication system [11], which was accepted by a full standardization group. UWB channels are quite different from narrow band wireless channels, especially in fading statistics and multipath clusters which cause a high challenge in acquisition design.

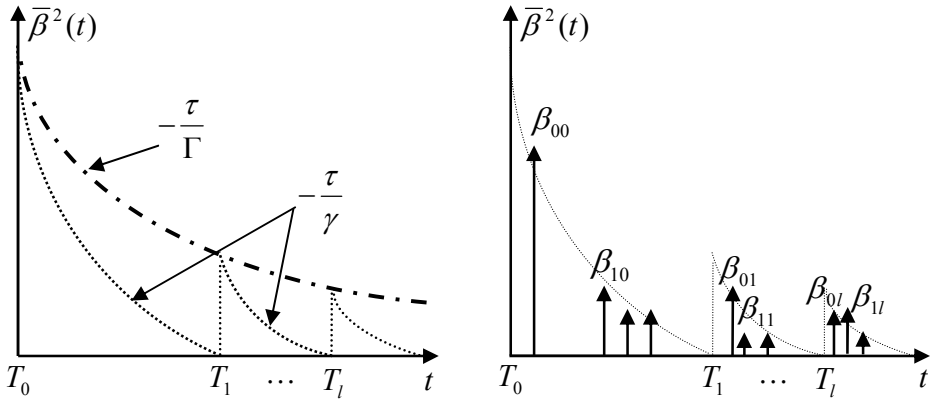

Figure 2.2 A graphical representation of S-V model:

(a) Exponentially decaying ray and cluster average powers.

(b) A realization of the impulse response.

Four types of UWB channels are defined by the IEEE 802.15.3a group to meet measurement results, namely CM1, CM2, CM3, and CM4, for different channel characteristics.

- CM1: LOS scenario with a separation between transmitter and receiver of less than 4m.
- CM2: the same range as CM1, but no LOS.
- CM3: a N-LOS scenario for distance between 4-10m.
- CM4: a situation with strong delay dispersion, resulting in a delay spread of at least 25ns.

For comparison purposes, Figure 2.3 presents impulse responses of the four IEEE channel models. The original Matlab code of the channel model is from [11].

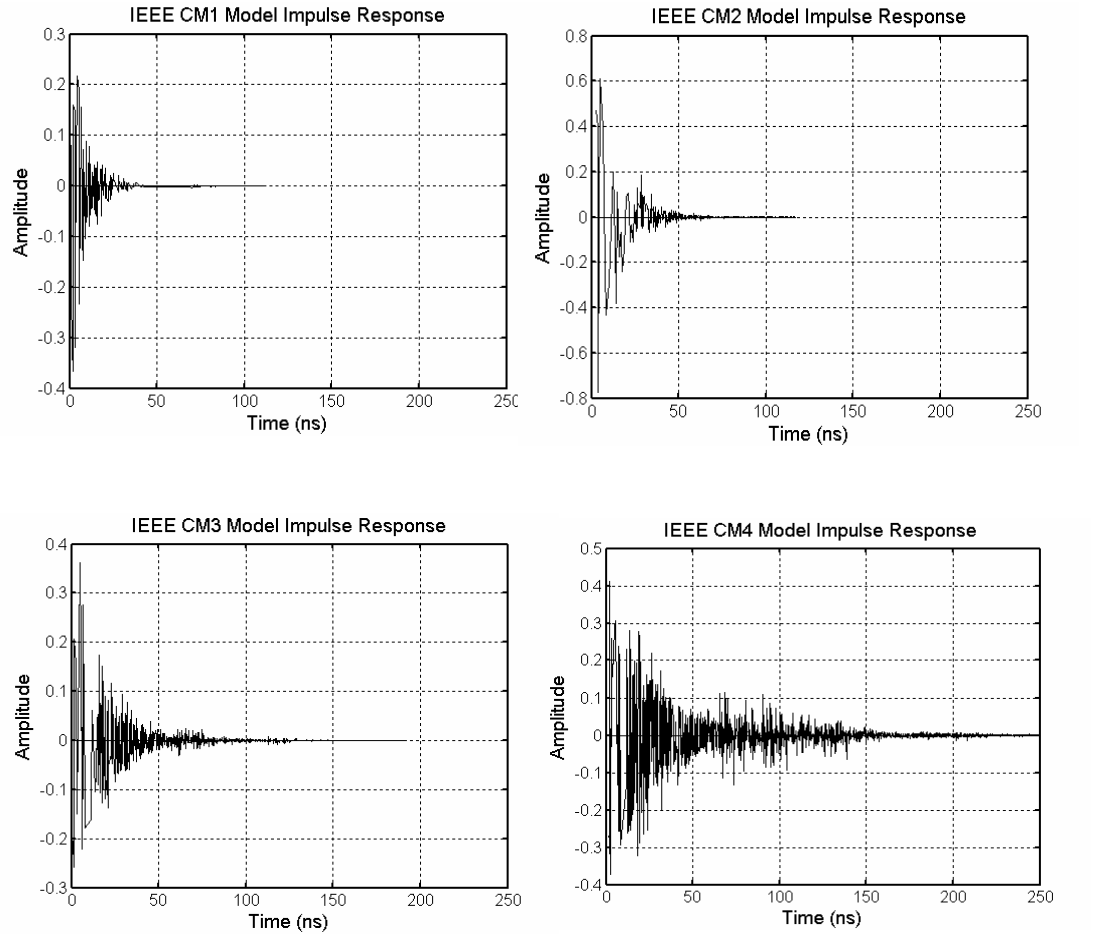

Figure 2.3 Impulse response of IEEE UWB Channel models

For a visual understanding the influence of UWB channel models with the modulated monocycle pulse, Figure 2.4 is one example of the waveform of monocycle pulse passing through a UWB IEEE standard channel. The Matlab simulation uses 125Mbps transmitting rate for IEEE CM3 model. The waveform in Figure 2.4(c) is similar to thermal noise.

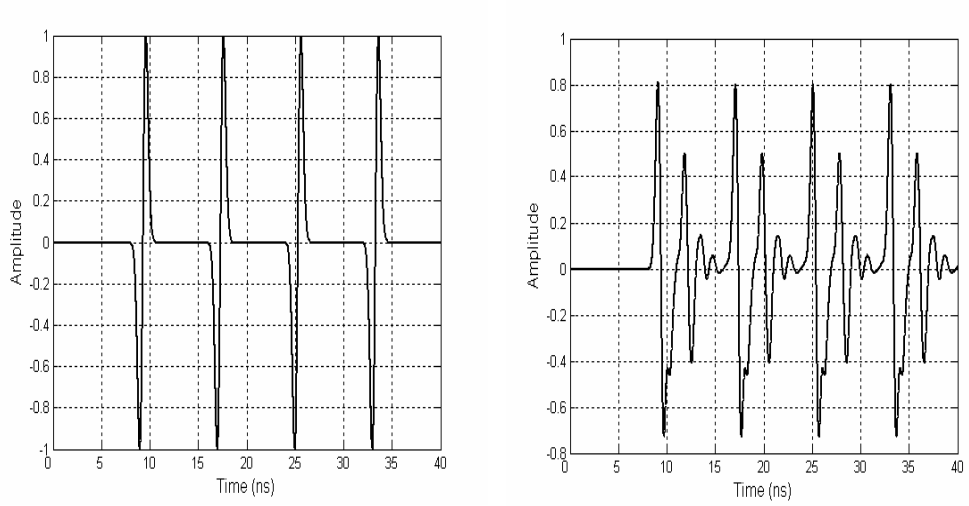

(a) Modulated BPSK waveform (b) Waveform after CM3

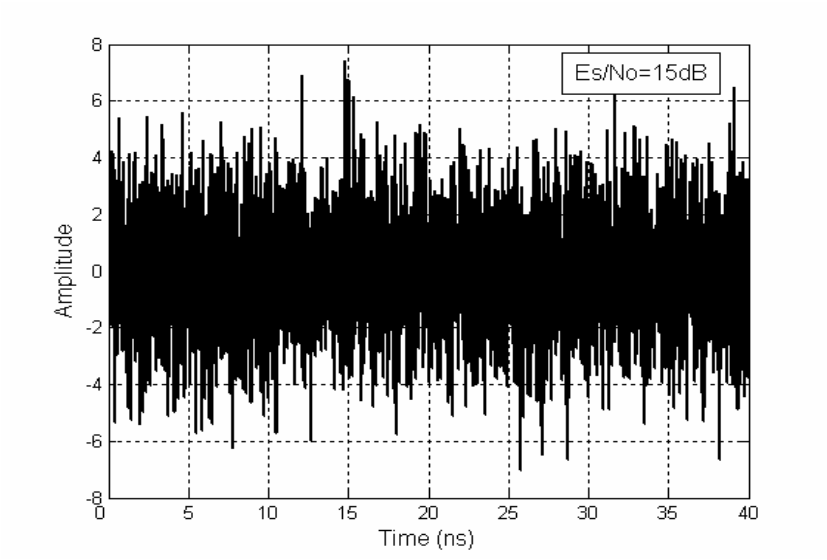

(c) Waveform after CM3 and AWGN channel

Figure 2.4 BPSK modulation under a UWB channel

The defined channel parameters for these four models are listed in Table 2.2. These models assume the channel impulse response is constant during transmission of one packet if the transmission is shorter than 200μs. Moreover, channel realizations are assumed to be independent between packets.

Table 2.2 IEEE UWB channel characteristics [11]

Target Channel characteristic	CM1	CM2	CM3	CM4
Distance(m)	0-4	0-4	4-10	
(Non) Line of sight	Yes	No	No	No
Mean excess delay τ_{rms}(ns)	5.05	10.38	14.18	
RMS delay spread τ_{rms}(ns)	5.28	8.03	14.28	25
NP_{10dB}			35	
$NP_{85\%}$	24	36.1	61.54	

Note: NP_{10dB} is the number of paths within 10dB of the strongest path and $NP_{85\%}$ gives the number of paths containing 85 per cent of the energy. Root mean square (RMS) of spread delay, r_{rms}, is also measured for all models.

2.3 Sampling Issue

Sampling rate plays a crucial role in signal processing and communications. As time passes, more and more analog techniques are being replaced by their digital counterparts. The choice of sampling rate is decided by the symbol rate and performance of the system.

2.3.1 Sampling Rate for UWB

It is well known from Nyquist-Shannon sampling theorem that unambiguous reconstruction is possible if the signal is bandlimited and the sampling frequency is greater than twice of the signal bandwidth. The error which corresponds to the failure of band limitation is referred to as aliasing. The condition for alias-free sampling at rate f_s called Nyquist sampling frequency is

$$2B \leq F_s \tag{2.7}$$

where B is the bandwidth of the signal. From signal processing perspective, the theorem includes two parts: a sampling process, in which a continuous time signal is converted into a discrete time signal, and a reconstruction process in which the continuous signal is recovered from the discrete signal.

UWB signal processing requires much higher sampling rate than general narrow band signal if the Nyquist sampling frequency is observed. The reason is that the UWB signal occupies a much wider bandwidth. High Nyquist sampling frequency makes alias-free signal possible but the system requires more expensive A/D converter and more power to support high speed signal processing. To avoid such design challenge, a new approach for sampling rate is indeed demanded in the UWB application.

2.3.2 UWB Sampling Strategy

It is a clear trend to design UWB system with digital implementation. Digital-oriented systems have well-known advantages, including less expensive technology, easy integration, and high stability. As discussed in section 2.3.1, the

sampling rate for signals should be higher than the spectrum of signals. Otherwise, the message can not be recovered if spectrum aliasing of the modulated signal occurs during under-sampling. In fact, spectrum aliasing does not necessarily lead to spectrum aliasing of the message signal [26]. Even though the modulated signal cannot be recovered, it is still possible to reconstruct the message using the received signal energy and phase.

In fact, spectrum aliasing of the modulated signal is not exactly equal to spectrum alias of the message signals. The modulated signal is Gaussian-monocycle pulse and the message data are digitalized as -1, or 1 for BPSK in this thesis. It is an obvious observation that the modulated signal is an ultra-wide bandwidth signals and the message data are narrow band signals which use a single frequency. This observation gives some clues to recover message signals without concerning spectrum alias of modulated signals. Under-sampling is achievable from such principle. This means that there is a symbol at every symbol time, if the communication begins (Figure 2.5).

The proposed acquisition for UWB communication systems is going to sample the incoming analog signal at the symbol rate which is much less than the mono-pulse bandwidth. The algorithm to be used in this proposed method acquires the system to move the sample phase which adjusts the sampling to near or on the highest energy point of the modulated signal. This algorithm will be discussed in Chapter 4.

2.4 Summary

A brief introduction of UWB communications is introduced to provide the background information which is used in later chapters to build a UWB communication system. There are four factors affecting acquisition algorithm in system design level: signal waveform, modulation method, communication channel model, and sampling rate. Communication channel models are defined by the IEEE 802.15.3a group. Signal waveform, modulation and sampling rate are selected based on signal bandwidth, PSD, design complexity, Nyquist sampling theorem and system performance. Gaussian monocycle pulse, BPSK and under-sampling rate are used to build the communication structure in the thesis.

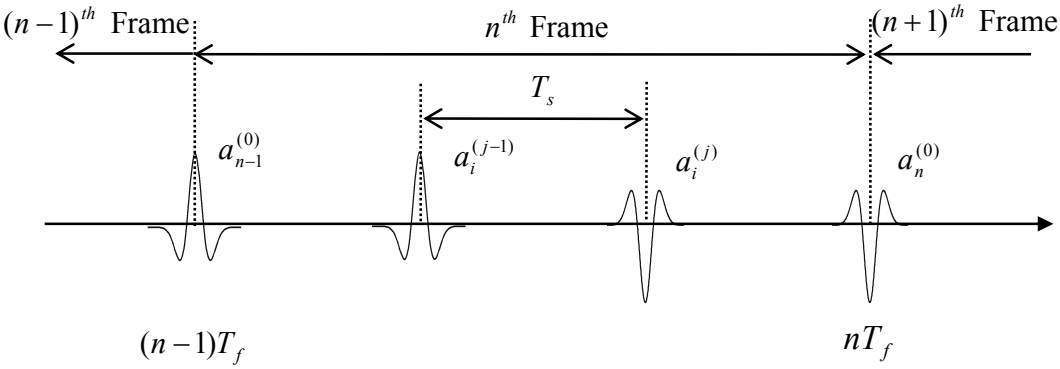

Figure 2.5 A modulated UWB data frame

CHAPTER 3 ACQUISITION TECHNIQUES IN UWB COMMUNICATIONS

One of the most challenging tasks in a digital demodulator is to acquire accurate symbol timing. Since propagation delay from a transmitter to a receiver is generally unknown, acquisition attempts to find optimum sampling phase in order to improve signal to noise ratio (SNR). The main features of acquisition methods used in traditional UWB communication systems are reviewed before proposing new acquisition approaches for UWB signal.

3.1 UWB Acquisition Overview

Acquisition is normally performed using a feedback or a feed-forward loop to control the phase of the sampling clock. These two typical UWB digital acquisition architectures are shown in Figure 3.1. Both structures serve for the timing offset estimation. The received signals are sampled by the local clock and thus sampling is not synchronized to the incoming data symbols. The feed-forward timing offset parameters are estimated by using analog method because signal processing is executed before A/D conversion. The feed-back timing estimation approach is a digital method since the signals are processed after A/D conversion. A local clock is generated by a voltage controlled oscillator (VCO). Then the clocks at the transmitter and the receiver are not synchronized until acquisition is achieved. Timing acquisition system is in charge of driving the local clock to run the same

tone as the incoming signal clock. In another word, the timing acquisition system knows where to sample the optimal position in order to enhance SNR. As a result, the performance of timing acquisition affects system performance.

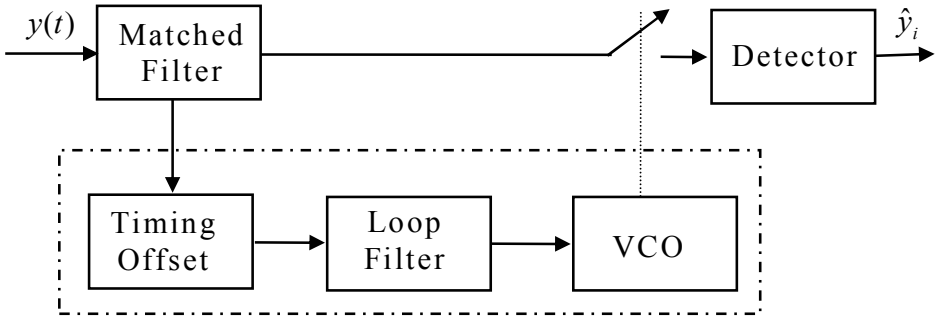

(a) Feed-forward timing estimation

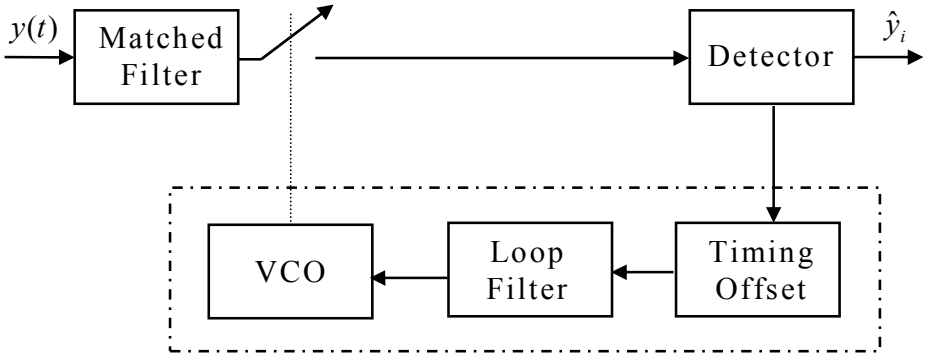

(b) Feed-back timing estimation

Figure 3.1 Timing offset estimation

3.2 The Effect of Timing Offset in System Performance

Timing offset d is defined as timing phase difference between the incoming signal and the local free running oscillator if the clock rate is the same in both sides. A typical acquisition attempts to bring the timing offset within a pull-in range of

the tracking loop by searching the timing uncertainty region in increments of a fraction of a chip. The conception of a chip is borrowed from CDMA where a chip is the transition time for individual bits of the pseudo-random data. The chip can be defined as the period of an impulse. It is necessary to analyze the relationship between timing offset d and UWB communication system performance.

Timing offset is a key function deciding system performance. The probability of the receiver errors for binary modulation is well analyzed in [27]. It is assumed that the binary signals are used as modulation with equal energy and AWGN channel is the transmission channel.

The received signal is expressed as

$$r(t) = s_m(t) + n(t). \tag{3.1}$$

in which $n(t)$ is AWGN noise and $s_m(t)$ is the modulated signal

$$s_m(t) = \mathrm{Re}[s_{lm}(t)g(t)], \qquad m = 1,2 \qquad 0 \le t \le T \tag{3.2}$$

where $s_{lm}(t)$ is the information signal and $g(t)$ is the symbol waveform. The corresponding optimum receiver for this received signal using envelope or square-law detector is presented in Figure 3.2. The MF 1 or 2 is applied to demodulate $r(t)$. The sampling instance is set at $d = 0$ when the optimum sampling phase is located. The envelope/square-law detector makes the decision to recover the received information digits same as $s_{lm}(t)$ if there is no error occurring in the system.

If there are only an AWGN channel and antipodal BPSK modulation in the system, the probability of errors is

$$P(e|s_{l1}) = Q\left(\sqrt{\frac{2\varepsilon}{N_0}}\right) \tag{3.3}$$

and

$$P(e|s_{l2}) = Q\left(\sqrt{\frac{2\varepsilon}{N_0}}\right) \tag{3.4}$$

in which ε is the energy of a symbol and N_0 is the AWGN noise level. Since binary signals are likely equal to be transmitted, the average probability of error is

$$P_b = \frac{1}{2}P(e|s_{l1}) + \frac{1}{2}P(e|s_{l2})$$

$$= Q\left(\sqrt{\frac{2\varepsilon}{N_0}}\right) \tag{3.5}$$

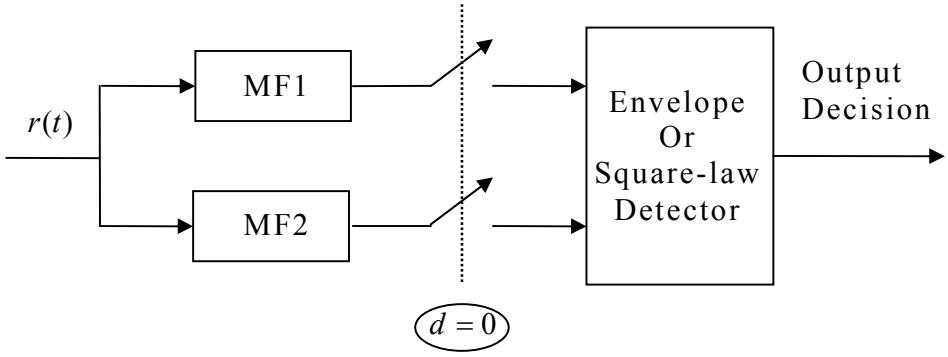

Figure 3.2 Optimum receiver for binary signals

Matlab numerical simulation was used to show the effect of timing offset on system performance. Simulation of five different types of channel models is presented in Figure 3.3.

In this simulation, sampling phase d is defined as the timing difference between the apex and sampling time in one period of a pulse. T_p is the Gaussian

monocycle pulse length. Here it is assumed that the sampling phase is located within the Gaussian monocycle pulse. After sampling, for BPSK modulation, the demodulator makes decision to recover the symbols and compares with transmitted symbols. Figure 3.3 provides several examples of the relationship between timing errors and system performance.

To obtain the numerical results, simulations were repeated 20 times for every timing offset setting and the results were averaged. System performance degrades propositionally with the sampling phase. For IEEE UWB channel model, system performance is more sensitive to the sampling phase errors for CM3 and CM4 than CM1 and CM2.

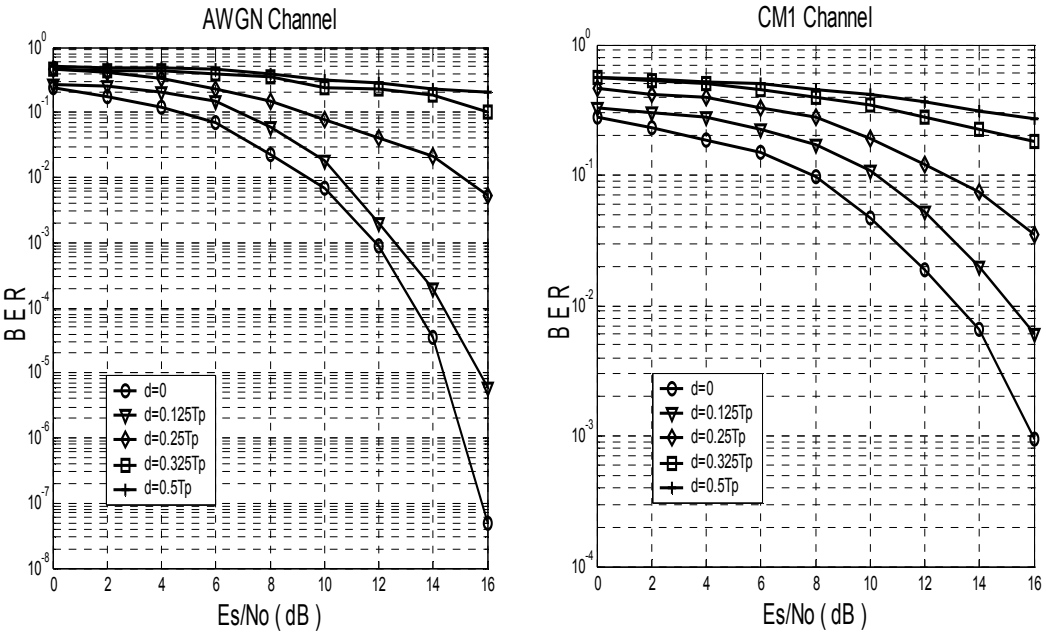

(a) (b)

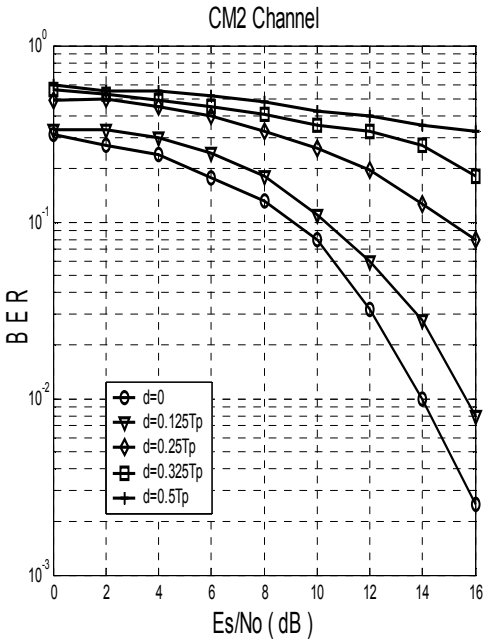

(c)

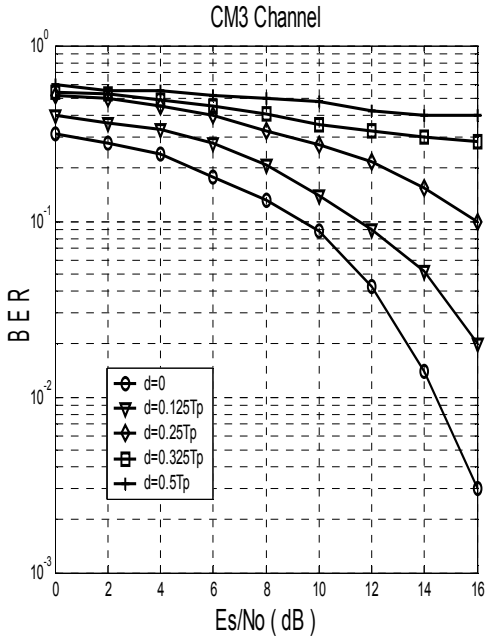

(d)

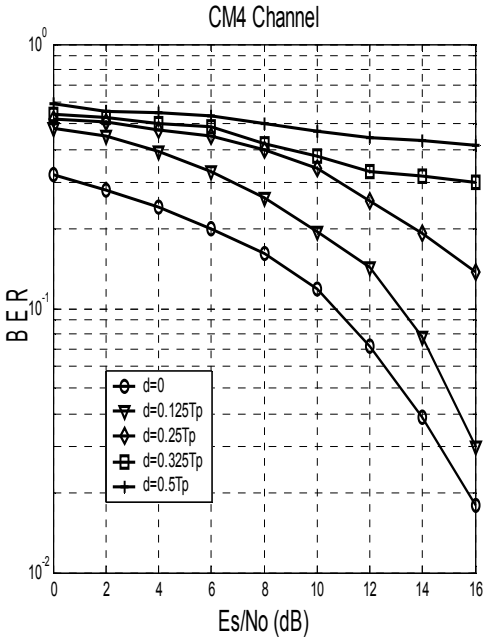

(e)

Figure 3.3 Effect of timing error on system performance

3.3 Potential UWB Acquisition Techniques

Acquisition techniques can be introduced from two folds: timing estimation and search strategies. A UWB signal waveform is very sharp which means there are a large number of resolvable paths after UWB channel response. The main difference between the acquisition for UWB systems and traditional wireless communication systems is the amount of acquisition states. UWB systems require more acquisition stages to meet larger search space. The main objective for UWB acquisition techniques is how to achieve acquisition faster than the traditional techniques through timing estimation and search strategies.

3.3.1 Timing Estimation

Traditionally, timing estimation is accomplished in one of several ways: decision-directed timing estimation, non-decision directed timing estimation, and early-late gate synchronization.

a) Decision-directed timing estimation

Decision-directed timing estimation treats the information symbols from the output of a demodulator as a known transmitted sequence. It is well known that maximum-likelihood (ML) criterion and maximum a posteriori probability (MAP) criterion are widely applied to signal parameter estimation. For timing estimation, the delay timing τ is modeled as random and characterized by a priori probability density function $p(\tau)$. In the ML criterion, τ is processed as deterministic but unknown.

BPSK modulation is considered at baseband here. The received signal is expressed as

$$r(t) = s(t;\tau) + n(t) \tag{3.6}$$

where

$$s(t;\tau) = \sum_n I_n g(t - nT_s - \tau) \tag{3.7}$$

in which I_n is the information digit which is 1 or -1, $g(t - nT_s - \tau)$ is the signal shape and T_s is the symbol period. An example of BPSK receiver is given in Figure 3.2. The demodulator output is sampled periodically at the symbol rate, T_s.

$$t_n = nT_s + \tau \tag{3.8}$$

The observation window is set as N samples of the received signals

$$r = [r_1, r_2, \cdots, r_N] \tag{3.9}$$

$$r_n = s_n(\hat{\tau}) + z_n = \int_{-\infty}^{+\infty} s(nT_s + \hat{\tau} - \tau) g(t) dt + z(n) \tag{3.10}$$

where $z(n)$ is a discrete expression of AWGN noise. From [27], the MAP estimate is the value of τ that maximizes the MAP:

$$p(\tau) = \frac{p(r/\tau)p(\tau)}{p(r)} = \frac{p(\tau)}{p(r)} \left(\frac{1}{\sqrt{\pi N_0}} \right)^N \exp\left[- \sum_{n=1}^{N} \frac{|r_n - s_n(\tau)|^2}{N_0} \right] \tag{3.11}$$

Maximization of the parameter τ is equal to the maximization of a likelihood function. In another word, the ML criterion for signal parameter estimation is given by

$$\Lambda(\tau) = \exp\left[- \sum_{n=1}^{N} \frac{|r_n - s_n(\hat{\tau})|^2}{N_0} \right] \tag{3.12}$$

$$s_n(\hat{\tau}) = I_n J(\Delta\tau) + \sum_{m=-\infty}^{+\infty} I_m J\left[(n-m)T_s - \Delta\tau\right] \quad m \neq n \tag{3.13}$$

where

$$J(t) = g(t) * g(-t) \quad \text{with } J(nT_s) = \begin{cases} 1, & n = 0 \\ 0, & n \neq 0 \end{cases} \tag{3.14}$$

$$\Delta\tau = \tau - \hat{\tau} \tag{3.15}$$

in which $*$ denotes a convolution. From the above processes, the ML function to estimate τ can be defined as follows

$$\Lambda(\hat{\tau}) = \frac{1}{N}\sum_{n=1}^{N} \frac{r_n}{I_n}$$

$$= J(\Delta\tau) + \frac{1}{N}\sum_{n=1}^{N}\sum_{m=-\infty}^{+\infty} \frac{I_m}{I_n} J\left[(n-m)T_s - \Delta\tau\right] + \frac{1}{N}\sum_{n=1}^{N} z_n \qquad m \neq n \tag{3.16}$$

Then the time delay $\hat{\tau}$ is the ML estimate of τ if

$$\frac{d\Lambda(\hat{\tau})}{d\hat{\tau}} = J'(\Delta\tau) + \frac{1}{N}\sum_{n=1}^{N}\sum_{m=-\infty}^{+\infty} \frac{I_m}{I_n} J'\left[(n-m)T_s - \Delta\tau\right] + \tilde{z}_L \quad m \neq n \tag{3.17}$$

where $\tilde{z}_L$ is AWGN noise. The implementation of (3.17) for timing estimation is shown in Figure 3.4, in which $g(-t)$ acts as a pulse MF.

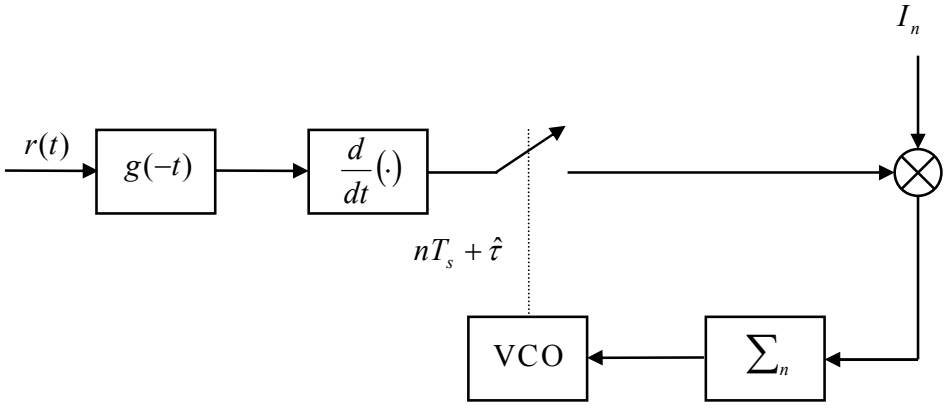

Figure 3.4 Decision-directed ML timing estimation

b) Non-decision-directed timing estimation

A non-decision-directed timing estimation is another popular method to obtain timing information of the received signal. Instead of using estimated symbols to calculate a likelihood function, this method averages the likelihood ratios $\Lambda(\hat{\tau})$ over the probability density function (PDF) of the information symbols. Again, the received sequence of N samples is given by (3.9). Combining (3.10) and (3.13), the individual sample is to be expressed

$$r_n = I_n J(\Delta\tau) + \sum_{m=-\infty}^{+\infty} I_m J\left[(n-m)T_s - \Delta\tau\right] + z_n = I_n J(\Delta\tau) + z_L \qquad m \neq n \tag{3.18}$$

where

$$z_L = \sum_{m=-\infty}^{+\infty} I_m J\left[(n-m)T_s - \Delta\tau\right] + z_n \qquad m \neq n \tag{3.19}$$

Since $J(t)$ is a real function, the ML criterion for non-decision directed timing estimation is to be obtained as

$$\begin{aligned}\Lambda(\hat{\tau}) &= \frac{1}{N}\sum_{n=1}^{N}\left|r_n\right|^2 \\ &= \frac{1}{N}J^2(\Delta\tau)\sum_{n=1}^{N}\left|I_n\right|^2 + \frac{1}{N}\sum_{n=1}^{N}\left(2\Re\left\{I_n z_L^*\right\}J(\Delta\tau) + \left|z_L\right|^2\right)\end{aligned} \tag{3.20}$$

where $\Re(\cdot)$ denotes the real part of a function. The time delay $\hat{\tau}$ is the ML estimate of τ if

$$\frac{d\Lambda(\hat{\tau})}{d\hat{\tau}} = C_{NE} J'(\Delta\tau) J(\Delta\tau) + NC = 0 \tag{3.21}$$

in which

$$C_{NE} = \frac{1}{N}\sum_{n=1}^{N}\left|I_n\right|^2 \tag{3.22}$$

$$NC = \frac{1}{N}\frac{d\left(\sum_{n=1}^{N}\left[2\Re\left\{I_n z_L^*\right\}J(\Delta\tau)+\left|z_L\right|^2\right]\right)}{d\tau} \tag{3.23}$$

An implementation of a non-decision-directed timing estimation on the derivative of (3.20) and (3.21) is presented in Figure 3.5.

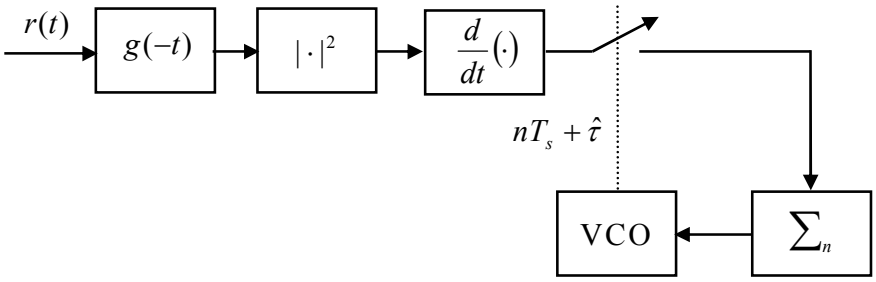

Figure 3.5 A non-decision-directed ML timing estimation

The performance between decision-directed timing estimation and non-decision-directed timing estimation was explored in [27]. The first method provides better performance than the later one, however it requires more overhead of the transmitted sequence. Decision-directed timing estimation is also known as data aided (DA) timing estimation. As the name suggested, DA timing estimation requires a sequence of known symbols or pilot codes. There is a very interesting observation in UWB acquisition according to [28]. The DA acquisition is faster than the non-decision-detected timing estimation.

c) Early-late gate tracking

Fine synchronization or tracking which complete the task of timing recovery is introduced to set foundation for the proposed acquisition structure. A system intends to sample a symbol at the highest SNR point if the timing recovery loop

operates properly. An example of a typical timing recovery loop is shown in Figure 3.6.

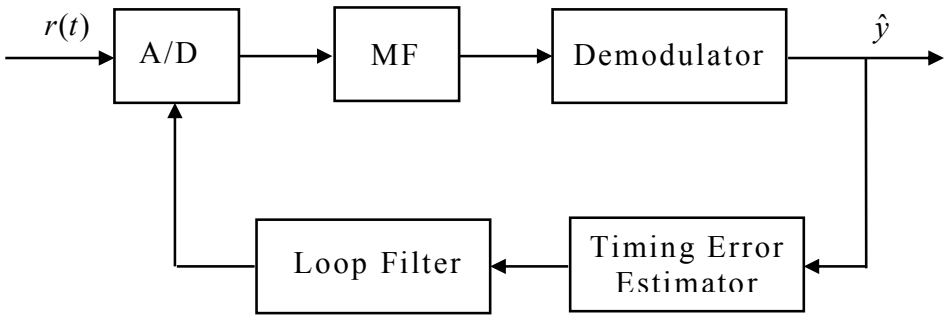

Figure 3.6 A timing recovery loop

The A/D converter is in charge of sampling the incoming analog signal and sending out digital data. After A/D converter conversion, the signal is passed through a matched filter. A timing error estimator then utilizes a number of different algorithms to generate a timing error. A controlled signal for adjusting sampling phase is formed by filtering this error signal using a standard first-order loop filter containing two paths: the proportional path and the integral paths as illustrated in Figure 3.7. The proportional path multiplies the timing error signal by a proportional gain K_p. From control theory, it is known that a proportional path can be used to track out the phase error. For the timing recovery loop to track out a sampling frequency error, a loop filter containing an integral path is needed. This path multiplies the error signal by an integral gain K_i and then integrates the scaled error using an adder and a delay block.

An early-late gate algorithm [27] is applied for an A/D converter and fine timing error estimator. This algorithm recognizes a timing error by using samples

that are early and late compared to an ideal sampling point. Generation of an error requires at least three samples per symbol as shown in Figure 3.8. The left plot in Figure 3.8 is for the case where the sampling is occurring late. Note that the early and late samples are at different amplitudes. The difference in amplitude is used to derive an error for the timing recovery loop. Once the timing recovery loop converges, the early and late samples will be at equal amplitudes. The sample to be used for later processing is the sample that lies in the middle of the early and the late samples. One drawback of the early-late gate algorithm is that it requires at least three samples per symbol. This drawback is compensated by using symbol sampling rate to reduce over samples comparing with when over-sampling is used.

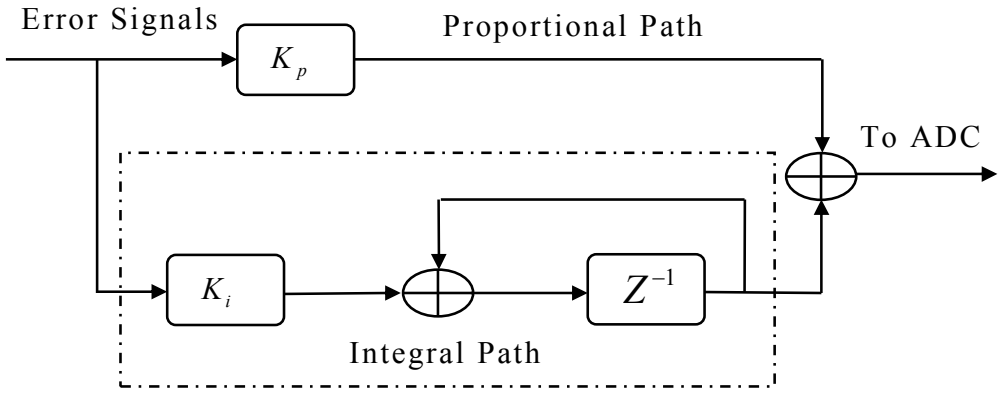

Figure 3.7 A typical first order loop filter

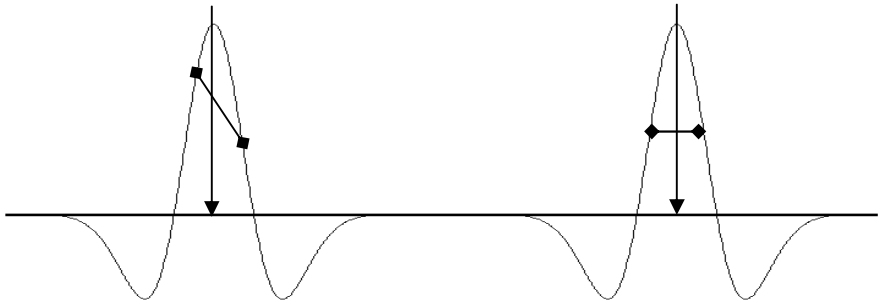

Figure 3.8 Early-late gate algorithm

3.3.2 Search Strategies

A search space of acquisition is random in nature. Mostly, a search for acquisition is based on the auto-correlation properties of the applied pilot codes. The auto-correlation is high if the receiver is synchronized with the incoming pilot codes. Acquisition search space is a set of all possible relative shifts of the local code with respect to the received signals. This search space is divided into q_{acq} search-cells. The process of acquisition is identified by the so-called sync-cell. The sync-cell corresponds to a situation in which the receiver is synchronized. The time takes to search a single cell called dwell-time, t_{dwell}. Power at the output of the data detector is cumulated during t_{dwell}. This power-level is used as a decision variable to select the sync-cell. Duration of a cell corresponds to half chip-period, $0.5T_p$ in normal narrow band applications. The relationship of acquisition time and the chip size for the same q_{acq} is: the acquisition-time increases when the size of a chip decreases.

3.3.2.1 Hybrid Search Scheme

There are two ways for acquisition search: the serial search, using a single correlator and searching the cells sequentially; the parallel search, examining more than one cell in a unit time. A clear disadvantage of a serial search is that it takes longer due to a large number of cells being analyzed sequentially to find the sync-cell. A number of correlators operate in parallel to reduce acquisition time in a parallel search. A parallel search increases complexity to analyze power-contents in

the parallel stages. The required amount of computational power easily grows so that a parallel search may exceed the available resources.

A hybrid scheme using both serial and parallel search balances the need for fast acquisition and low complexity. Multiple correlators, but not all, search the sync-cell simultaneously. A general structure of hybrid acquisition for UWB is presented in Figure 3.9.

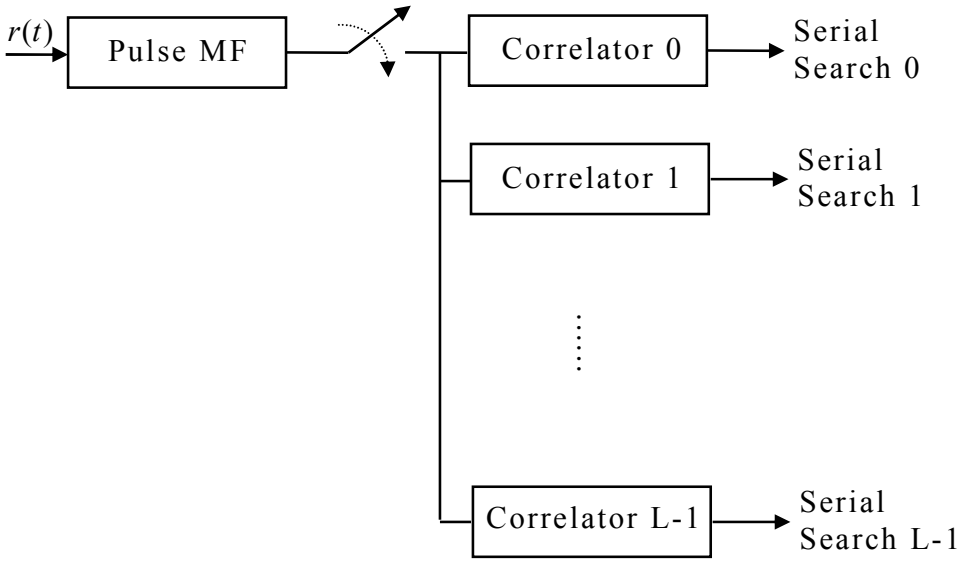

Figure 3.9 Hybrid search for acquisition

There are two important measures determining the performance of an acquisition scheme

- The false alarm probability is the chance that an acquisition is declared at a wrong cell.
- The detection probability is the chance that an acquisition is detected at a sync-cell.

Denoting the j^{th} correlator output as Z_j and assuming the detection threshold as T_h, the detection probability of the j^{th} correlator is

$$P_d = P_r(|Z_j| > T_h | \ H_j) \tag{3.24}$$

Here the hypothesis H_j represents the event that the timing error falls within $\pm\lambda$ of the j^{th} correlator peak where λ denotes a sync-cell size. The notation $\overline{H}_j$ represents the event that timing error falls out of a window $\pm\lambda$ around the j^{th} correlator. False alarm probability is defined as

$$P_f = P_r(|Z_j| > T_h | \ \overline{H}_j) \tag{3.25}$$

P_d and P_f have a relationship of

$$P_d + P_f = 1 \tag{3.26}$$

A search is the process of converting multiple hypothesis tests into a series of simpler binary hypothesis tests. The inherent trade-off here is the reduction of complexity at the cost of increasing the time to reach final decision. The first stage of the search tests an observed random cell (in this case, the correlator output) against two hypotheses, say H_j and $\overline{H}_j$ as defined above. If the selected hypothesis is H_j then the search is terminated, otherwise the process continues with another pair of hypotheses, H_k and $\overline{H}_k$. H_k is the hypothesis of timing error falling within $\pm\lambda$ of the k^{th} correlator peak. In general, k is unrestricted and can be equal to j, as to be the case for a truly random search.

3.3.2.2 Serial Search Scheme

An important parameter to evaluate acquisition performance is the mean acquisition time (MAT). For one search path, serial search is straightforward to be considered in design. It is simple to implement but suitable only for short uncertain search positions. A search strategy specifies the order in which the candidate phases in the timing uncertainty region are evaluated by the acquisition system. When there are more than one acquisition phases in the uncertainty region, the serial search which linearly searches the uncertainty region is no longer the optimal search strategy. More efficient non-consecutive search strategies are required for fast acquisition. Four different search schemes are investigated and Figure 3.10 provides block diagrams for each case.

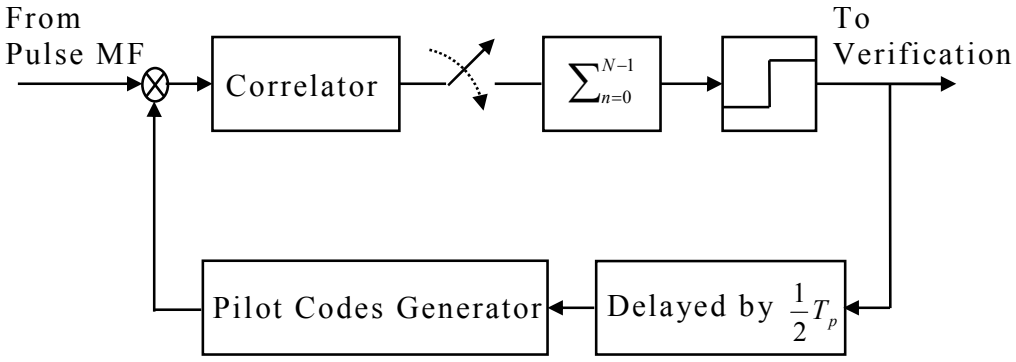

(a) Serial search

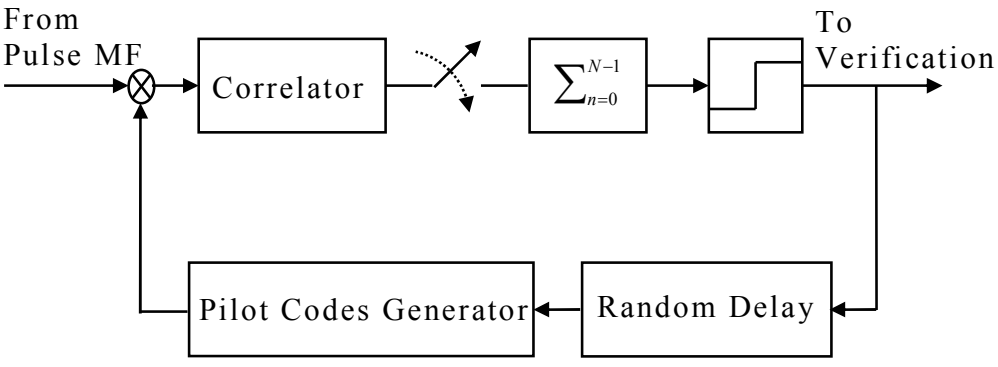

(b) Random search

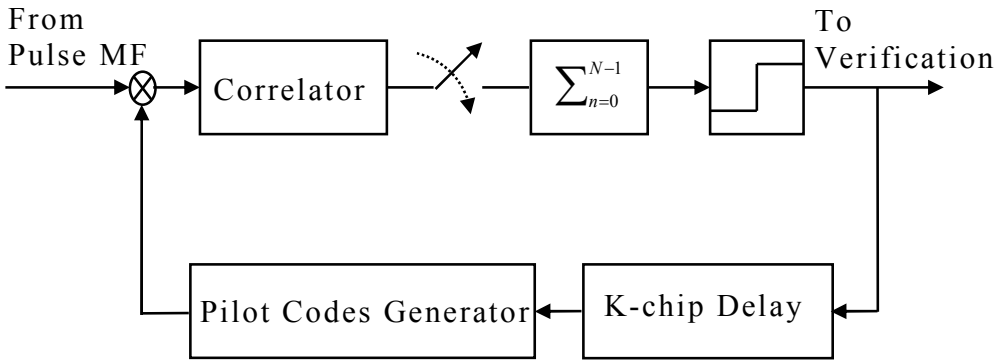

(c) Look-and-jump search

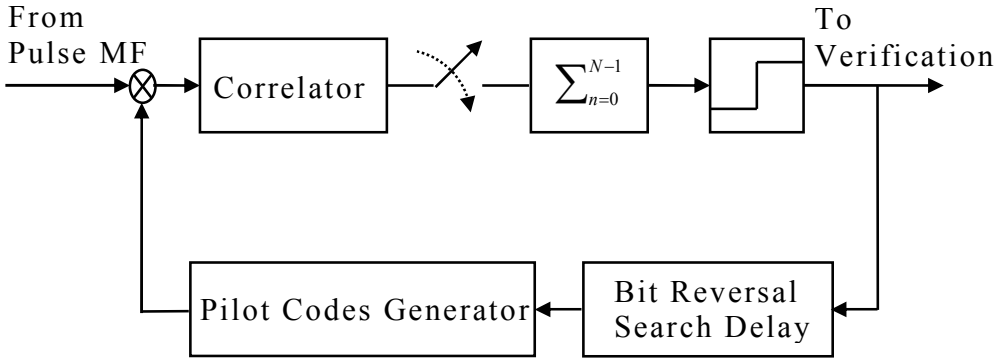

(d) Bit reversal search

Figure 3.10 Search strategy schemes

a) Linear search

The phase of the locally generated code is progressively shifted in sequence in steps of a unit search interval $\frac{1}{2}T_p$. Assuming the minimum multipath resolution is $\frac{1}{2}T_p$, the correlator dwell time is one full period of the packed code. The decision variable is then compared with a decision threshold T_h. If the decision variable exceeds the threshold, the corresponding cell is declared to be a sync-cell (H_1 cell) and the search is terminated. Otherwise, the cell is declared to be a non sync-cell (H_0 cell) and the next cell is tested. The entire process repeats until the codes are

aligned to within a step size. This total number of cells in the uncertainty region is thus $q = N \times T_s / (\frac{1}{2} T_p)$. In the event of a false alarm, it is assumed that the search resumes after a penalty time of J correlator dwell times. Penalty time is the time taken to confirm a false alarm.

b) Random search

The random search acquisition receiver is very similar to the serial search except that the local code is not shifted serially. Instead, the correlator step size at any time is chosen randomly. The random delay generator changes the phase of the pilot codes randomly between 1 and $(q-1)$-step size. The receiver continues to run with random jumps at each step until acquisition is achieved.

c) Look-and-jump search

The basic idea of look-and-jump search is assuming the timing uncertainty region divided into bins indexed by 0, 1, …, $N-1$. In look-and-jump by K-bin search, starting at bin 0, the search continues to the K^{th} bin, then $(2K)^{th}$ bin. K is the number of bins to terminate an acquisition. For $N = 12$ and $K = 3$, the look-and-jump search operates in the following bin order: {0, 3, 6, 9, 1, 4, 7, 10, 2, 5, 8, 11}.

d) Bit reversal search

For UWB acquisition, the delay spread of a channel can not be exactly known regardless any assumption. Due to the characteristics of the UWB channel, there might not be K consecutive bins to terminate the search. From Figure 2.4(b), it is easy to find that certain bins have higher probability to end the acquisition because they have larger amplitude. Some bins have lower probability of

terminating the search because of smaller amplitude. For this reason, an efficient search is needed in that the knowledge of K is mostly unknown for a search. Let use a binary representation of the integers 0, 1, …, $N-1$, and set N is assumed to be a power of 2. For example, if $N=16$, the bit reversal search pattern is denoted as 0000, 1000, 0100, 1100, …, 0111, and 1111 in binary for each search-cell. The index set for a bit reversal search permutation is named as I = {0, 8, 4, 12, …} in decimal fashion. The jump between two consecutive search-cells is not a constant but in a forward move and backward move approach.

3.3.2.3 Serial Search Performance Analysis

Hybrid search reduces the search space for a single serial search path. As a result, the performance of the individual path search is critical for MAT. To simplify the deduction, a search without AWGN noise is considered here. Assuming N available search states and a zero false alarm probability, the first finding of H_j, $j \in \{0,1,\cdots,K\}$ hypothesis terminates the acquisition. From [29,30], the MAT for these four search approaches is

- Serial search

$$MAT_{serial} = \frac{(N-k)^2 + (3N-K)}{2N} \tag{3.27}$$

- Random search

$$MAT_{random} = \frac{N}{K} \tag{3.28}$$

- Look-and-jump search

$$MAT_{look-and-jump} = \frac{1}{2}\left(\frac{N}{K}+1\right) \tag{3.29}$$

- Bit reversal search

$$MAT_{BRS} = \frac{1}{2}\left(\frac{N}{K}+1\right) \tag{3.30}$$

The result showing normalized MAT for these four search strategies is plotted in Figure 3.11. The normalized MAT is defined as MAT/N versus K/N. It is obvious that the look-and-jump search and bit reversal search is the most promising search approaches and random search is the second optimum choice. Serial search is the slowest method. In [30], the author analyzed the performance of serial search and random search under a channel model based on IEEE 802.15.3a with parameter $\frac{1}{\Gamma} = 10\,\text{ns}$ and $\frac{1}{\lambda} = 1\,\text{ns}$. This channel model is somewhat similar to the IEEE UWB models. It again proves that the random search slightly better than the serial search for SNR over 9dB as indicated in Figure 3.12.

In practice, since the knowledge of K is unknown, bit reversal search and random search are supposed to be more popular in UWB acquisition researches.

3.4 Summary

A brief discussion about traditional acquisition and potential UWB search approaches is presented in this chapter. The contents includes timing acquisition structure, communication system performance relative with timing error, timing estimation algorithm and normal UWB search methods.

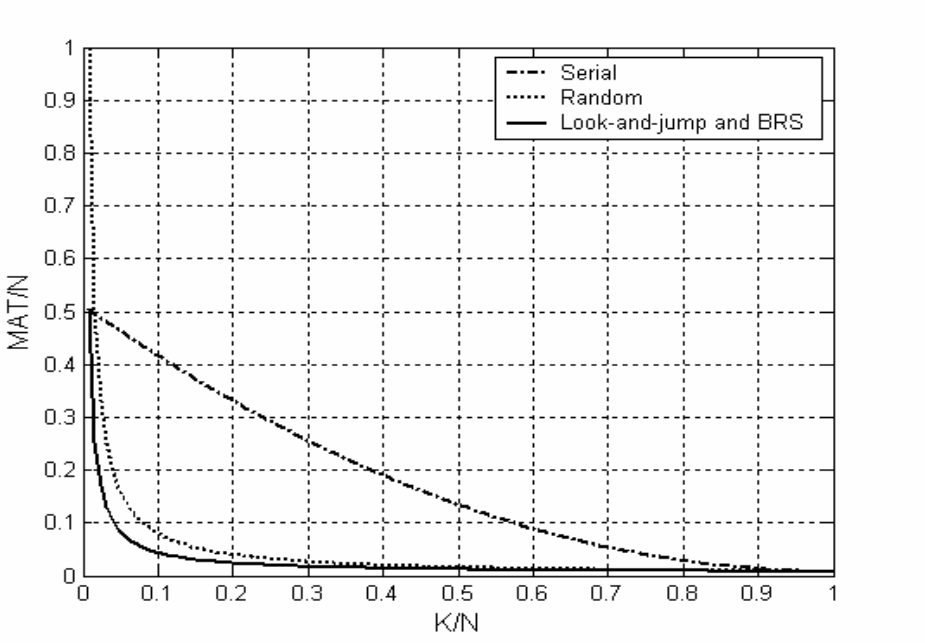

Figure 3.11 Normalized MAT for discussed search approaches

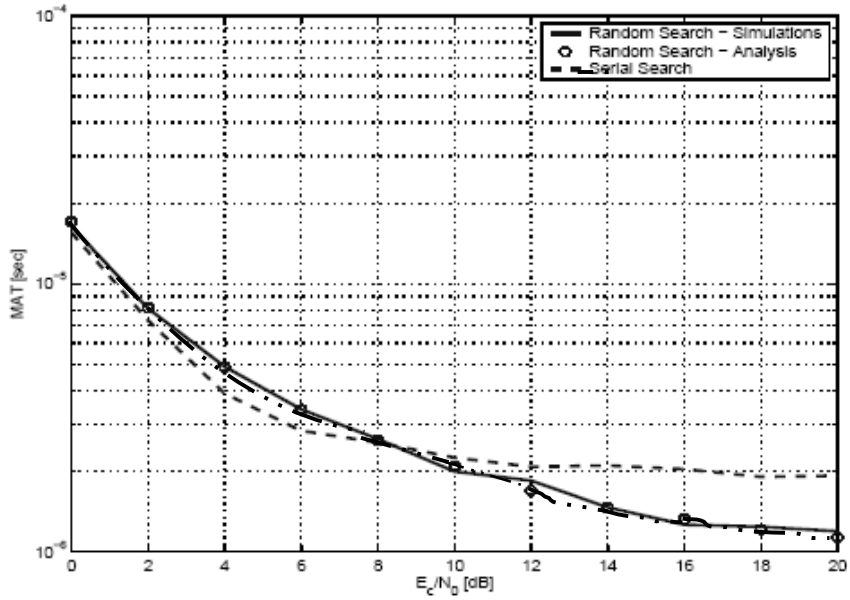

Figure 3.12 Simulation results of three search methods [30]

CHAPTER 4 PROPOSED UWB ACQUISITION STRATEGIES

Synchronization processes in two stages. The first stage is acquisition which achieves a coarse synchronization to a reasonable accuracy in a short time. The second stage is the tracking process which is responsible for achieving fine synchronization and maintaining system synchronization through clock drifts. Acquisition is more challenging than tracking because acquisition aligns the free running local clock to the incoming signals within one chip interval. Due to the constraint of signal power level and more search space in UWB than narrow band communications, acquisition strategies focus on how to suppress noise level and shorten MAT by means of simple implementations. From the previous chapter description, there are two candidates for timing estimation: the data aided (DA) timing estimation and the non-decision-directed timing estimation. DA timing estimation is selected since this method provides faster acquisition. The drawback of DA timing acquisition is that it requires an overhead of the transmitted sequence. This research makes use of this overhead to collect signal energy. A well-designed architecture for UWB acquisition is proposed using DA timing acquisition approach in this chapter. The architecture includes: a pilot code design, a hybrid MF timing estimation, a post detection integration (PDI) technology, and a bit iteration search (BIS).

4.1 Pilot Code Design

In a typical DA communication system, pilot codes provide the receiver with a known sequence of symbols. The receiver constantly looks for these codes to locate the timing information [31]. Figure 4.1 illustrates the concept of received symbols with a DA sequence.

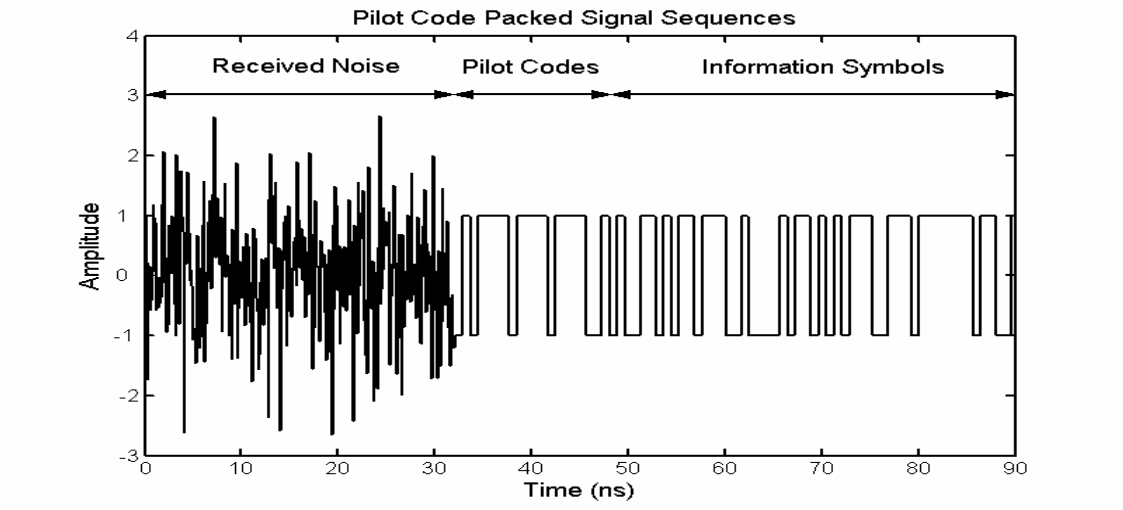

Figure 4.1 Pilot codes of a signal sequence with noise

A sequence of pilot codes is defined as $X(i), i \in [0, N_p - 1]$, where N_p is the length of the pilot header code. The autocorrelation property of a set of pilot codes affects acquisition performance. A higher degree of autocorrelation yields a better result in acquisition. One successful autocorrelation function of pilot codes from [32] is

$$R(k) = \sum_{n-1}^{N_p} X(n)X^*(n+k) = \begin{cases} N_p & k = 0 \\ -1 & 1 \le k \le N_p - 1 \end{cases} \tag{4.1}$$

Because the sequence of pilot codes is periodic with a period N_p, its autocorrelation function is also periodic with period N_p. From the above expression, when two identical N_p -sequences are exactly aligned, the autocorrelation reaches the peak value during the period N_p. With any other offset autocorrelation decreases dramatically to –1. N_p-sequence autocorrelation property motivates its use as pilot codes for the purpose of acquisition. When the pilot sequence is entirely captured within the correlator and maximum correlation value is obtained, the receiver can estimate the timing of the incoming symbols.

UWB communications are processed in relative high speed rate. Long acquisition preambles significantly reduce throughput of a network. Cyclic pilot codes are successfully applied in orthogonal frequency division multiplexing (OFDM) as a guard interval to suppress inter-symbol-interface (ISI) [33]. There are very few reports for cyclic pilot codes in DA acquisition. Cyclic pilots supply a repeated peak if the correlator captures the pilot codes. This property motivates this research to build a pilot code MF to suppress dense ISI for UWB channel models. The relatively low transmission power of UWB systems requires the receiver to process the received signals in longer time in order to obtain a reliable estimation of the timing information. The receiver is able to conform the reliable timing phase in time domain. An example with two repeated pilot codes structure is shown in Figure 4.2.

4.2 Hybrid MF Timing Offset Estimation

Short pulses and low duty cycle signaling employed in UWB systems place stringent timing requirements at the receiver for demodulation [8], [11]. The wide bandwidth results in a fine resolution of the timing uncertainty region. Thereby there is a large search space for acquisition. In the absence of any aided information regarding the timing of received signals, the receiver must search through a large number of timing phases in the acquisition stage. This causes a long acquisition time if the system evaluates timing phases in serial as discussed in Chapter 3. If the timing phases are evaluated using a hybrid technique, the receiver needs sub-optimum hardware supports to achieve acquisition in a short time.

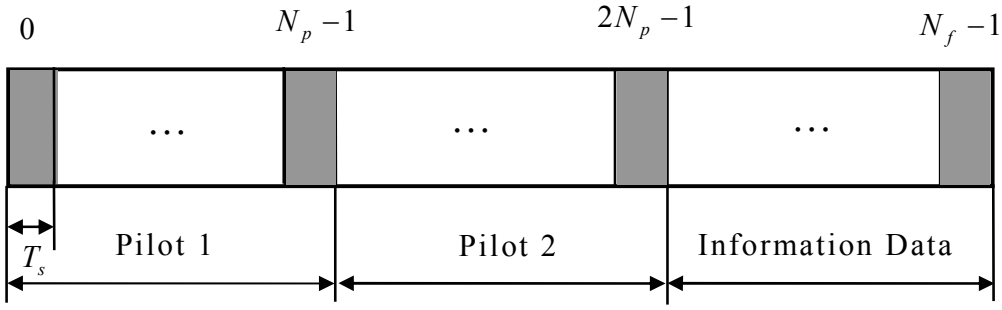

T_s : Symbol period.
N_{p-1} : Length of one section of pilot codes.
N_f : Length of one frame of packed data.

Figure 4.2 Format of a packed information data

The transmitted pulse is distorted by the antenna and the transmitting channels. The receiver does not have an exact knowledge of the received signal waveform. Short pulses used in UWB systems also result in high resolvable multipaths with a large delay spread at the receiver. ISI effect occurs when the

symbol length of the system is shorter than the multipath delay spread of the channel. Individual symbols are "smeared" into each other, which typically require an equalizer to compensate such channel affect. However, synchronization is accomplished before signals going through an equalizer in this case. Acquisition without equalizer to reduce ISI is studied in this thesis.

Acquisition is realized by active or passive method or a combination of both. In the active method, the received signal is multiplied with a local generated replica of the spreading code and the result is integrated over some observation intervals. Multiplications and integrations in the process are performed step-by-step for each chip phase and tested, i.e., serially. In the passive method, a pulse shape or a pilot code matches to the MF impulse response. Therefore, the impulse response of the MF is a time-reversed and delayed version of the pulse shape or the pilot code. The MF waits until the code in the received signal obtains a predetermined phase, which leads to the name “passive”. MF acquisition is more useful especially in the case when fast acquisition is needed or a chosen pilot or preamble is sent before data transmission. The output of MF is either sent to a threshold detector or a ML algorithm during a given observation window is selected, from which the acquisition decision is made.

4.2.1 MF Timing Estimation with Down-sampling Rate

Data transmission over a dispersive channel, i.e. low pass channel, results in ISI, which is a major source of errors. ISI can be minimized by optimal signal design. Errors which are caused from the receiver and the channel noise are

simplified as thermal noise. Thus the received waveform is distorted by ISI and the thermal noise. Detection a pulse signal of known shape which immersed in additive white noise is an important and well-studied problem in communications. The optimum detection of a noisy pulse is the use of MF. MF is a linear-time-invariant (LTI) system. When the receiver is switched on, an A/D converter needs to know when to sample the output of the MF in order to make decision. In general, there are two types of MF. One is continues signal processing and another is discrete signal processing. It is very difficult to process a pulse MF in digital form for UWB communications due to its ultra wide bandwidth. A continuous pulse MF is used to compress the AWGN noise.

In the presence of noise, an optimal filter is the one having its own impulse response matching with the incoming pulse shape. If $g(t)$ is the impulse response of the pulse shape filter in the transmitter and $h(t)$ is the impulse response of the receiver filter, matched filter theory requires that $g(t) = h(-t)$. MF output is the autocorrelation of the transmitted pulses, therefore MF averages the noise and provides a peak value to reduce noise during correlating the signal with its noisy replica. The algorithm for timing recovery assumes that the incoming UWB signals are sampled with an unknown timing offset τ, i.e. $T = T_s + \tau$. A general MF receiver with symbol sampling rate is shown in Figure 4.3, where $n(t)$ denotes the AWGN noise. In order to estimate τ, output of the MF, $O_p(\cdot)$, is suitably expressed as

$$O_p(t) = \int_{t=0}^{T_s} r(t+\tau) * h(t)dt \tag{4.2}$$

where $r(\cdot)$ is the received symbol waveform. Perform the maximum operation over $O_p(\cdot)$ provides

$$(\hat{\tau}) = \arg\max_t(O_p(t)) \tag{4.3}$$

where $\arg\max_t(\cdot)$ denotes the maximum value among a set of $t \in [0, T_s + \tau]$. The maximum of $O_p(T)$ indicates location of the timing phase. This algorithm can be implemented by either analog or digital method. Traditional MF digital timing estimation uses over-sampling, generally higher than the Nyquist sampling rate, and interpolating incoming waveform to locate the maximum value of $O_p(\cdot)$ in order to estimate the timing phase. For a UWB receiver, it is challenging to over-sample the received pulses and process the MF digitally. The theoretical architecture of a MF receiver is presented in Figure 4.3.

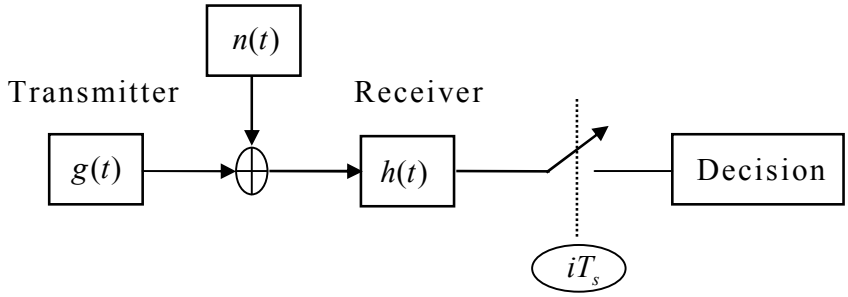

Figure 4.3 Basic architecture of a MF receiver

4.2.2 Pilot Code MF Timing Offset Estimation

Pilot code MF timing offset estimation makes use of code MF filter for timing estimation. Different from the pulse MF, a code matched filter stores a sequence of codes as it coefficients. Same as the pulse MF, output of the code MF

is the autocorrelation of the transmitted codes. Pilot codes MF uses a copy of pilot codes as its coefficients. Since the chosen pilot codes having a peak value of its autocorrelation function in (4.1), the pilot MF has similar property as a pulse MF to locate the timing phase digitally.

The basic pulse MF time estimation in Figure 4.3 is not able to detect the timing information for UWB communications. If a pilot MF is added, the architecture of the receiver is sketched in Figure 4.4. The received data are sampled in an optimal timing phase after a pulse MF to reduce the AWGN noise. The equispaced samples are collected into the pilot MF to calculate the autocorrelation of the pilot codes. Normally, an optimum decision rule based on the MAP estimation criterion is used to detect the received symbol sequence coupling with noise [33]. This decision criterion attempts to choose values of the sampled phase in each transmitted signal interval from the observation vectors, such that a set of posteriori probabilities is maximized. The prior probabilities are all equal (assuming symbols are uniformly distributed). MAP criterion makes decision from the maximum of the conditional probability density functions, known as ML criterion. An optimal ML receiver performs both data detection and synchronization parameter estimation. In another word, an optimal ML receiver selects a set of values $\{y(i)\}$ which maximizes the likelihood function $\mathrm{p}(y/\hat{\tau})$ as follows

$$(\hat{\tau}) = \arg\max_{y} \left(p(y/\hat{\tau})\right) \tag{4.4}$$

where $\arg\max_{y}(\cdot)$ denotes the maximum value $(\cdot)$ among a set of y. The function structure of the pilot MF timing offset is given in Figure 4.4.

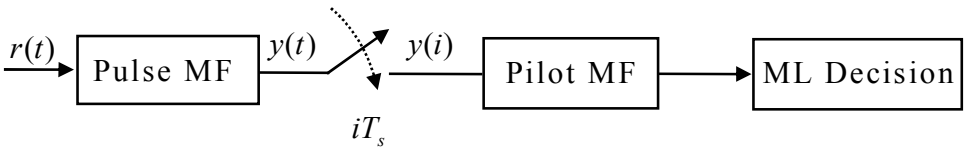

Figure 4.4 An architecture of pilot MF acquisition

4.2.3 Reference Aided Matched Filter Acquisition

Pilot MF acquisition is a common way for DA acquisition. Due to the dense ISI in UWB communications, a modified pilot MF acquisition is proposed here. There are two identical sections of the pilot codes in the cyclic pilot codes in Figure 4.2, Pilot 1 and Pilot 2. A new code MF uses Pilot 1 as the reference MF for Pilot 2. This pattern is named as reference aided matched filter. The conception structure is presented in Figure 4.5, where T_Δ is the length of pilot codes.

$$T_\Delta = N_p T_s \tag{4.5}$$

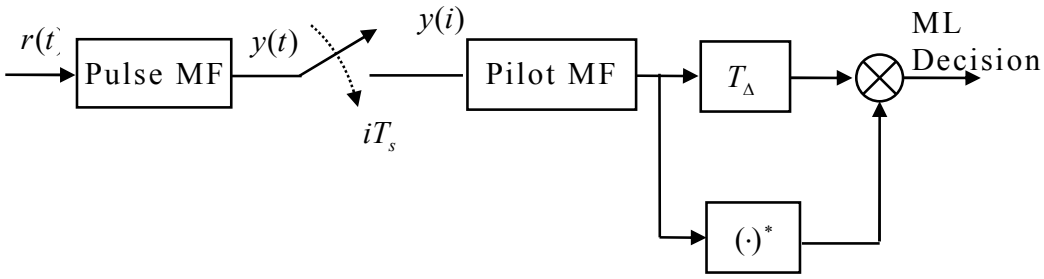

Figure 4.5 Basic architecture of RAMF

The original idea of RAMF is to suppress the dense ISI further and implement acquisition with a practical, fully digital architecture without over-sampling. The two-repeated cyclic pilot in Figure 4.2 is used to build a RAMF. This MF is an adaptive digital filter storing a delayed copy of incoming sequence to match the following sequence for jointly timing estimation. Why is this filter adaptive? Its coefficients are changed from one frame to another. The UWB multipath channel models represent dense multipath interference. If the delay time of multipath interference is longer than the symbol period, such interference leads to the delayed pulse echoing jointly to autocorrelation with the current pulse. The output of the traditional pilot MF is not robust to compress these interferences. RAMF is adaptive, which means the updated coefficients can depress such dense multipath interference. The signal format after pulse MF is denoted by $y(t)$ as

$$y(t) = \sqrt{E_p} \sum_{i=-\infty}^{+\infty} \sum_{l=0}^{L-1} \int_{-\infty}^{+\infty} I_i \alpha_l g(t - \upsilon - iT_s - \tau_l) g(\upsilon) d\upsilon + n(t) * g(t) \qquad (4.6)$$

where τ_l stands for l^{th} path timing delay and α_l is the multipath gain coefficient . The transmitted pulse autocorrelation function is

$$R_p(\lambda) = \int_{-\infty}^{+\infty} g(t) g(\lambda - t) dt \qquad (4.7)$$

The received signal (4.6) becomes

$$y(t) = \sqrt{E_p} \sum_{j=-\infty}^{+\infty} \sum_{l=0}^{L-1} I_i \alpha_l R_p(t - jT_s - \tau_l) + n(t) * g(t) \qquad (4.8)$$

Simplifying this equation as

$$y(t) = r_p(t) + n_C(t) \qquad (4.9)$$

in which

$$r_p(t) = \sqrt{E_p}\sum_{j=-\infty}^{+\infty}\sum_{l=0}^{L-1} I_i \alpha_l R_p(t - jT_s - \tau_l) \tag{4.10}$$

$$n_c(t) = n(t) * g(t) \tag{4.11}$$

Sampling time $\theta(i)$ after pulse MF in Figure 4.5 for a serial search is

$$\theta(i) = iT_s \tag{4.12}$$

After sampling, the continuous signal becomes discrete as

$$r_p(i) = r_p(\theta(i)) \tag{4.13}$$

And the resulting output of sampling with noise is

$$y(i) = r_p(i) + n_c(i) \tag{4.14}$$

where $n_c(i)$ is correlator noise sequence, which is an independent and identically distributed sequence of a zero-mean, variance $\sqrt{E_p}\sigma^2$ Gaussian random variables.

Then the incoming signal is filtered by a cyclic code MF, whose coefficients are copies of the cyclic codes, defined as

$$g_I(i) = \sum_{k=0}^{N_c-1} I_i u(k-i) \tag{4.15}$$

in which $u(\cdot)$ is a rectangular waveform with period T_s. Two channel models, AWGN channel and UWB channel are discussed for ML estimation as follows.

a) General AWGN Channel Model

In the following analysis, a statistical AWGN channel is assumed. In fact, AWGN is a special case of multipath channels when the number of paths equal to one. The beginning sample index is set at zero. The observation window is set at $2N_p$ length, which means RAMF connects $2N_p$ samples for the ML estimation. Then the vector $Y\{\cdot\}$ of the $2N_p$ samples is

$$Y\{y(0), y(1), \cdots, y(2N_p - 1)\} \tag{4.16}$$

Through cyclic pilot MF, the vectors are convoluted with the cyclic code copy, $g_I(i), i \in [0, N_p - 1]$, yielding an output as

$$\tilde{y}(i) = \sum_{k=0}^{N_p - 1} y(k) g_I(i - k) \tag{4.17}$$

Inserting (4.17) into (4.16), the output of the RAMF becomes

$$\tilde{Y} = \{\tilde{y}(0), \tilde{y}(1), \cdots, \tilde{y}(2N_p - 1)\} \tag{4.18}$$

From statistic viewpoint, $\tilde{Y}$ inherits the following property for an average function of $E(\cdot)$.

$$E\{\tilde{y}(i) * \tilde{y}(i + k)\} = \begin{cases} \sigma_w^2 + \sigma_n^2 & k = 0 \\ \sigma_w^2 & k = N_p \\ 0 & otherwise \end{cases} \tag{4.19}$$

where $\sigma_w^2 = E\{|\tilde{y}(i)|^2\}$, $\sigma_n^2 = E\{|\tilde{n}(i)|^2\}$, and $\tilde{n}(i)$ is the noise.

A pilot aided ML estimation aims at achieving a maximum output of MF so that the receiver can estimate the optimum sampling position. ML estimation requires determination of the signal $y(i)$ which maximizes the conditional probability density function (PDF) is $p(y \mid g_I)$, that is, the most likely signal, $g_I(i)$. $g_I(i)$ produces a set of observations, $y(i)$, over a specific observation period $2N_p$. The timing offset τ is treated as deterministic but unknown. The MAP estimate is

$$\hat{\tau} = \arg\max_{\tilde{y}_m} \left\{ p(g_I(i), \tilde{y}_n \left| r_p(i) \right.) \right\} \tag{4.20}$$

where $\tilde{y}_m$ stands for $\tilde{y}(i) * \tilde{y}(i + N_p)$. Based on Bayes' theorem, MAP is able to be transferred into ML as

$$p(g_I(i),\tilde{y}_m|y(i)) = p(y(i)|g_I(i),\tilde{y}_m)\frac{p(g_I(i),\tilde{y}_m)}{p(y(i))} \tag{4.21}$$

where the PDF $p(r_p(i))$ and $p(g_I(i),\tilde{y}_m)$ are constant among the search because the possibility of $y(n)$ is simply a normalized parameter. In addition, the possibility of $g_I(i)\cap\tilde{y}_m$ is the same for all samples.

Assuming no ISI in AWGN channel, the log-likelihood function $\Lambda(\tau)$ is similar to [34],

$$\Lambda(\tau) = \ln(\prod_{i=\beta}^{\beta+N_p-1}\frac{p(y(i),y(i+N_p))}{p(y(i))\,p(y(i+N_p))}) \tag{4.22}$$

in which $p(y(i))$ and $p(y(i+N_p))$ is assumed as normalized parameters, so they are constant. The joint PDF $p(y(i),y(i+N_P))$ is simply assumed as Gaussian-like distribution. Then the log-likelihood function can be simply expressed as

$$\Lambda(\tau) = \sum_{i=\beta}^{p+N_p-1}\ln\left(p(y(i),y(i+N_p))\right) \tag{4.23}$$

The received signals are based on [35],

$$y(t) = \sqrt{E_p}\sum_{i=-\infty}^{+\infty} d_i\alpha R_p(t-iT_s-\tau) + n(t) * g(t) \tag{4.24}$$

Combining (4.24) with (4.12) and (4.13) yields

$$y(k) = y(\theta_i(k)) = \sqrt{E_p}\sum_{i=-\infty}^{+\infty} d_i\alpha R_p(kT_s - iT_s - \tau) + n(i)g(i) \tag{4.25}$$

If it is assumed that there is no ISI in the AWGN channel and the noise item, $n(i)g(i)$, is still AWGN noise , then (4.25) becomes as

$$y(k) = \sqrt{E_p}d_k\alpha R_p(k) + n(k) \tag{4.26}$$

where

$$R_p(k) = R_p(kT_s - \tau) \tag{4.27}$$

The log-likelihood function of the cyclic prefix has joined Gaussian PDF property from above equations [36].

$$p(y(k), y(k+N_p)) = \frac{\exp(-\frac{(\tilde{y}_i(k))^2 - 2\rho\tilde{y}_i(k)\tilde{y}_i(k+N_p) + \tilde{y}_i(k+N_p)^2}{(\sigma_w^2(T_\beta)+\sigma_n^2)(1-\rho^2)})}{\pi^2(\sigma_w^2(T_\beta)+\sigma_n^2)(1-\rho^2)} \tag{4.28}$$

where ρ is cross-correlation coefficient as

$$\rho = \frac{E\{\tilde{y}_i(k)\tilde{y}_i(k+N_p)\}}{\sqrt{E\{(\tilde{y}_i(k))^2\}E\{(\tilde{y}_i(k+N_p))^2\}}} \tag{4.29}$$

This leads to

$$\Lambda(\tau) = \sum_{k=\beta}^{\beta+N_p-1} \ln\left[\frac{\frac{\exp\left((\tilde{y}(k))^2 - 2\rho\tilde{y}(k)\tilde{y}(k+N_c) + (\tilde{y}(k+N_p))^2\right)}{\pi^2\left(\sigma_w^2(T_\beta)\right)^2(1-\rho^2)}}{\frac{\exp\left(-\frac{(\tilde{y}(k))^2}{\sigma_w^2(T_\beta)+\sigma_n^2}\right)\exp\left(-\frac{(\tilde{y}(k+N_p))^2}{\sigma_w^2(T_\beta)+\sigma_n^2}\right)}{\pi^2\left(\sigma_w^2(T_\beta)+\sigma_n^2\right)^2}}\right]$$

$$= C_1(T_\beta) + C_2(T_\beta)\sum_{k=\beta}^{\beta+N_p-1}(2\tilde{y}_i(k)\tilde{y}_i(k+N_p) - \rho((\tilde{y}_i(k))^2 + (\tilde{y}_i(k+N_p))^2)$$

$$= C_1(T_\beta) + C_2(T_\beta)d_\beta \tag{4.30}$$

in which

$$C_1(T_\beta) = \ln\left(\frac{\pi^2}{1-\rho^2}\right) = \ln\left(\frac{\pi^2}{1-\left(\frac{\sigma_w^2(T_\beta)}{\sigma_w^2(T_\beta)+\sigma_n^2}\right)^2}\right) \tag{4.31}$$

$$C_2(T_\beta) = \frac{\rho}{(\sigma_w^2(T_\beta)+\sigma_n^2)(1-\rho^2)}$$

$$= \frac{\sigma_w^2(T_\beta)}{\sigma_n^4 + 2\sigma_w^2(T_\beta)\sigma_n^2(T_\beta)} \tag{4.32}$$

$$d_\beta \propto E\left\{\tilde{y}(k) * \tilde{y}(k + N_p)\right\} \tag{4.33}$$

Although $C_1(T_\beta), C_2(T_\beta)$ are variables, the fluctuation region is very limited. Then they are processed as constants to simplify the equation. Finally, the ML estimation becomes

$$\Lambda(\tau, \tilde{y}_m) = E\left\{\tilde{y}(k) * \tilde{y}(k + N_p)\right\} \tag{4.34}$$

For a frame of information data

$$\hat{\tau} = \arg\max_{\tilde{y}_m}\left\{\Lambda(\tau, \tilde{y}_i)\right\} \tag{4.35}$$

Timing offset is estimated through (4.35) when the receiver detects the largest output, $\tilde{y}_m$, within a predefined observation window. This $\tilde{y}_m$ corresponds to a timing phase for the optimal sampling echo.

b) UWB Channel Model

Under UWB dense multiple channel fading, the received signals after pulse expansion are given by (4.6). ISI is very serious if the parameter τ_l is longer than the symbol period T_s. The statistic character of τ_l for the IEEE UWB channel models is mentioned in Table 2.2. UWB CM3 and CM4 channel models suffer more serious ISI than CM1 and CM2 for the same symbol period. ML estimator is applied to detect the strongest path for optimal sampling.

Combining (4.8), (4.9) and (4.10), a digitalized symbol is expressed as

$$y(j) = \sqrt{E_p}\sum_{i=-\infty}^{\infty}\underbrace{\sum_{l=0}^{L-1} d_i \alpha_l R_p(\theta(j) - iT_s - \tau_l)}_{\text{ISI item}} + n(\theta(j)) * p(\theta(j)) \tag{4.36a}$$

$$= \sqrt{E_p}\left(\sum_{i=-\infty}^{\infty}\sum_{l=0}^{L-1} d_i \alpha_l R_p(jT_s - iT_s - \tau_l) + n(\theta(j))\right) \quad (4.36b)$$

$$= \sqrt{E_p}\left(\sum_{i=-\infty}^{\infty}\sum_{l=0}^{L-1} d_i a_l R(j-i) + n(j)\right) \quad (4.36c)$$

where $R(\cdot)$ denotes $R_p(\cdot)$ in (4.36b). The ISI item is marked in (4.36a). Since the template of the pilot codes is kept in pilot MF, the output after pilot MF is denoted as $\vec{y} = \vec{r} \times \vec{g}$, where $\vec{y}$ is a vector output after pilot MF and $\vec{g}$ is a pilot MF coefficient vector. Comparing (4.36c) with (4.26) in AWGN channel, the pilot code MF output of a UWB channel model is much complex due to the ISI. The receiver can cancel part of the noise from multipath through cross-correlation function of the pilot codes when $R(\cdot)$ arrives a maximum value among one frame. From (4.36c), it is easy to understand that the pulse cross-correlation function $R(\cdot)$ is multiplied by information bits d_i, which is similar to the modulation rule. The correlation of RAMF extracts the strongest section which matches the expected pilot code and treats the weak multipaths as white noise. ML estimation calculation is the same as previous discussion in the AWGN channel analysis, using the maximum value of $\tilde{y}_m$ to estimate the optimal sampling phase.

For UWB, a search might be properly terminated with multiple hypotheses of the estimated timing phase for an optimal sampling. At a result, a hypothesis requires to be conformed as true acquisition timing. Then a proper verification must be added to terminate searches. Post detection integration (PDI) is desired to complete such task.

4.3 Post Detection Integration Technology

PDI is proposed to assist RAMF acquisition to reduce the effect of the noise-signal crossing terms and dense multipath interference introduced by the UWB channels. These distortion factors can cause a false alarm in the RAMF timing estimation. Many PDI schemes have been explored in literatures [38-40], amongst which the non coherent PDI (NCPDI) and the differential PDI (DPDI) are commonly used.

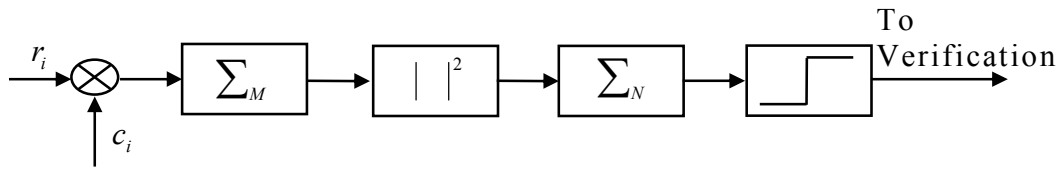

a) Non-coherent PDI

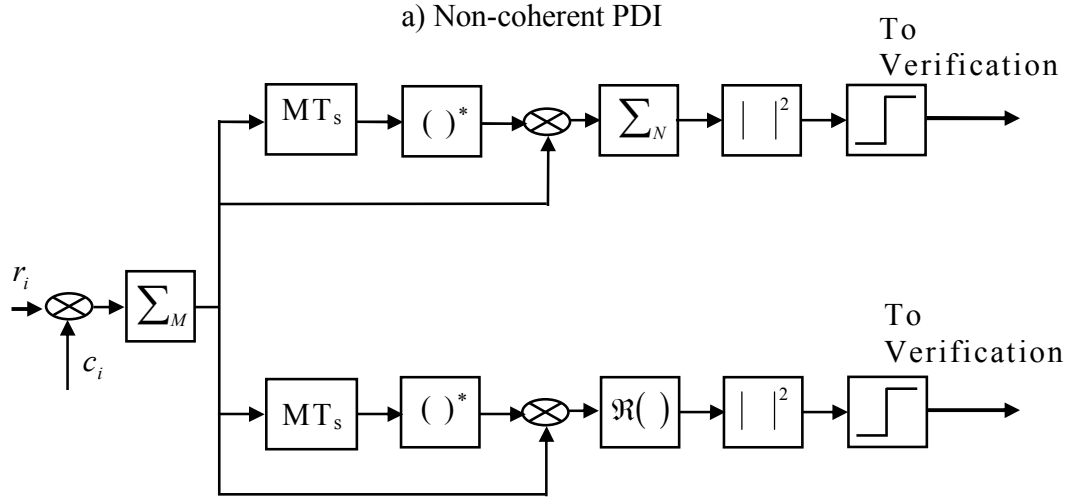

(b) DPDI of absolute value channel and real value channel

c_i : known pilot codes. $(\cdot)^*$: convolution. $|\ |^2$: absolute value. $\sqcup\!\sqcap$: threshold.

Figure 4.6 Protocols of NCPDI and DPDI

Cartier [37] and Viterbi [38] considered NCPDI as shown in Figure 4.6(a), which is strictly making use of the energy detector to the case of frequency uncertainty. NCPDI is widely used in practical applications, however, the technique can be outperformed by the DPDI techniques (Figure 4.6 (b)) in many cases [37], [39]. DPDI sums the complex conjugate products of adjacent coherent correlation outputs and takes either the absolute value (DPDI-Abs) or the real part (DPDI-Real) for energy detection. NCPDI and DPDI are robust practical approaches to generalize and average likelihood ratio testing solution. They are fundamental elements for acquisition. The parameters of M and N in Figure 4.6 are chosen depending on code formulation or system performance requirements, i.e., there is no strict definition for them. Output of a PDI is compared with preset threshold to fulfill acquisition decision.

To simplify the DPDI structure, a modified PDI is presented for this thesis as shown in Figure 4.7. This PDI makes use of the information kept by the pilot codes. M is omitted and N is defined as the length of one frame. $\vec{\Gamma}$ is generated locally. There are two parts in $\vec{\Gamma}$. One is a copy of known pilot codes and another is padded with zeroes. The length of $\vec{\Gamma}$ is the same as the packed incoming data.

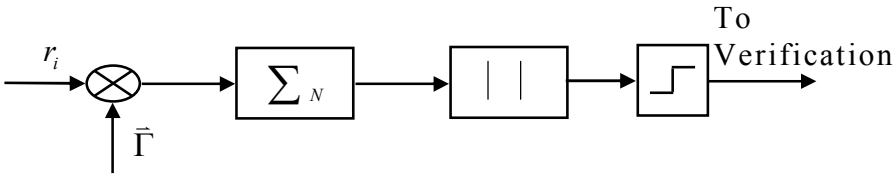

Figure 4.7 Modified PDI structure

PDI provides a simple approach to setup a threshold for RAMF. The receiver is able to use an error possibility of the pilot codes to estimate the

threshold. Format of one frame is defined first. $\vec{X}$ is defined as the vector of one frame incoming symbols before entering into the RAMF.

$$\vec{X} = [C_{p0} \quad \cdots C_{pi} \cdots C_{pl} \, C_{d0} \cdots C_{dj} \cdots C_{dk}] \quad i \in [0, l-1]; j \in [0, k-1] \tag{4.37}$$

where $\vec{X}$ stands for one frame data, C_{pi} denotes the pilot code, and C_{dj} is useful information symbols, $l + k = N$. After coarse estimation from RAMF, the estimated received codes $\vec{Y}$ are passed into PDI.

$$\vec{Y} = [\hat{y}_{p0} \cdots \hat{y}_{pi} \cdots \hat{y}_{pl} \cdots \hat{y}_{d0} \cdots \hat{y}_{dj} \cdots \hat{y}_{dk}] \quad i \in [0, l]; j \in [0, k] \tag{4.38}$$

where $\hat{y}_{pi}$ represents estimated pilot codes and $\hat{y}_{dj}$ denotes useful information. The system generates a template code $\vec{\Gamma}$ to correlate with the vector $\vec{Y}$. K bits of 0s are padded into the frame to mimic the unknown useful data.

$$\vec{\Gamma} = [C_{p0} \quad C_{p1} \cdots C_{pi} \cdots C_{pl} \quad 0 \cdots 0] \tag{4.39}$$

After integrating $\sum_N$ and absolute value calculation, it is much easier to compare the estimated pilot codes with pre-selected threshold.

During this research, it was found that the traditional PDI can not provide a reliable acquisition performance. An adaptive PDI (APDI) was developed to achieve a higher performance. The significant modification of APDI is that the estimated received code $\vec{Y}$ does not come from RAMF but from the tracking loop output. Figure 4.8 illustrates the structure of APDI.

The obvious advantage is APDI can update the estimated $\vec{Y}$ from one symbol period to another to reduce the risk of losing the candidate sync-cell. Because of short pulses, low duty cycle signaling and dense multipath interference,

a timing drift in the order of a chip width might happen in a short time. There is a graphic explanation showing such scenario in Figure 4.9.

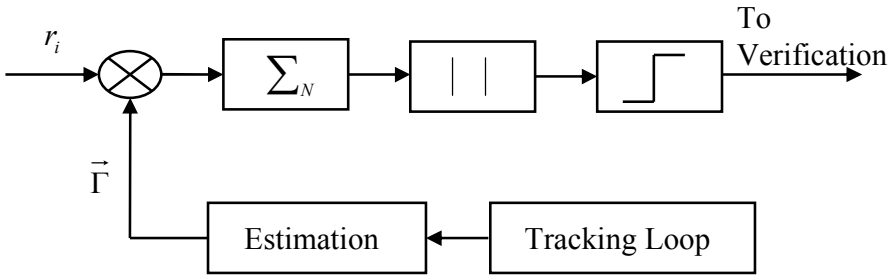

Figure 4.8 The structure of APDI

Figure 4.9 presents a waveform after a UWB CM3 channel, where the AWGN noise is 15dB. The ideal sampling echo is assumed and plotted using the dash lines in upper graph of Figure 4.9(a),(b). Figure 4.9(a) also shows the extraordinary energy variation on the sampling phase. A zoomed-in graph at this point of the waveform is provided in Figure 4.8(b). The energy reading of this sampling phase is near to zero, which may cause an acquisition failure.

The reason to sample the weaker energy output in the assumed optimum sampling phase is from the dense multipath interface and deep ISI. These two factors push the output pulse joint correlated with each other during one symbol period. It is well known that the correlation output becomes small when the inputs are in opposite phase. UWB dense channel models may process the input of a Gaussian monocycle pulse into its opposite phase counterpart. Then this opposite phase is correlated with the non-opposite pulse after the matched filter. Finally, the scenario of the output after the matched filter happens here.

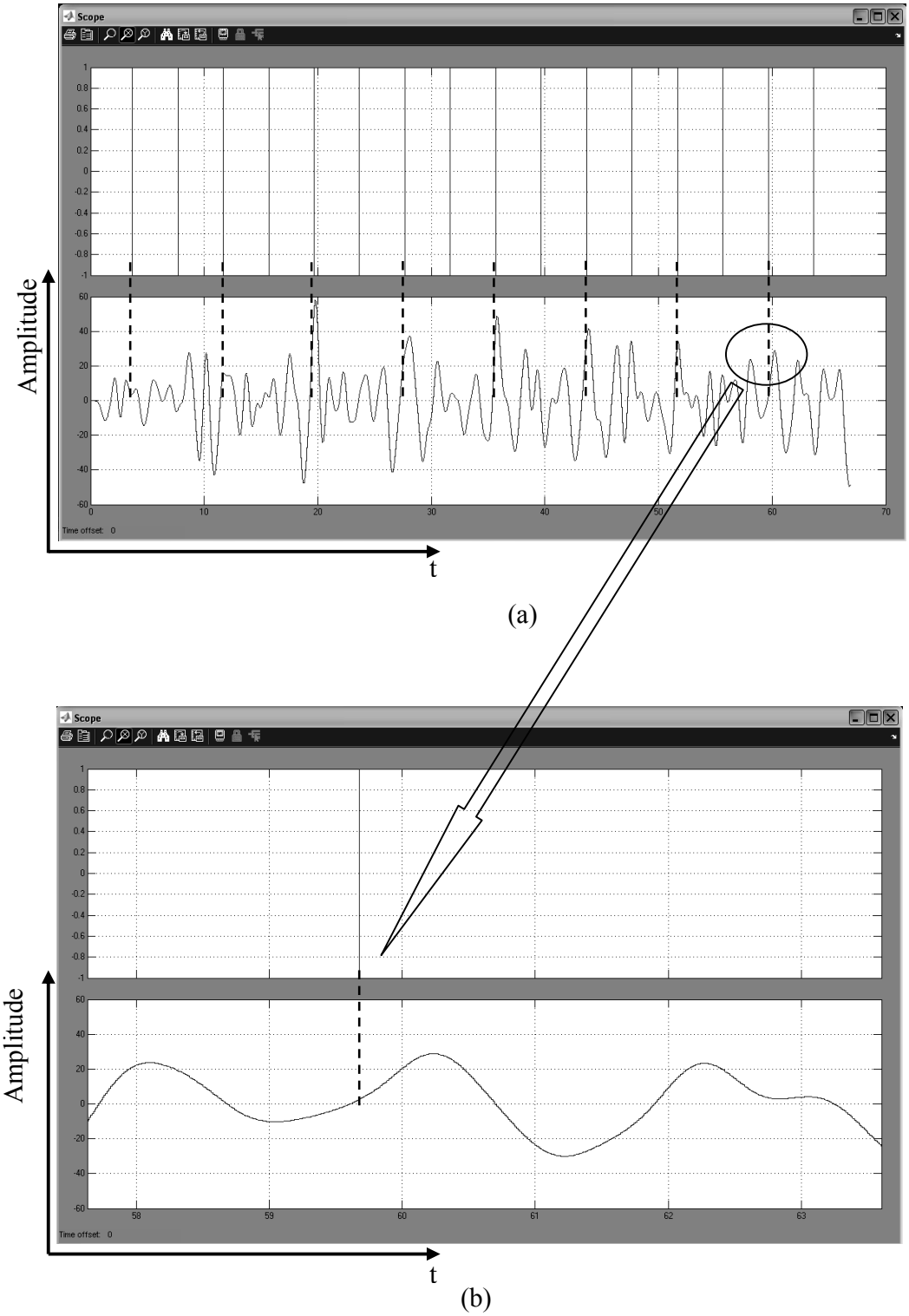

Figure 4.9 Energy variation after a UWB CM3 channel

An ultra sharp pulse shape means a very narrow chip width, that is, a very tiny margin for sampling points. There is an example of the waveform after a UWB channel model in Figure 2.4 (b) on page 17, where the second highest energy peak is over 50 percent of the highest energy peak. To avoid such dense multipath inference, the sampling region can not be at 50 percent of the pulse width, which is about 0.5ns for the pulse width of 1ns. The sampling margin is much smaller than 0.5ns if the sharp curve of the Gaussian monocycle waveform is concerned.

There is a simple method to estimate the width of a sampling margin for Gaussian monocycle pulse after IEEE UWB channel models, for example, CM3. The highest normalized energy level in Figure 2.4(b) is 0.8 and the second highest energy level is around 0.7 if the AWGN noise is omitted. Then the sampling margin order is about 0.01-0.1ns. When the signals pass through an AWGN channel, the peak of the pulses is varied slightly from time to time. Figure 4.9 is an example of such case. The sampling margin of 0.01-0.1ns is not wide enough to resist such variation. APDI makes use of the technology of tracking loop to force the sampling phase tracing the energy level as high as possible. Therefore APDI reduces the risk of energy variation after the AWGN channel.

4.4 Bit Iteration Search

As discussed in 4.3.2, the chip width for a UWB pulse is extremely narrow. The search strategies presented in section 3.2.2.3 must assume the receiver knowing the chip width and partition the search space into a number of known chips in a pre-designed searching procedure. The scenarios are quite different among four types of

UWB channel models and the minimum multipath resolution is not fixed for each type. Thus there is a task that must be done before the receiver tests which type of UWB channel model is used. If the assumed chip width is too wide, acquisition is possible to be missed; on the other hand, the acquisition time may be longer. Bit iteration search (BIS) is proposed to solve such task. BIS does not need to assume the minimum multipath resolution to generate a move step. Because delay generator changes the phase of the pilot codes depending on an algorithm which is able to partition the search space as small as possible technically. At the same time, BIS is not a serial search but a reversal search. The procedure is illustrated in Figure 4.10.

The search position number is double at every scan from original position to the end position of this path, but the same search location will not be repeated. The receiver keeps moving with a half size jump at each step until acquisition is achieved. Figure 4.10 presents a graphical explanation for BIS. There are two definitions for BIS procedure. One is half-size partition, which means the search space is doubled from this moment. Another is same-size move, which means a search move is in the same distance from this position to the next. The detail algorithm of BIS is as follow

- A delay generator randomly chooses a search position as initial timing phase, and marks it.
- First half-size partition begins. The delay generator moves sampling echo to the same-size move 0 and then to the same-size move 1.
- Second half-size partition begins. The delay generator moves sampling echo to same-size move 0, same-size move 1, and so on.

- Third half-size partition begins and the delay generator repeats the same-size moves until acquisition is achieved.

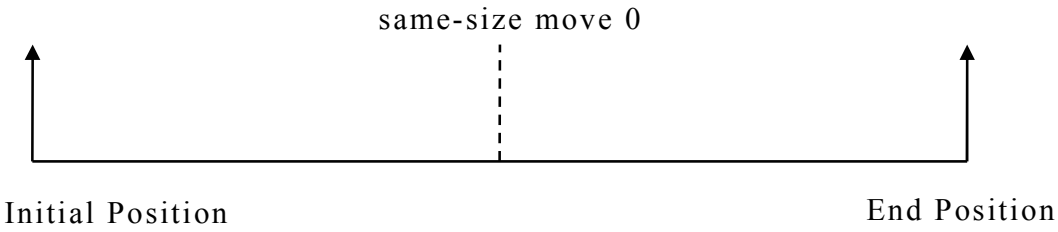

(a) First half-size partition

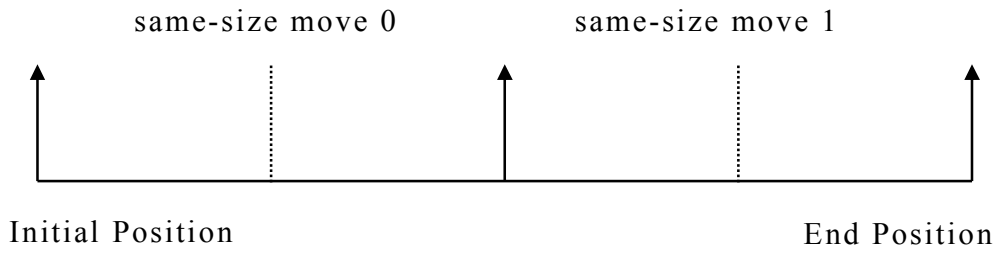

(b) Second half-size partition

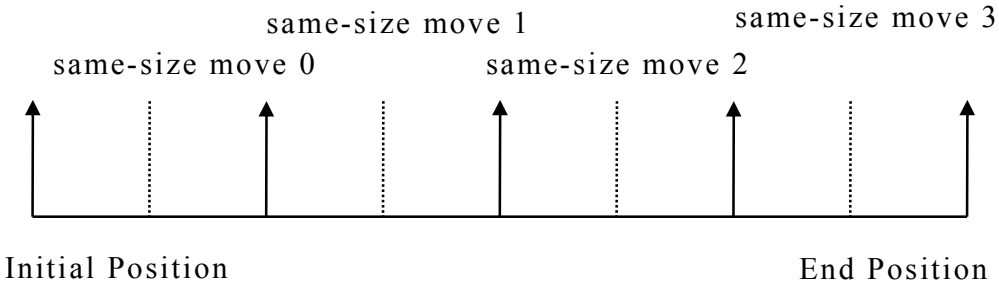

(c) Third half-size partition

...

SP : search position.

↑ : Spots searched before.

⋮ : Spots to be searched after half-size partition.

Figure 4.10 BIS algorithm flow chart

The mathematic expression of BIS is presented here. N searchable timing phases are assumed for the following equations and N is in a power of 2, i.e., $N = 2^n$, in which n is a positive integer. N is unknown but determined for each channel. If the symbol period of packed data is set as T_s, then

$$T_s = N \times \Delta \tag{4.40}$$

where Δ is the determined chip width for that channel.

When a BIS starts, it randomly picks an initial time and moves to a different timing space at each move as shown in Figure 4.10. For any stage m, there is an appropriate polynomial for BIS.

$$m = A_{n-1}X^{n-1} + A_{n-2}X^{n-2} + \cdots A_i X^i + \cdots + A_0 X^0 + 1 \quad A_i = 0,1 \quad i \in [0,n) \tag{4.41}$$

There is a variable corresponding with each move, ω. ω decides how far from the current search spot to the next based on the idea of Figure 4.10. ω is described as

$$\omega = \begin{cases} \dfrac{N}{2^{k+1}} \times \Delta & half-size \quad partition \\ \dfrac{N}{2^{i+1}} \times \Delta + \dfrac{N}{2^i} \times \Delta \times l & same-size \quad move \end{cases} \tag{4.42}$$

in which k expresses the half-size partition stage and i denotes the index of same-size move while one partition. Except at the zero timing phase, the BIS calculates the highest order of coefficient, A_k in (4.42) to get ω listed as Table 4.1.

4.5 Summary

This chapter proposes several new strategies serving for fast acquisition in UWB applications: RAMF, PDI, APDI and BIS. This thesis proposes three

architectures using these strategies for UWB acquisition. Figure 4.11 shows three architectures: pilot MF with APDI acquisition, RAMF with PDI acquisition, and RAMF with APDI acquisition. BIS is used after the verification to control the sampling phase for each acquisition.

Table 4.1 NCO iteration bit search control flow

index	Binary expression	Timing Phase	Polynomials
0	1	0	2^0-1
1	2^0+1	$\frac{N}{2^1}\times\Delta$	2^0
2	2^1+1	$\frac{N}{2^2}\times\Delta$	2^1
3	2^1+2^0+1	$\frac{N}{2^2}\times\Delta+\frac{N}{2^1}\times\Delta\times1$	2^1+1
4	2^2+1	$\frac{N}{2^3}\times\Delta$	2^2
5	2^2+2^0+1	$\frac{N}{2^3}\times\Delta+\frac{N}{2^2}\times\Delta\times1$	2^2+2^0+1
6	2^2+2^1+1	$\frac{N}{2^3}\times\Delta+\frac{N}{2^2}\times\Delta\times2$	2^2+2^1+1
7	$2^2+2^1+2^0+1$	$\frac{N}{2^3}\times\Delta+\frac{N}{2^2}\times\Delta\times3$	$2^2+2^1+2^0+1$
8	2^3+1	$\frac{N}{2^4}$	2^3+1
	…	…	…
N-1	$2^{n-1}+2^{n-2}+\cdots+2^0+1$	$\frac{N}{2^n}\times\Delta+\frac{N}{2^{n-1}}\times\Delta\times n$	$2^{n-1}+2^{n-2}+\cdots+2^0+1$

Compared with traditional acquisition approaches and previous UWB search methods, the new strategies for fast acquisition in UWB applications focus on solving the challenge. To speed up acquisition, the proposed acquisition

structures use hybrid search method. Performances of these proposed acquisitions are to be evaluated in the next chapter.

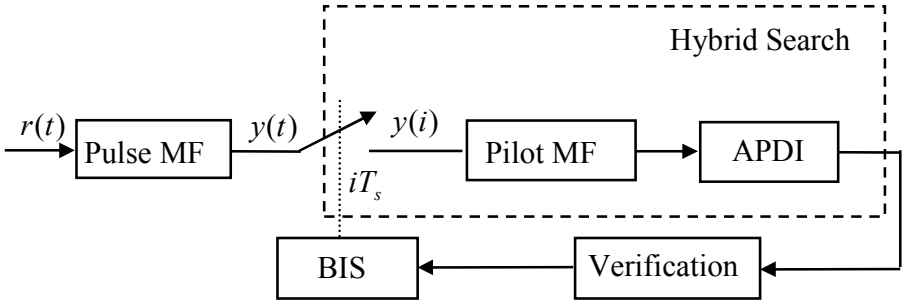

(a) Pilot MF with APDI acquisition

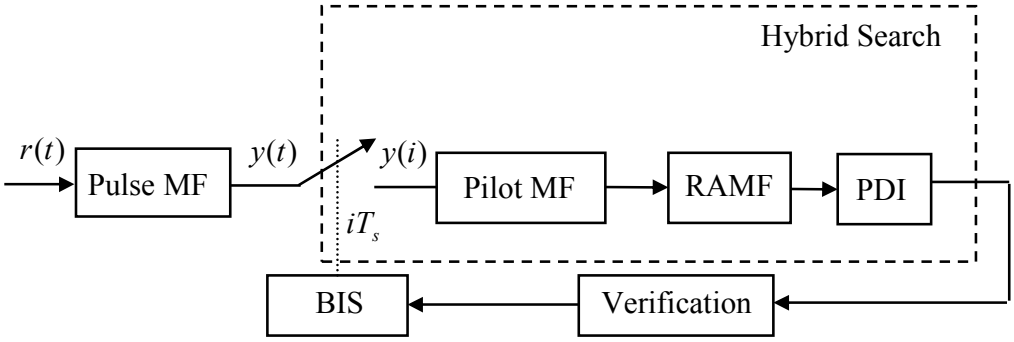

(b) RAMF with PDI acquisition

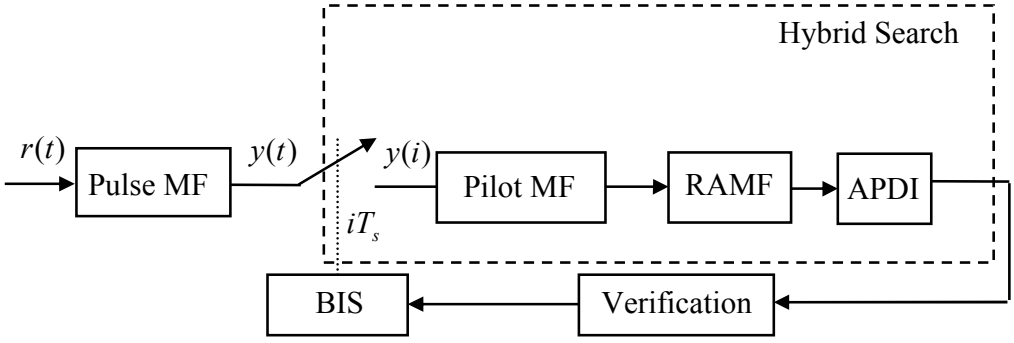

(c) RAMF with APDI acquisition

Figure 4.11 Three proposed acquisitions for UWB communications

CHAPTER 5 EVALUATION OF PROPOSED ACQUISITIONS

It is necessary to use Matlab simulations to verify and evaluate performance and effectiveness of the proposed acquisition strategies in terms of MAT and bit error rate. A UWB transceiver system structure is briefly described in section 1. Acquisition simulation is discussed in section 2. Section 3 provides analysis of the acquisition performance.

5.1 UWB System Simulation Setup

Simulation set-up includes the transmitter and receiver, and provides observation windows to monitor the acquisition performance. This work is based on the existing knowledge of UWB system, related modulation technology and the acquisition algorithm.

5.1.1 System Simulation Overview

The UWB system simulation is implemented in Matlab and designed in a flexible manner: the Simulink approach. This method enables quick modification and better visual simulation result than using simulation commands. Figure 5.1 depicts the structure of the UWB system simulation. The system contains these

blocks: UWB signal generator, UWB IEEE channel, AWGN channel, pulse MF, pilot MF, acquisition, and demodulator.

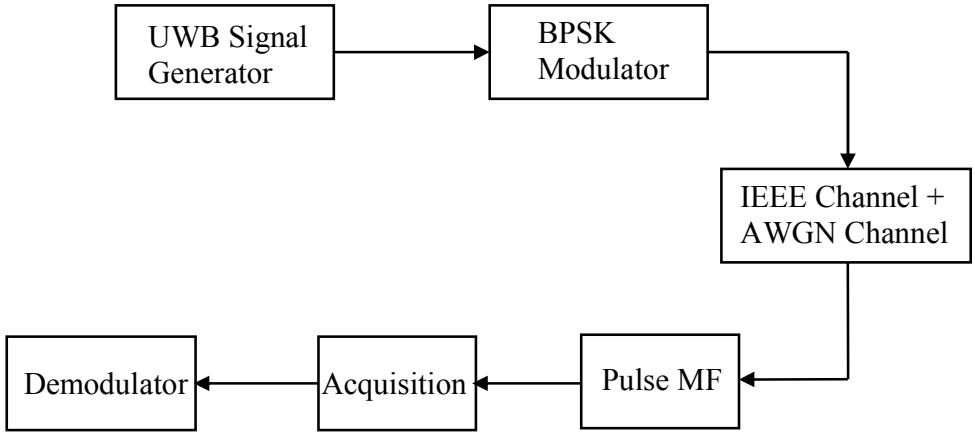

Figure 5.1 UWB system signal flow for simulations

5.1.2 UWB Signal Generator Module

The signal generator in Figure 5.2 is one of the major components in the UWB communication system.

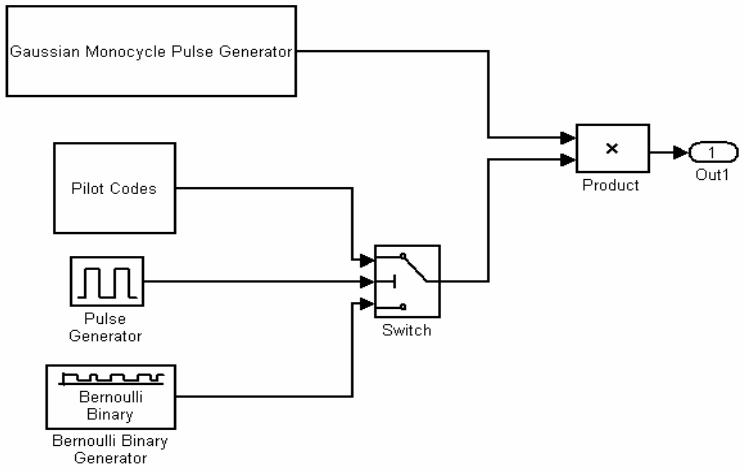

Figure 5.2 UWB signal generator

This generator loads the pilot codes as a header of the transmitted data train described in Figure 4.2. A pulse generator block controls the frame package. The modulation is BPSK as presented in section 2.1.3. The modulator output is the product of a Gaussian monocycle pulse and a framed data.

5.1.3 UWB IEEE Channel Module

This module is built to stimulate the multipath channel environment of UWB communications in which one transmitted pulse transformed multiple delayed pulses. The IEEE UWB standard channel models assume more than 100 multipaths as described in Chapter 2. RMS of the signals after UWB channels is measured in Figure 5.3. This value is presented as the input signal power of the AWGN module in Figure 5.4.

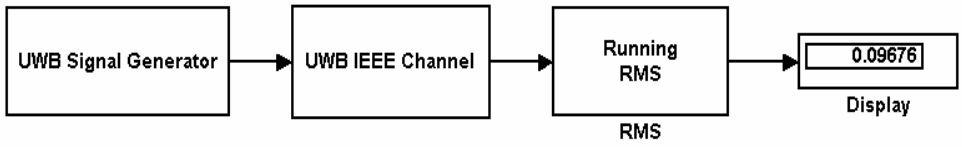

Figure 5.3 RMS of UWB signal after a UWB IEEE channel

5.1.4 AWGN Channel Module

In simulations, data are sent through the AWGN channel block where noise is added to the propagating UWB signal. AWGN channel module from Simulink is used as shown in Figure 5.4. The input signal energy is calculated for each system simulation because the energy level varies for different channels.

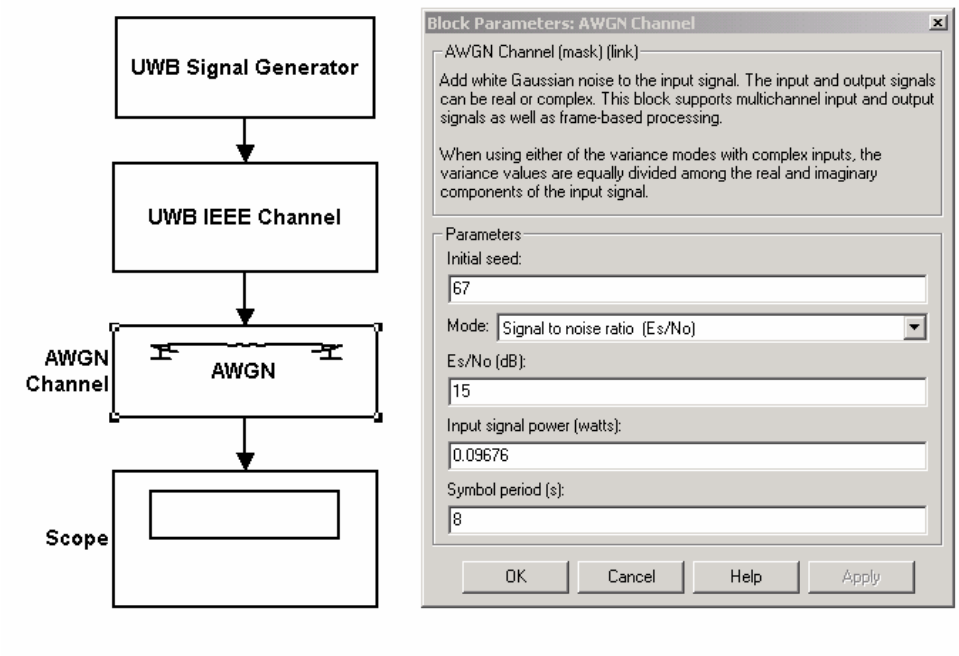

Figure 5.4 AWGN channel module parameter setting

5.1.5 Pulse MF Module

It is assumed that the transmitted pulse shape is known by the receiver. The pulse MF is a copy of the Gaussian monocycle pulse. A discrete filter module in Simulink library was selected. The coefficients of the pulse MF were calculated as follows

```
% This function generates mono Gaussian pulses
%  with a center frequency fc in 0.5 Giga hertz.
% Time resolution is 0.01 ns.
fc=0.5;
tc = gmonopuls('cutoff',fc);
t = -2.0*tc : 1e-2: 2.0*tc;
% Pulse MF coefficients are created  here.
pulse = gmonopuls(t,fc);
```

mono_pulse=pulse;

end;

The module of pulse MF was given in Figure 5.5

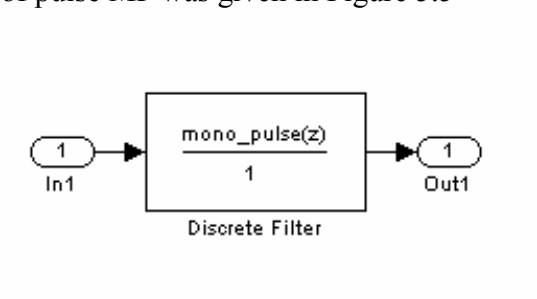

Figure 5.5 Pulse MF module

5.1.6 Acquisition Module

The acquisition module uses the proposed strategies in Chapter 4: hybrid search, pilot MF, RAMF, ML algorithm, PDI/APDI, and BIS. This module also includes two elements not described in Chapter 4: VCO and verification. Corresponding to the three proposed acquisition scheme, there are three different types of acquisition modules: the pilot MF with APDI acquisition, the RAMF with PDI acquisition and the RAMF with APDI acquisition. The simulation flow chart is given in Figure 5.6. An acquisition process is in the dash rectangular block. The VCO controls sampling rate and the BIS control sampling phase. Pilot MF and RAMF blocks contain ML algorithm and hybrid search algorithm. The verification points out when to stop moving the sampling phase to the BIS.

5.1.7 Demodulator Module

Demodulator applies a sign function to check polarities of the sampled bipolar signals and aligns the incoming signal into +1s or -1s. BER calculation is performed in the demodulator module.

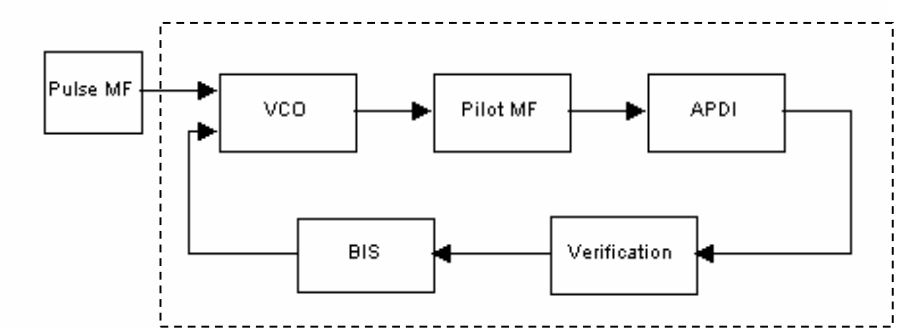

(a) Pilot MF with APDI acquisition

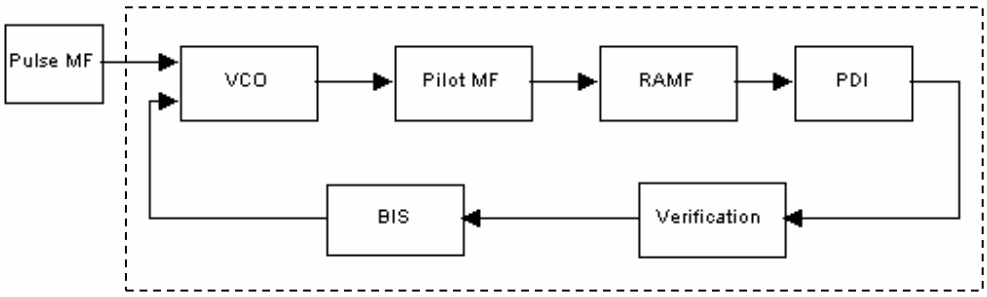

(b) RAMF with PDI acquisition

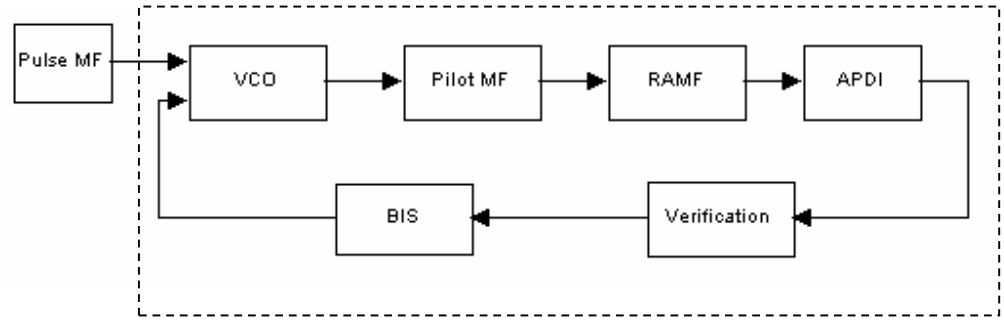

(c) RAMF with APDI acquisition

Figure 5.6 Three types of acquisition modules

5.2 Acquisition Simulation Modules

This section presents the detail simulations of the acquisition schemes in Figure 5.6.

5.2.1 VCO Module

The VCO module provides the sampling signals to transform continuous signals into discrete signals as shown in Figure 5.7. The oscillation function is generated by a cosine function. The initial phase of this cosine function is randomly selected in the contant1 block which is $\frac{2}{3}\pi$. The variable sampling phase is from the BIS module.

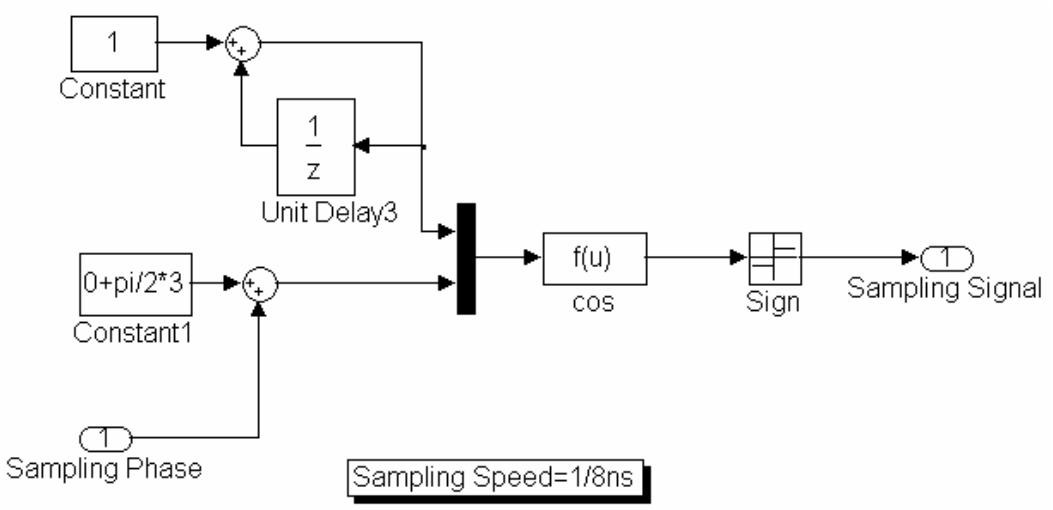

Figure 5.7 The VCO scheme in the simulation

5.2.2 BIS Module

A numerical control algorithm in BIS for sampling without the knowledge of channel parameters and searching bin is simulated here. The kernel of the BIS is the numerical control oscillator (NCO). The NCO calculates the sampling phase ω and moves each sampling phase. Figure 5.8 illustrates the NCO realization. The NCO is triggered by the verification module as presented in Figure 5.6 and it will stop when acquisition is achieved.

One example of the NCO simulation is scoped in Figure 5.9. The parameter, T_s in (4.38), is set at 32 (the unit is default as ns).

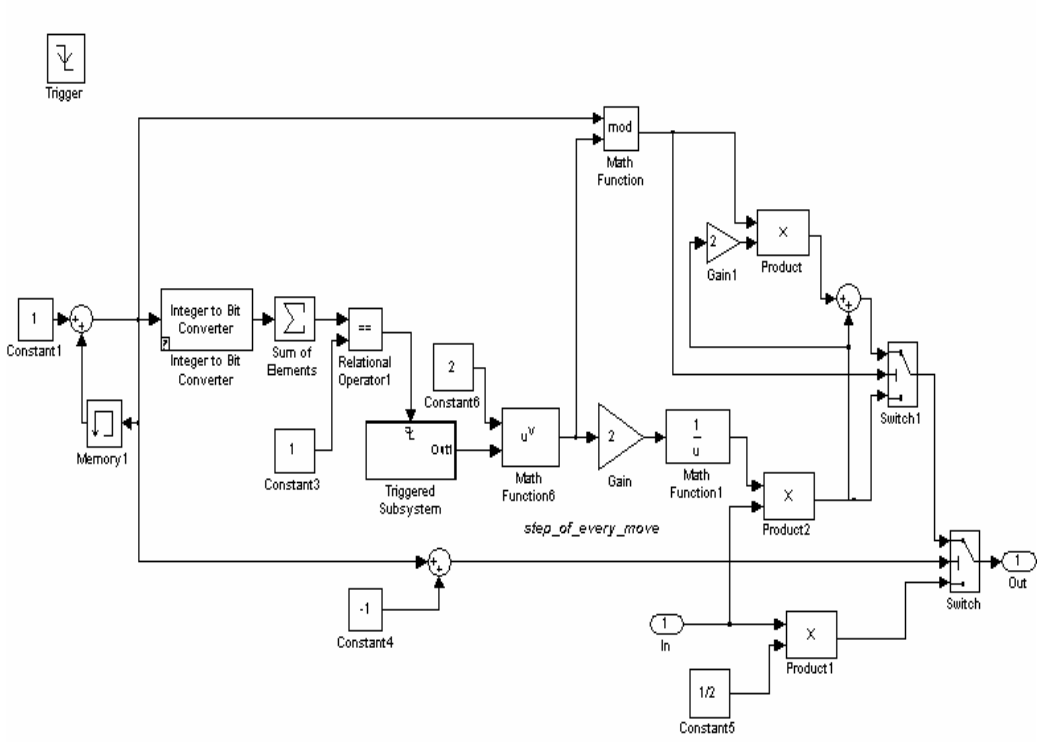

Figure 5.8 The NCO structure in the simulation

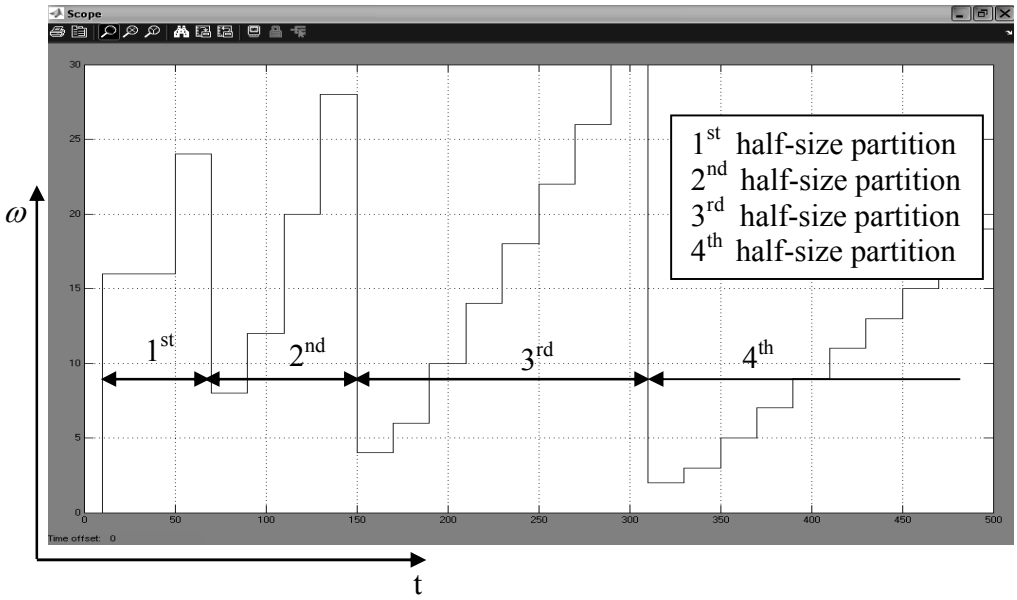

Figure 5.9 Simulation result of NCO

Figure 5.9 shows the information of ω (Y-axis) and the corresponding acquisition time (X-axis). After the first half-size partition ω is 16 and 24 if the initial position is not the sync-cell. After the second half-size partition, ω becomes 8, 12, 20 or 28, if the sync-cell is not detected. Then the third half-size partition starts, and the process repeats until acquisition achieved.

5.2.3 Pilot MF Module

The pilot MF module is a bank of matched filters. Figure 5.10 is set up for hybrid search. If the symbol period is set as $8\,ns$ and one serial search timing region is chosen as 2ns, four parallel paths are needed for a complete symbol time. The unit delay block corresponds to 2ns.

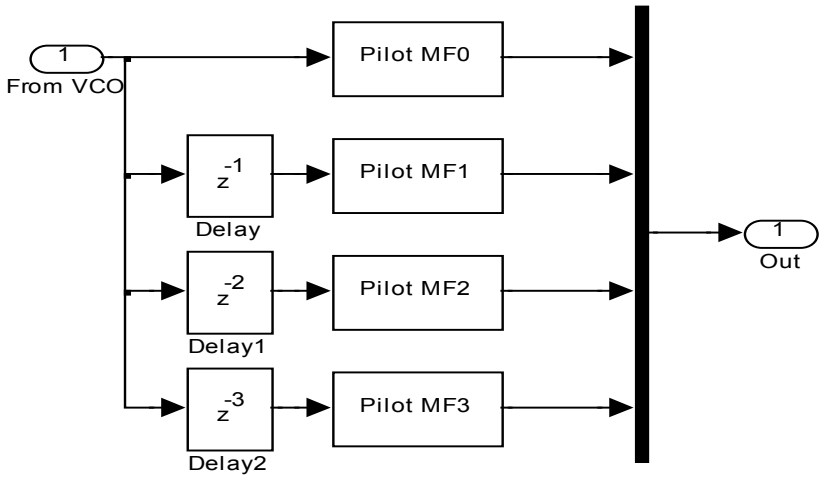

Figure 5.10 Simulink of the pilot MF module

5.2.4 RAMF Module

The RAMF module is also a 4-channel parallel search. The simulation structure is sketched in Figure 5.11. The unit delay block delays the incoming

symbols N_p-symbol time. The RAMF lets one section of the pilot codes convolute with another delayed section of the pilot codes.

A simulation waveform is the best way to easily understand the function of RAMF for the ML algorithm. One example of simulation results is scoped and provided in Figure 5.12. The simulation uses the following parameters

- Channel model: IEEE UWB CM3.
- AWGN noise level: E_s / N_o=15dB.
- Frame structure: two periodic pilot codes, $N_p = 16$, $N_f = 8N_p$ (N_p and N_f are defined in Figure 4.2).
- Symbol rate (sampling speed): $T_s = 8\,\text{ns}$.

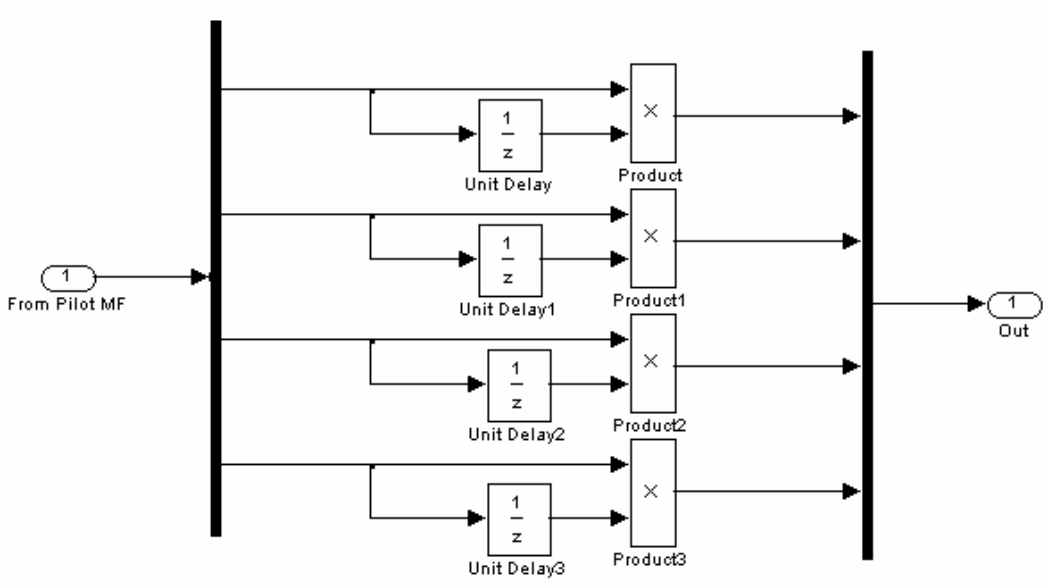

Figure 5.11 The RAMF module structure

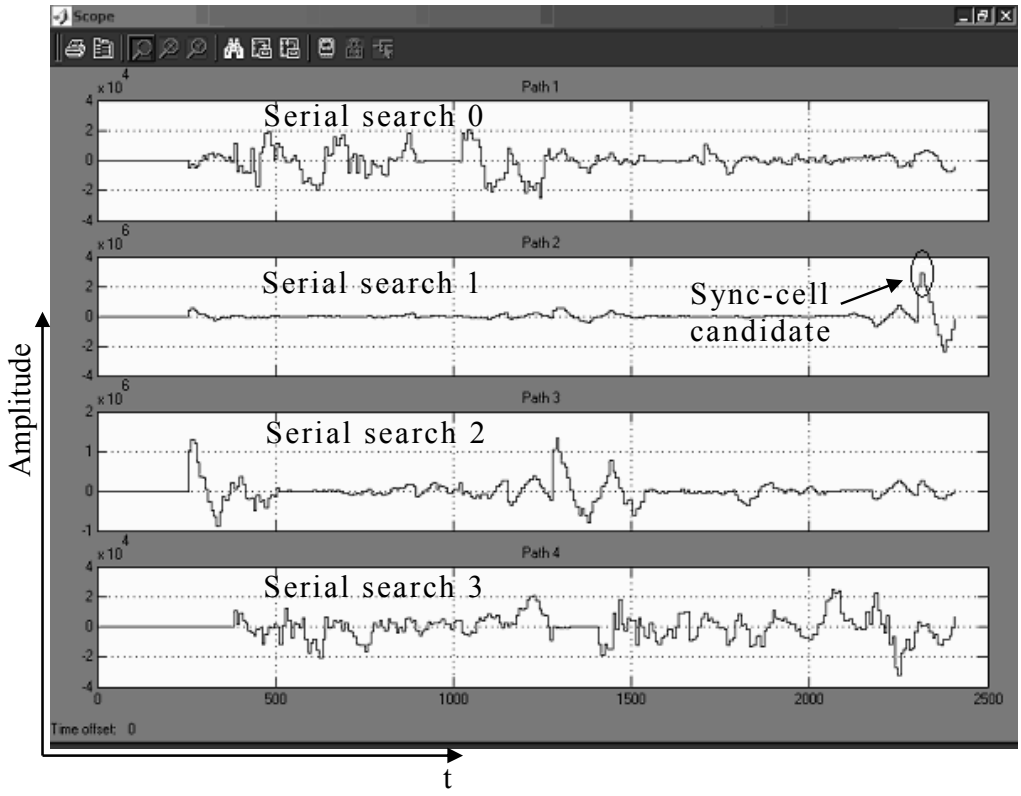

Figure 5.12 Waveform after RAMF during a hybrid search

As seen in Figure 5.12, if a sync-cell candidate exists in the path, the waveform after the ML algorithm I will provide the highest energy among these four search paths during one frame package. The serial search 1 in Figure 5.12 contains this candidate.

5.2.5 PDI Module

The strongest energy path among one frame package is passed into the PDI. The PDI uses decision-detected method comparing the detected pilot symbols with the stored pilot symbols. Thus the PDI is able to calculate an estimated error rate of the pilot codes. A PDI is a filter which assists in extracting the pilot code header

from estimated incoming signals. The output of PDI is one when the detected pilot codes is the same as the pilot template and less than one if there is noise during the detection. The Simulink blocks are given in Figure 5.13.

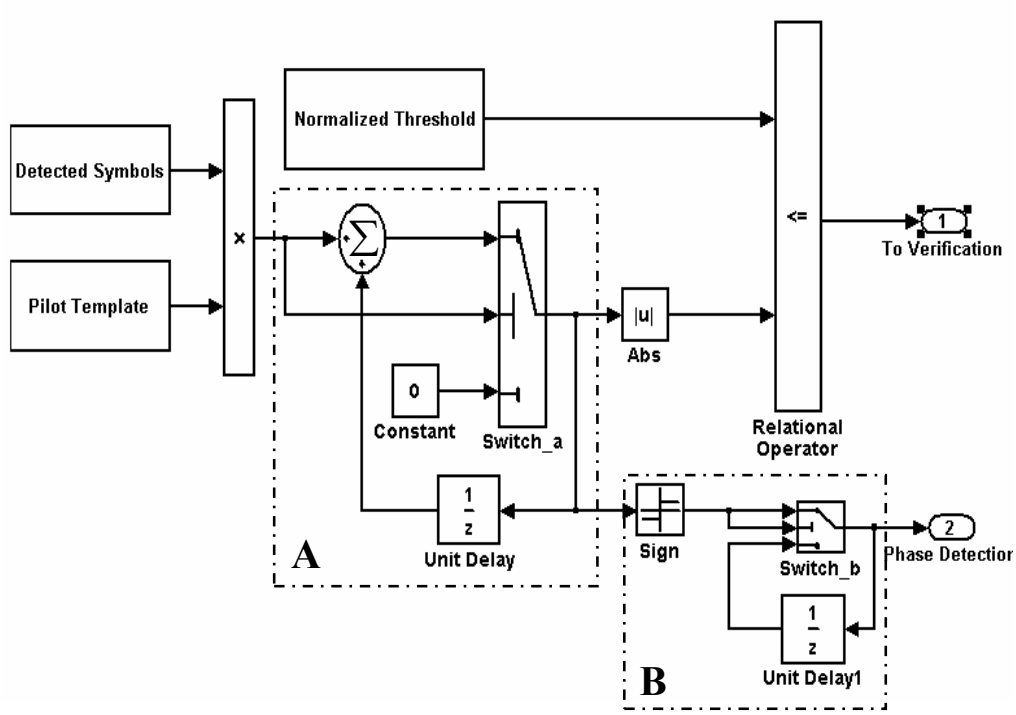

Figure 5.13 Simulink of the PDI scheme

Brief operation procedures of the PDI are described as follows

- The pilot template is multiplied with a frame of the detected symbols which are assumed to be synchronized. The detected symbols are not from the output of the tracking loop.
- The product after the multiplication is fed into block A which is an accumulator. This step attempts to measure the error rate of the assumed synchronized pilot within one frame package.

- There exists phase detection because of bipolar modulation. Block A checks the phase and sends it to B, which stores the sign of the phase and transfers this sign to a coherent demodulation.
- The result after the accumulator is taken as an absolute value in order to compare with a threshold. The result of this logic calculation is sent to the verification module.

A normalized threshold in Figure 5.13 is defined as the estimated bit right rate of the pilot header within one frame package. This value matches the output of the accumulator. This processing avoids the actual signal energy changing from time to time.

5.2.6 APDI Module

APDI is an advanced PDI version with only a minor difference between them. The detected symbol in Figure 5.13 is from the demodulator after the tracking loop for APDI. The tracking loop shown in Figure 5.14 includes an early-late gate block, a second order filter, a gain adjustment, and an oscillator.

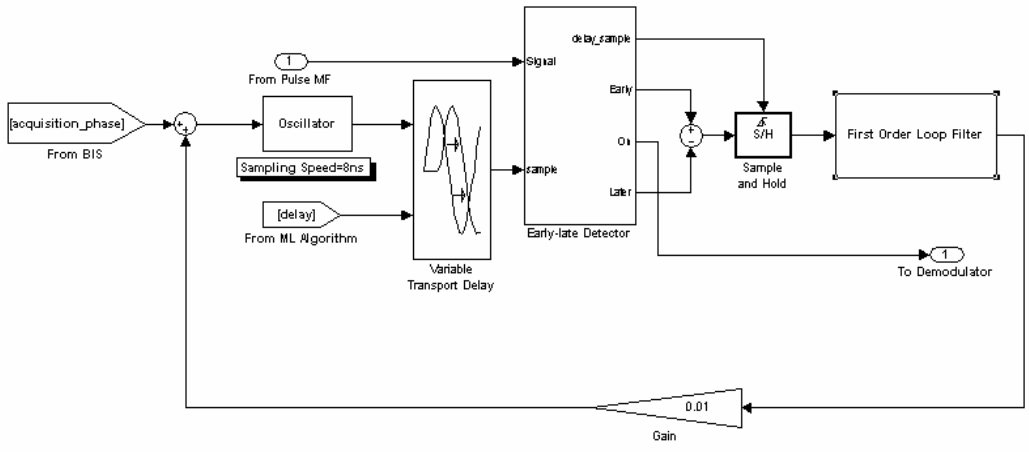

Figure 5.14 Simulink set-up of the tracking loop

5.2.7 Verification Module

The output of PDI/APDI is higher than the threshold does not mean a real sync-cell is detected because false alarm is possible to mislead the system to stop the acquisition. Verification is necessary to check the reality of this sync-cell [40]. This simulation uses a very simple s-function in Simulink to check a number of the pilot headers in the same sampling phase. This sync-cell is conformed as true if a specific percentage of these outputs after PDI/APDI are over the threshold. Otherwise, a new acquisition is asserted.

5.3 Acquisition Performance Analysis

Acquisition performance can be classified into several categories: a) mean acquisition time (MAT) is the most important factor to evaluate an acquisition algorithm. Fast acquisition means the communication between a transmitter and a receiver is established in a short time. b) False alarm occurs when a false detection in the noise-only portion of the signal is regarded as a sync-cell. c) The probability of detection measures capability of the proposed architectures acquisition. Acquisition performance can also be analyzed in terms of acquisition time and acquisition accuracy.

5.3.1 Performance of the Three Proposed Acquisition Methods

MAT provides a tool to measure an acquisition speed and BER is another means to evaluate acquisition accuracy. Performances of the three proposed

methods for UWB acquisition were evaluated. Coherent detection was used for demodulation. The following parameters were used for the simulation

- Cyclic pilot header $N_p = 16$, there were two cyclic pilots.
- One frame length: $N_f = 16 \times 8 = 124$.
- Symbol period $T_s = 8ns$, sampling rate 125MHz.
- Threshold of the PDI was normalized at 0.75 which was tested in section 5.3.2.
- Verification procedure: checking three consecutive frames after a candidate sync-cell was chosen by the PDI. The acquisition was ended if there were two frames passing the threshold PDI.

The hybrid search was used for all of three proposed methods. The MAT and BER were the average values after repeating 50 simulations for each case.

a) Pilot MF with APDI acquisition

The pilot MF timing acquisition is the simplest method to estimate timing offset. Simulation result in Figure 5.15 provides information on speed and accuracy for this approach. The MAT value indicates the sync-cell detection time which includes the verification time. BER shows the average accuracy of the sync-cell detection. BER is affected by the false alarm because the false alarm definitely causes higher error rate than the true sync-cell detection. The shortest MAT of CM1 at Es/No=15dB is about 1,399 symbols and the corresponding BER is about 0.01. It means that the true sync-cell detection time is 1,399 symbols after verification. This detection time is equal to $1{,}399 \times 8\text{ns} = 11.192\mu\text{s}$. For CM4 channel model, the MAT is 3,284 symbols at Es/No=15dB.

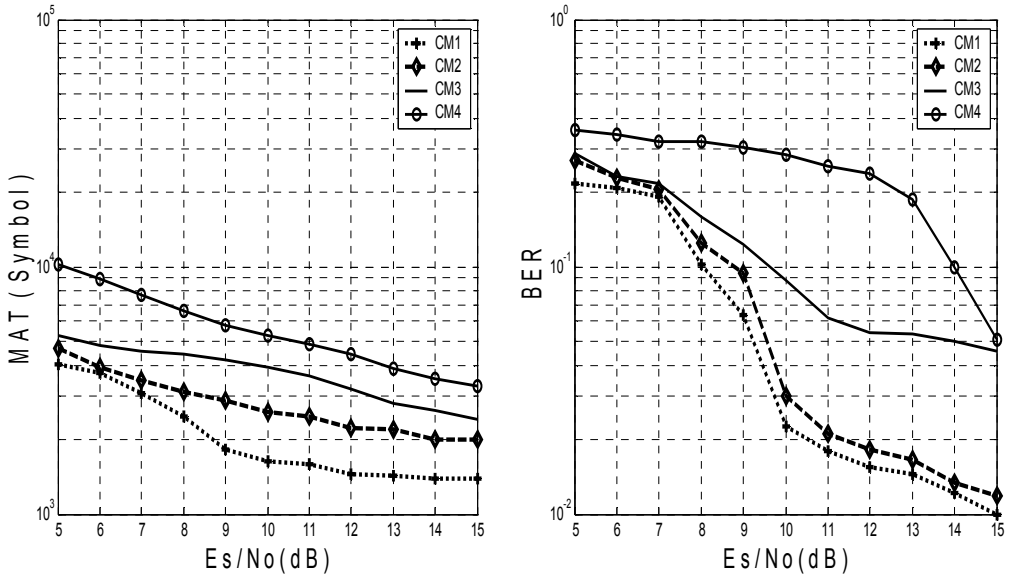

Figure 5.15 Performance of pilot MF with APDI acquisition

At Es/No equals to 13dB for CM1, MAT is limited in the range of 1,400-1,422 symbols. For CM2, MAT is limited in the range of 2,000-2,190 symbols. For CM3, the MAT limitation trends to 2,400 symbols when Es/No is equal to 15dB. For CM4, MAT is the worst performance among these four channel models.

b) RAMF acquisition with PDI

The performance for this proposed strategy is the worst compared with other two methods as the results are shown in Figure 5.16. BER of the four UWB channel modes in overall is over 0.01 for AWGN level between 5dB and 15dB. The reason of such high BER values is that the false alarm of acquisition happens more frequently. False alarm probability P_f is calculated and provided in Figure 5.19. Because the P_f is below the accept level, there is no meaning to explain the MAT performance further in this case.

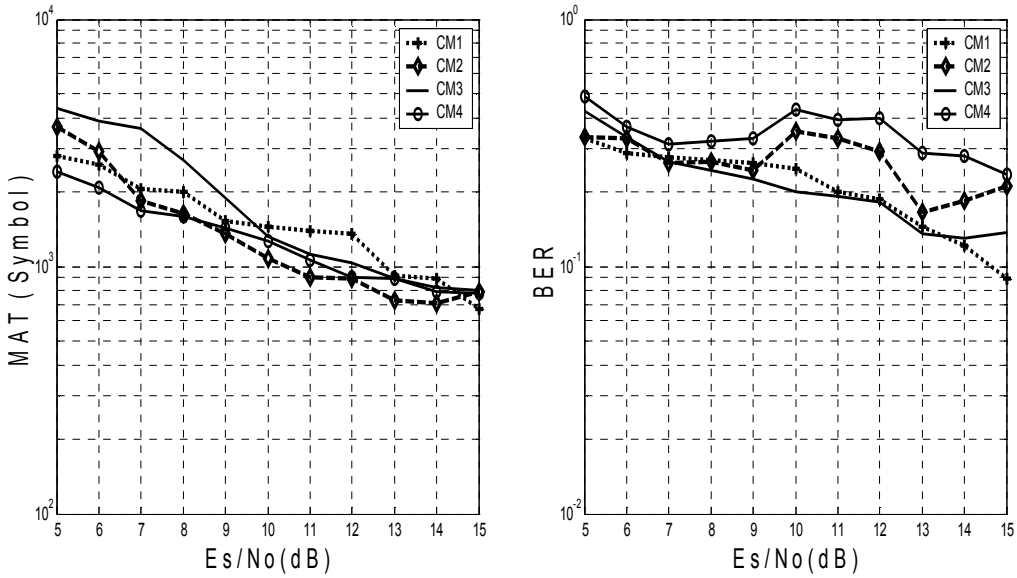

Figure 5.16 Performance of RAMF with PDI acquisition

c) RAMF acquisition with APDI

The simulation result of this strategy is the best among the three approaches for all UWB channel models and shown in Figure 5.17.

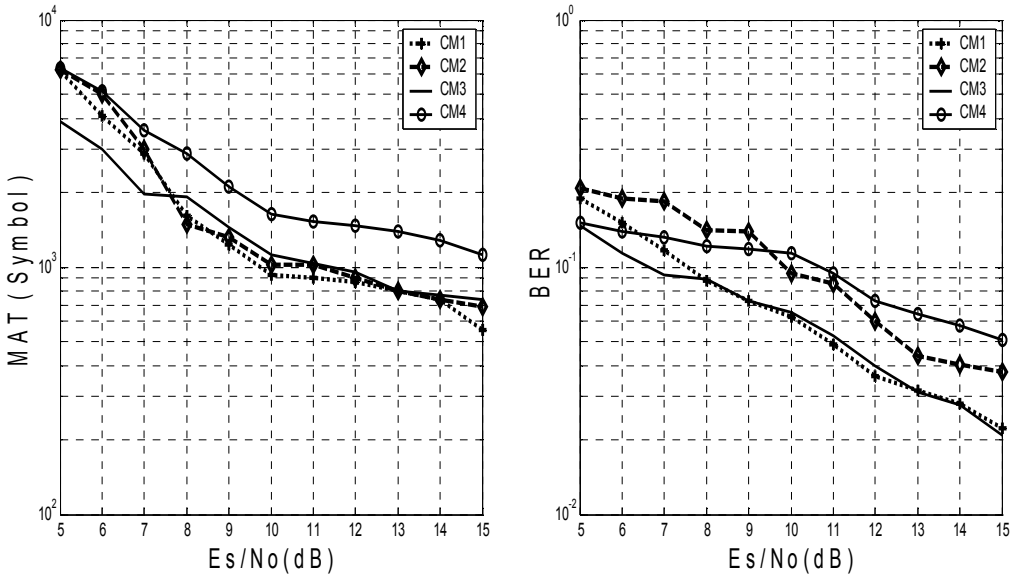

Figure 5.17 Performance of RAMF with APDI acquisition

There are three advantages of this method comparing with the other two strategies

- Fastest acquisition: at Es/No=15dB, MAT for CM1 is approximate 656 symbols and MAT is 1,118 symbols for CM4. Acquisition time is reduced to half compare with the other two methods.
- Accuracy of this proposed approach is the highest for CM3 and CM4 models.
- For CM1 and CM2: the bound of MAT is much higher than 15 dB in terms of SNR. For CM3 and CM4: the bound of MAT limitation is around 15dB. The concept of bound for MAT means the acquisition time is not improved further when the SNR is over a certain value. This property of MAT points out the possibility of improvement of an acquisition approach. RAMF with APDI has more room to improve the performance.

The MAT performance for CM1 and CM2 is worse than CM3 and CM4. The reason for this may come from the threshold setting, which means different channel model needs different thresholds.

Figure 5.20 shows the performance comparison between the three proposed acquisition methods. CM3 results are used in this comparison since this channel model presents a much "close to" practical environment. The graph clearly illustrates the strategy of using RAMF with APDI provides the best performance in both MAT and BER. However, the acquisition accuracy of this method is not as high as the one using MF with PDI.

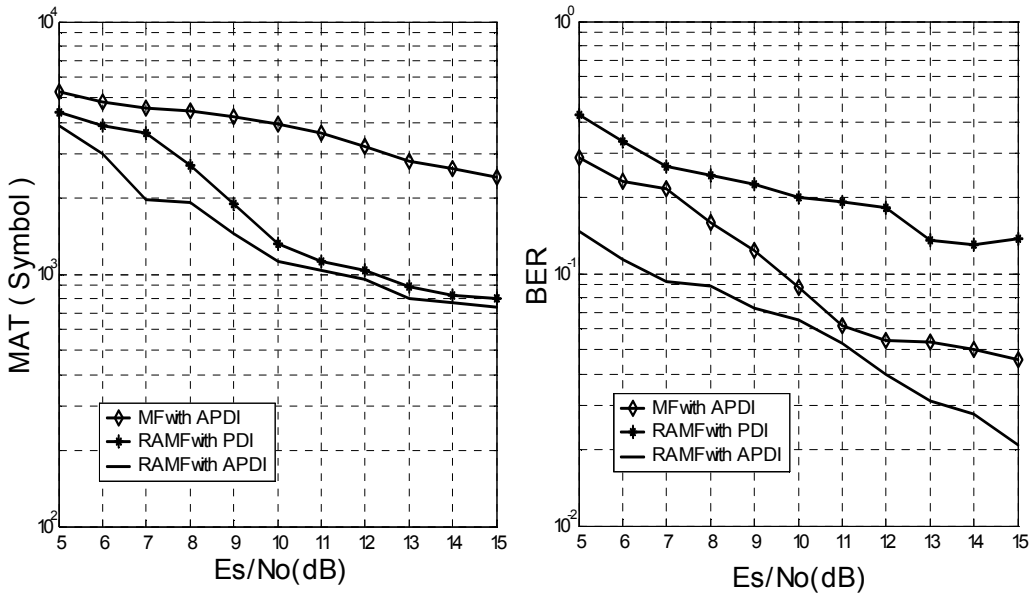

Figure 5.18 Performance comparison among three proposed acquisition methods

5.3.2 Threshold Setting Selection

The criteria to select an optimal threshold is based on the fixed false alarm rate, minimum MAT, or minimum BER. In another word, setting threshold affects acquisition time.

There is no direct relationship between optimum threshold and MAT. Author in [41] concluded that it is very difficult to build a good threshold-based UWB acquisition system. A numerical approach is capable to test an approximate optimum threshold for the proposed acquisition scheme under the assumption that the false alarm probability is fixed. Matlab simulation results are provided in Figure 5.19 based on the structure of APDI in Figure 5.14 with the RAMF acquisition strategy. Because the acquisition performance of APDI with RAMF is the best among these three proposed acquisition methods. The verification is unified as testing consecutive three frames until a candidate sync-cell is detected. The

acquisition is terminated if the accumulator output of the APDI module exceeds the threshold twice. There are six thresholds presented here for four IEEE UWB channel models: 0.9, 0.85, 0.8, 0.75, 0.7 and 0.65. The rule of threshold setting for the proposed acquisition scheme is the balance between performance of MAT and BER for each channel model.

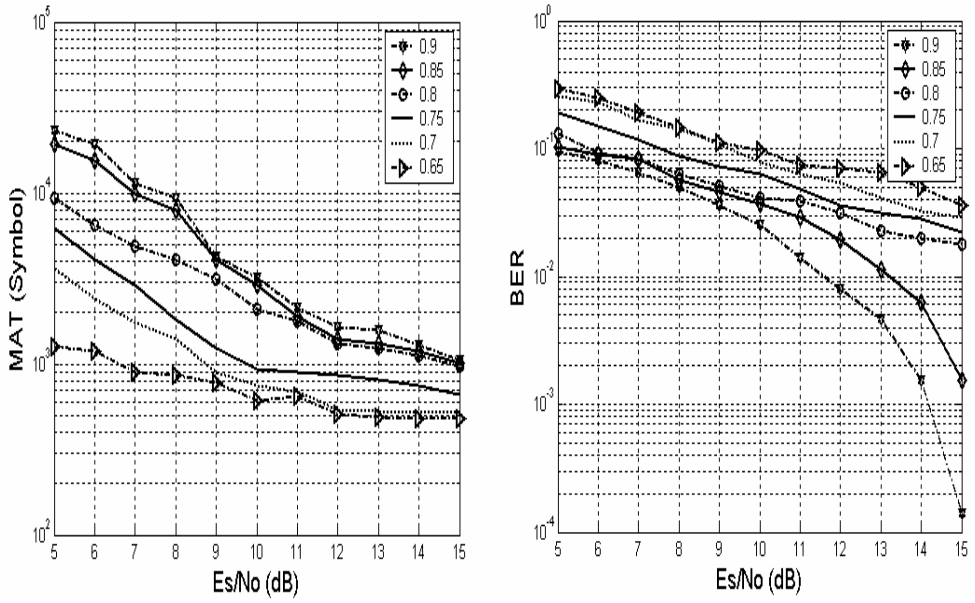

(a) IEEE CM1 channel model

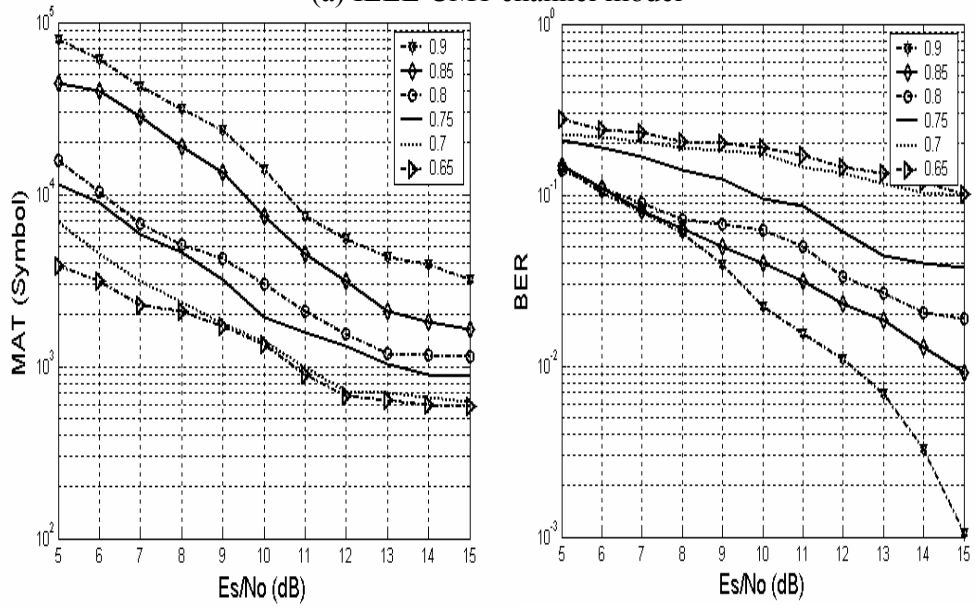

(b) IEEE CM2 channel model

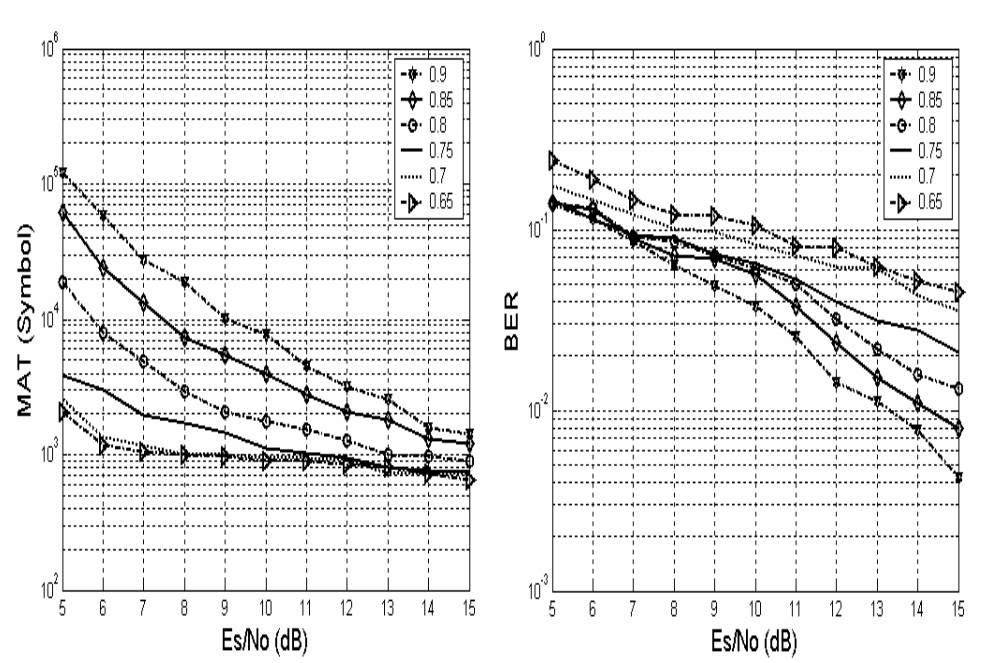

(c) IEEE CM3 channel model

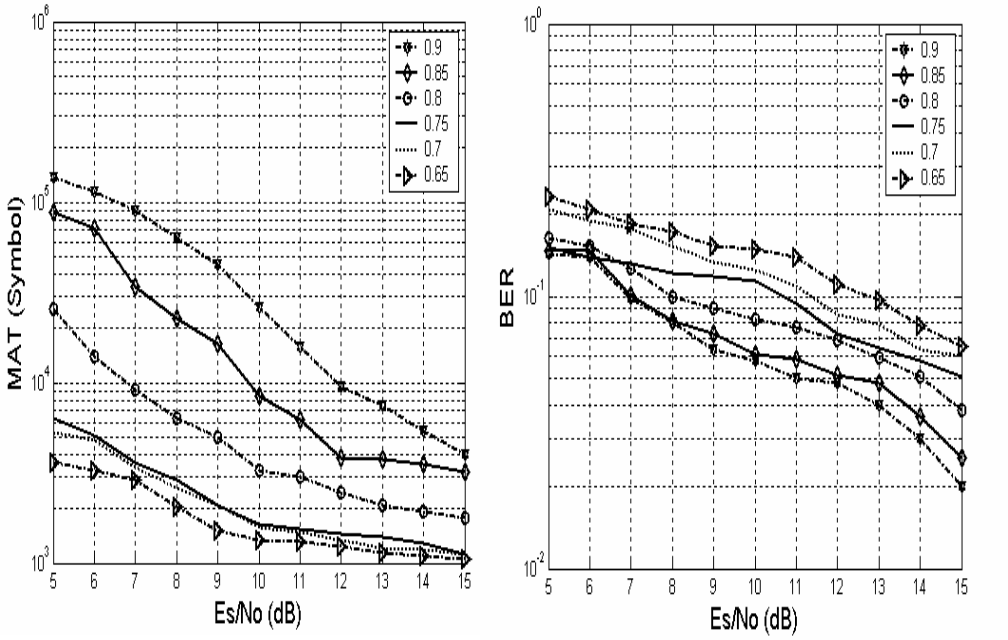

(d) IEEE CM4 channel model

Figure 5.19 Threshold settings of the RAMF with APDI strategy

Followings are brief discussions of the simulation results.

a) IEEE CM1 model

For thresholds of 0.9 and 0.85, there is a similar performance and MAT of the threshold 0.8 is almost identical for the threshold 0.9 and 0.85 for Es/No over 11dB. The performance of the threshold 0.8 is much better than other three threshold settings. Acquisition time for threshold 0.75 is shorten the threshold 0.8 but the BER is worse.

b) IEEE CM2 model

The thresholds of 0.65 and 0.7 have better MAT performance but BER is not satisfied compared with other thresholds. Threshold 0.9 and 0.85 uses much longer MAT to trade off for better BER. Threshold 0.8 is the best choice after balancing the MAT and BER performance.

c) IEEE CM3 model

The thresholds of 0.8-0.9 have much longer MAT but yield better BER performance. The threshold 0.75 has similar MAT as the threshold of 0.65 and 0.7 for Es/No higher than 10 dB. This threshold also has better BER result.

d) IEEE CM4 model

Similar to CM3, the threshold 0.75 is the best choice among these threshold settings.

From the above discussions, threshold 0.8 is selected for IEEE CM1 and CM2. IEEE CM3 and CM4 should have a threshold of 0.75.

5.3.3 Verification Procedure

False alarm probability P_f and probability of detection P_D are affected by the threshold value γ and verification method. The threshold value γ is selected based on the performance of MAT under the assumption that the false alarm rate is constant. False alarm is the acquisition choosing a H_0 cell as a H_1 cell. Because of dense multipath interference and noise, the output after PDI over the threshold might be from H_0 cells instead of the H_1 cells. How to decrease the false alarm rate if the threshold is fixed? The common resolve method is using a verification module to reduce the false alarm probability. It is difficult to distinguish between a sync-cell and a false sync-cell from a good verification scheme [41]. A coarse verification method is discussed here. The verification module evaluates a sync-cell candidate for a few frames. If there are a specific number of frames passing evaluation among these consecutive frames, the sync-cell is declared to be found.

Verification module inherits such property: the longer verification time, the lower false alarm possibility and the longer MAT. A verification parameter, V, is introduced. V denotes the possibility of a system passing the threshold as

$$V = \frac{N_{sync}}{N_v} \tag{5.1}$$

where N_{sync} is the successful time of the detected sync-cell candidate when the acquisition performing in the same sampling phase. N_v is the overall time of verification after a sync-cell candidate is declared. For the purpose of getting a short MAT, if the system performance permits, two candidates of the verification

module are considered here: $V = 2/3$ and $V = 3/4$. $V = 1/2$ and $V = 2/2$ are not used in the simulation, because $V = 1/2$ is not able to reduce P_f and $V = 2/2$ can cause very high missing possibility for CM3 and CM4 at the beginning of observation. Missing probability is not the major research of this thesis and the data is not provided.

Matlab simulations to compare between these two cases are presented in Figure 5.20. False alarm possibility is defined as

$$P_f = \frac{N_f}{N_{sum}} \tag{5.2}$$

where N_f records the number of bit errors in one simulation over the threshold value γ. N_{sum} is the number of all simulation frames for each channel model.

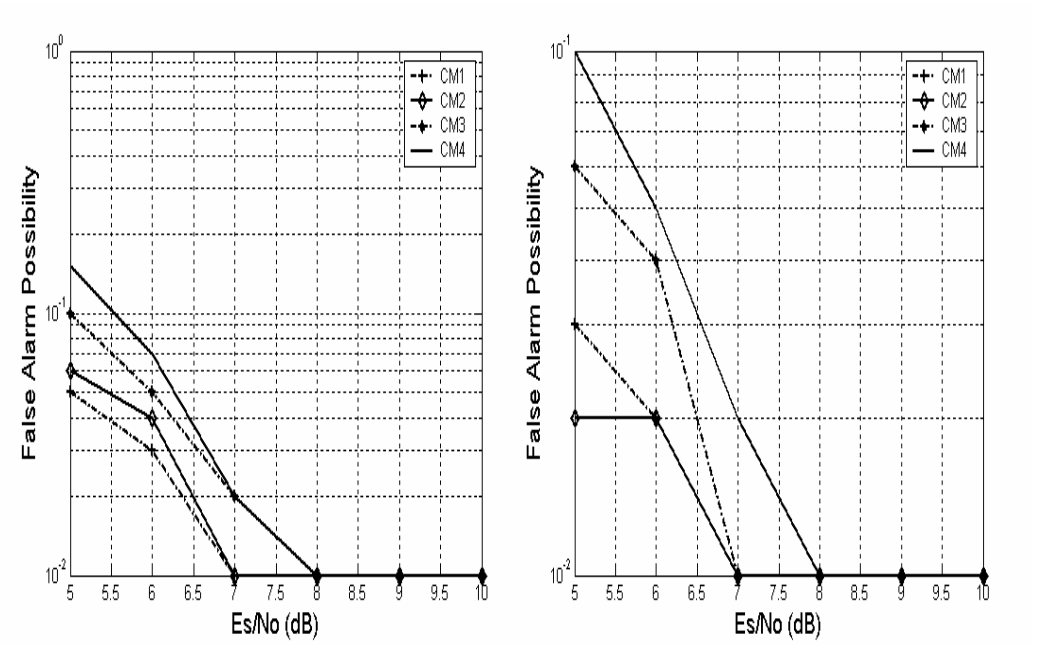

(a) $V = 2/3$ (b) $V = 3/4$

Figure 5.20 P_f of RAMF acquisition with APDI

There are three sections on the E_s / N_o axis for comparison between the verification parameters, $V = 3/4$ and $V = 2/3$ in Figure 5.20

- E_s / N_o below 7dB: $V = 2/3$ corresponds with higher P_f than $V = 3/4$ and the same P_f for both verification parameters using CM1-CM3.
- E_s / N_o between 7dB and 8dB: there is no strict rule to select P_f. In this thesis, 1% is assumed to be acceptable based on simulation time. Therefore, $V = 3/4$ does not mean higher performance than $V = 2/3$ for the overall noise level. $V = 2/3$ is selected for the final UWB acquisition research.

5.3.4 Performance of RAMF with APDI Acquisition

Figure 5.21 depicts the optimum performance for RAMF acquisition with APDI after combining the MAT, threshold setting and BER. The threshold for CM1 and CM2 is 0.8 and the threshold for CM3 and CM4 is 0.75.

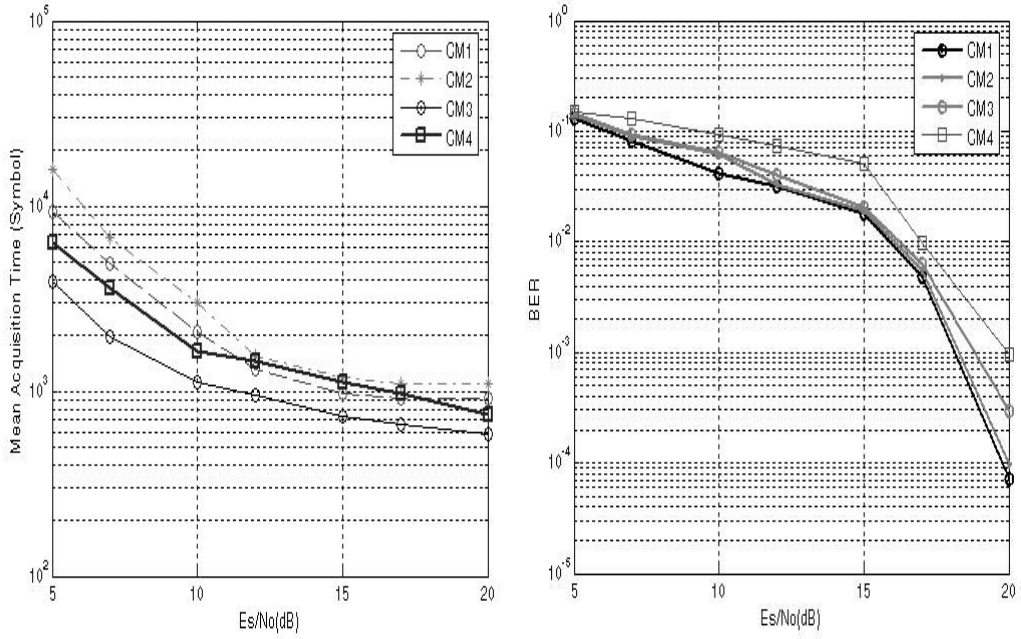

Figure 5.21 Acquisition performance of RAMF with APDI

5.4 Performance Comparison with other UWB Acquisitions

One of the best ways to evaluate the proposed acquisition scheme is to compare its performance with other similar works. MAT is used as the main parameter for comparison. There were works exploring UWB acquisitions in terms of the MAT and BER in the past three years: timing acquisition for transmitted reference [42], acquisition for serial and parallel code search [43] and another performance evaluation for transmitted reference [44]. Simulation results from [42-44] provide the comparison with this thesis work from the viewpoints of MAT, BER, and channel models in Table 5.1

Table 5.1 Perform comparison of acquisition researches

	[42]	[43]	[44]	This work
Symbol rate	220ns	5.344ns (pulse width: 0.167ns)	150ns (pulse width: 0.5ns)	8 *ns* (pulse width: 1ns)
Channel model	Multipath for 10m communications	IEEE UWB CM1,	IEEE UWB CM1-4	IEEE UWB CM1-4
MAT	7×10^{-3} s at E_s / N_o=15-18dB, 1.4×10^{-2} s at E_s / N_o=10dB.	6.68×10^{-8} s at E_s / N_o=18dB		Given in Figure 5. 20
BER at 15dB			Given in Figure 5.22	Given in Figure 5.21

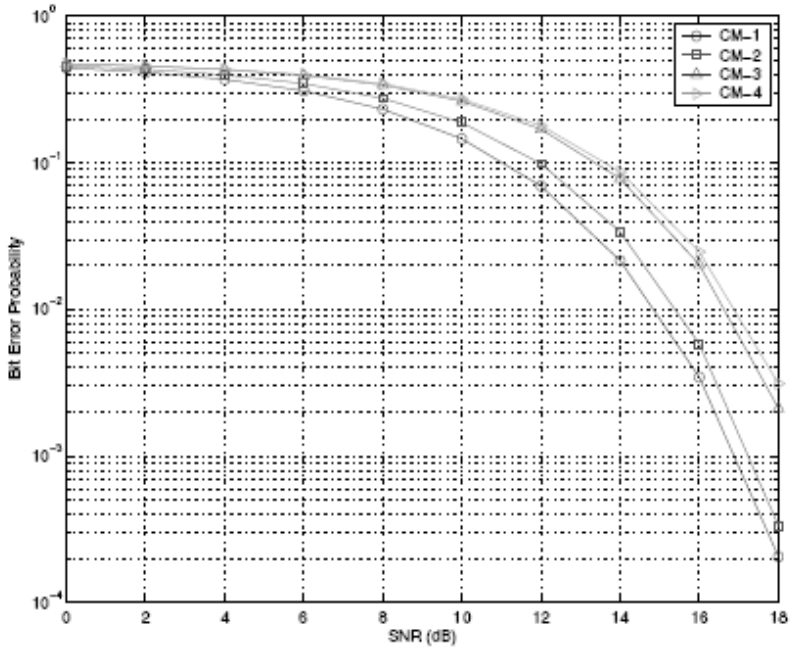

Figure 5.22 Performance of the UWB receiver in [44]

There is no ISI in [42] because the symbol rate is longer than the multipath delay time. The proposed acquisitions using RAMF with APDI and pilot MF with APDI are faster than [42]. The accuracy of proposed acquisitions using RAMF with APDI and pilot MF with APDI is slightly worse than [44]. But ISI in these two proposed acquisition is more serious than [44]. The speed of symbols in [43] is faster than these two proposed acquisition methods, but the pulse width in [43] is much narrower than this research. Narrower width pulse causes more resolvable paths [3]. MAT in [43] is better than the proposed acquisition strategy if not concerning about difference of the pulse width. However, the method in [43] focused on the higher SNR level and CM1 channel model. The simulation of this research was done before the work in [43].

5.5 Summary

This chapter describes detailed simulation structures for three proposed acquisition strategies. A system structure is presented to provide an overview of the simulation scheme. Simulink modules consists of a mono-Gaussian pulse generator, a BPSK modulator, communication channel models, a pulse MF, a VCO, a hybrid ML module, a PDI, a tracking loop, and a verification block. Three proposed acquisition methods are analyzed in terms of MAT and BER performance. The last two sections provide numerical results to select approximate optimum setting for thresholds and verification parameters. The proposed acquisition methods are compared with other works. The overall acquisition performance of RAMF with APDI and pilot MF with APDI is the most promising method.

CHAPTER 6 CONCLUSION AND FUTURE WORK

6.1 Conclusion

In any communication system, synchronization is of fundamental importance. Without proper synchronization, information cannot be reliably exchanged. There are two stages in synchronization: acquisition and tracking. Acquisition is a very critical issue in synchronization since acquisition must be established first with less information to aid in the design. For an ultra-wideband (UWB) system, acquisition architecture design faces many difficulties. These challenges include ultra short pulse, dense multipath channels, low signal emission, and very serious ISI. Since UWB technology is a new field in wireless communications, optimum acquisition methods in UWB usage still require more investigations. The objectives of this thesis are to find a simple, implementable and reliable acquisition scheme. The scheme should be verified through simulations. Background of UWB communications and traditional acquisition approach are introduced first to give the readers an overview of the UWB technologies and acquisition concepts.

The Gaussian monocycle pulse is selected in this thesis due to its simple design in hardware. Its pulse shape is qualified for FCC part 15 rules. The ultra wide spectrum of the Gaussian monocycle pulse leads to the need for a sampling

rate in GHz range. This requires high power consumption and very high cost to build such system. Under-sampling technology is expected to resolve such challenge. A symbol rate sampling is proposed in this thesis because the sampling rate is at the order of MHz which is practical for the hardware implementation. One risk for the under-sampling rate is the negative effect in the system performance. In [45], the author mentioned that the under-sampling rate is not significant as long as the sampling rate is greater than 2GHz and it only affects synchronization accuracy. The author explored timing recovery in the UWB CM1 channel model which used channel estimated coherent method. System performance of the reference aided matched filter with adaptive post detection integration acquisition proposed in this thesis is 2-3dB better than the approach for a single user using 8 times of the symbol rate in [45]. From this point, the proposed under-sampling rate timing recovery improves synchronization accuracy at much lower sampling rate.

Bit iteration search is a modified bit reversal search aiding in shortening acquisition time. The ultra sharp signal of UWB communications means more search space for the sync-cell detection than narrow band communications for the same unknown delay time. In another word, there are more resolvable chips in UWB communications. There are three non-serial search patterns: random search, look-and-jump search, and bit reversal search. The random search has the same mean acquisition time (MAT) performance with bit reversal search in noiseless environment. Bit iteration search is another version of bit reversal search but with one difference. Bit iteration search does not need to assume the minimum resolvable chip width to move the search. The performance of bit iteration search is

not different from bit reversal search in noise free channel models if the minimum resolvable chip width is the same in both cases.

ISI is very difficult to suppress when a symbol period is shorter than the multiple path delay. UWB channel models IEEE 802.15.3a are dense multipath channels, especially for CM3 and CM4 models. The RMS delay spread for CM3 is 14.28ns and for CM4 is 25ns. The symbol period is set at 8ns for the simulations in this thesis. The dense ISI has to be suppressed so that the timing information can be extracted before channel estimation. The transmitted reference technique is popular in the UWB research because transmitted reference is very robust to suppress the dense ISI. This thesis proposed pilot frame transmitted reference, named as reference aid matched filter, for the data-aided acquisition comprising with the pulse transmitted reference scheme. The pulse transmitted reference scheme makes use of the correlation between a UWB pulse and its delayed pulse shape to depress ISI. The reference aid matched filter method uses two repeat pilot frames in one package data to calculate the correlation. One section of pilot codes acts as a template for another copied pilot codes. Simulation results indicate this simple strategy working not effectively to extract correlated information in noise-like signals after matched filter if there is no addition of other techniques. Then the modified post detection integration, called as adaptive post detection integration, is proposed in this thesis. The simulation proved that reference aided matched filter without adaptive post detection integration is not able to achieve the desired UWB acquisition. The reason for this is from dense ISI that distorts the optimum sampling points. That means the optimum sampling points are not always at the

highest value after reference aided matched filter correlation. Adaptive post detection integration introduces the early-late gate tracking loop to effectively improve performance of acquisition. To prove this viewpoint, this thesis also presents another UWB acquisition strategy: pilot matched filter with adaptive post detection integration. This method does not use transmitted reference technique. Simulation result reveals sub-optimum promising results.

This thesis also presents work for threshold setting and verification choice. The threshold setting and verification procedure affect MAT. Fixed threshold and a simple verification are developed to decrease the false alarm probability.

Simulations of aforementioned schemes have been performed for IEEE standard UWB channel models and AWGN channel. The results show better system performance over similar researches in UWB synchronization.

Above all, the followings are the conclusion of this research

1 Under-sampling rate is effective in UWB acquisition. Sample rate does not increase MAT of UWB acquisition compared with other over-sampling schemes for the UWB acquisition.

2 Bit iteration search is a solution to avoid estimation of the minimum resolvable chip width for the UWB acquisition.

3 Acquisition using reference aided matched filter with adaptive post detection integration is capable of suppressing the multipath interference in all four channel models from IEEE 802.15.3a. The tradeoff for the improvement is the addition of an early-late gate tracking loop to accurately estimate timing offset during acquisition. Adaptive post detection

integration is more complex than post detection integration. The overall design complexity does not increase because synchronization comprises of both acquisition and tracking. Adaptive post detection integration just forces the system to open the tracking loop for acquisition.

4 Transmitted reference technique is not always effective for UWB communications. Reference aided matched filter with post detection integration fails to acquire synchronization. The pilot matched filter with adaptive post detection integration is proven to be successful.

5 Adaptive acquisition is promising in UWB communications.

6 Optimum threshold setting and verification algorithm can decrease false alarm probability.

6.2 Future Work

The UWB acquisition is a new field in wireless communication research. There are many topics remained to be solved. It is found in this thesis that the tracking loop helps in improving search performance. The early-late gate tracking loop is simple and there were few studies about the tracking loop in UWB synchronization. An optimum tracking strategy will improve overall acquisition performance for UWB communications.

This thesis finds that reference aided matched filter with post detection integration method fails because of ISI. In general, transmitted reference technique used in [42], [44] assuming there was no ISI between the translated frames in order

to decease the interference from a dense multipath environment. More researches about transmitted reference technique in dense ISI environment are required.

REFERENCES

[1] G.F. Ross, "The Transient Analysis of Multiple Beam Feed Networks for Array Systems," *Ph.D. dissertation, Polytechnic Institute of Brooklyn*, Brooklyn, NY, 1963.

[2] Federal Communications Commission (FCC), "Revision of Part 15 of the Commission's Rules Regarding Ultra-Wideband Transmission Systems," *First Report and Order*, *ET Docket 98-153*, FCC 02-48, Apr. 2002.

[3] D. Porcino and W. Hirt, "Ultra-wideband Radio Technology: Potential and Challenges ahead", *IEEE Commun Mag*, vol. 41, pp. 66-74, Jul. 2003.

[4] V.S. Somayazulu, J.R. Foerster, and S. Roy, "Design Challenges for very High Data Rate UWB Systems Signals," *Systems and Computers*, Conference Record of the Thirty-Sixth Asilomar , vol. 1, 3-6, pp. 717 – 721, Nov. 2002.

[5] M.Z. Win, and R.A. Scholtz, "Impulse Radio: How It Works," *IEEE Communications Letters*, vol. 2, pp. 36 – 38, Feb. 1998.

[6] G. Leus, and Alle-Jan van der Veen, "Noise Suppression in UWB Transmitted Reference Systems," *Fifth IEEE Workshop on Signal Processing Advances in Wireless Communications*, Lisboa, Portugal, Jul. 11-14, 2004.

[7] W.M. Lovelace, and J.K. Townsend, "The Effects of Timing Jitter on the Performance of Impulse Radio," *Proc. of IEEE Conf. on UWB Sys. & Tech.*, Baltimore, MD, pp. 251-254, 2002.

[8] I. Maravi´c, M. Vetterli, and K. Ramchandran, "High-Resolution Acquisition on Methods for Wideband Communication Systems," *IEEE ICASSP*, Hong Kong, 6-10, Apr. 2003.

[9] Maravic and M. Vetterli, "Low-complexity Subspace Methods for Channel Estimation and Synchronization in Ultra-wideband Systems," *Proc. of IWUWB*, Jun. 2003.

[10] L. Yang, and G.B. Giannakis, “Low-complexity Training for Rapid Timing Acquisition in Ultra Wideband Communications,” *IEEE Global Telecommunications Conference, 2003. GLOBECOM '03.*, vol. 2, 1-5, pp. 769 – 773, Dec. 2003.

[11] A.F. Molisch, J.R. Foerster, and M. Pendergrass, “Channel Models for Ultrawideband Personal Area Networks,” *IEEE Wireless Communications*, vol. 10, pp. 14 – 21, Dec. 2003.

[12] L.P.B. Christensen, “A Low-Complexity Joint Synchronization and Detection Algorithm for Single-Band DS-CDMA UWB Communications,” *EURASIP, Journal on Applied Signal Processing*, UWB - State of the Art Year 2005.

[13] E. A. Homier, and R. A. Scholtz, “Hybrid Fixed-Dwell-Time Search Techniques for Rapid Acquisition of Ultra Wideband Signals,” *IWUWBS2003*, Oulu, Finland, Jun. 2003.

[14] F. Ramirez-Mireles, “Signal Design for Ultra-wide-band Communications in Dense Multipath Vehicular Technology,” *IEEE Trans. Comm*, vol. 51, pp. 1517 – 1521, Nov. 2002.

[15] R. Scholtz, “Multiple Access with Time-hopping Impulse Modulation,” *Military Communications Conference*, 1993. MILCOM '93. Conference record. 'Communications on the Move', IEEE, vol. 2, 11-14, pp. 447 – 450, Oct. 1993.

[16] J. D. Taylor, “Introduction to Ultra-Wideband Radar Systems,” *CRC Press*, Boca Raton, FL, 1995.

[17] J. Balakrishnan, A. Dabak, S. Lingam, and A. Batra, “Complexity and Performance Analysis of a DS-CDMA UWB System,” *IEEE P802.15-03/388r2*, Sept. 2003.

[18] R. Scholtz, “Multiple Access with Time-hopping Impulse Modulation,” *IEEE MILCOM '93. Conference record. 'Communications on the Move'.*, vol. 2, 11-14, pp. 447 - 450, Oct. 1993.

[19] “Time Modulated Ultra-wideband for Wireless Applications,” *Pulson Techology*, Technical Description, 2000.

[20] Ismail Güvenç, and Hüseyin Arslan, “On the Modulation Options for UWB Systems,” *IEEE Military Communications Conference*, vol. 22, no. 1, pp. 892 – 897, Oct. 2003.

[21] N.H. Lehmann, and A.M. Haimovich, “The Power Spectral Density of a Time Hopping UWB Signal: a Survey,” *'03 IEEE Conference on Ultra Wideband Systems and Technologies*, pp. 234 – 239, Nov. 2003.

[22] F. Zhu, Z. Wu, and C.R. Nassar, “Generalized Fading Channel Model with Application to UWB,” *'02 IEEE Conference on Ultra Wideband Systems and Technologies*, pp. 13 – 17, May 2002.

[23] B. Uguen, E. Plouhinec, Y. Lostanlen, and G. Chassay, “A Deterministic Ultra Wideband Channel Modeling,” *'02 IEEE Conference on Ultra Wideband Systems and Technologies*, pp.1 – 5, May 2002.

[24] “UWB Channel Modeling Contribution from Intel”, *IEEE P802.15-02/279r0-SG3a*, Jun. 2002.

[25] S.S. Ghassemzadeh, R. Jana, C.W. Rice, W. Turin, and V. Tarokh, “Measurement and Modeling of an Ultra-Wide Bandwidth Indoor Channel,” *IEEE Trans. Comm*, vol. 52, pp. 1786 – 1796, Oct. 2004.

[26] Y. Xiong, Y. Huang, J.F. Ralph, W. Al-Nuaimy and P. Sun, An FM Dmodulation lgorithm with an Udersampling Rte,” *IEEE 2003 International Conference on ICASSP* , vol. 6, pp. VI - 245-8 , Apr. 2003.

[27] John G. Proakis, *Digial Communications*, 4th edition, McGraw-Hill, 2001.

[28] T. Zhi , L. Wu, and S.A. Zekavat, “Blind vs. Taining-based UWB Tming Aquisition with Efective Mltipath Cpture,” *Signals, Systems & Computers, 2003 The Thirty-Seventh Asilomar Conference on*, Vol.2, pp.1771-1775, Nov, 2003, Pacific Grove, California, USA.

[29] E. A. Homier and R. A. Scholtz, “Rapid acquisition of ultra-wideband signals in the dense multipath channel,” *Proc. 2002 IEEE Conf*, Ultra Wideband Sys, Tech., pp. 105–109, 2002.

[30] I. Ramachandran, and S. Roy, “Acquisition of Direct-sequence UIltra-wideband Signals,” *'05 IEEE Wireless Communications and Networking Conference*, Vol.2, pp. 752 – 757, Mar. 2005.

[31] S. W. Golomb, *Shift Register Sequences*, Revised Edition, Aegean Park Press, 1982.

[32] Czylwik, “Low Overhead Pilot-aided Synchronization for Single Carrier Modulation with frequency domain equalization,” *IEEE Global Telecommunications Conference* (*GLOBECOM)*, vol. 4, pp. 2068–73, 1998.

[33] E. Homier, “Initial Phase Estimate Statistics,” TRW Space and Electronics Group Interoffice Correspondence, C80-99-SE-041, May 1999.

[34] J. J. Spilker, “Delay-lock Tracking of Binary Signals”, *IEEE Trans. on Space Electron. Telemetry*, vol. SET-11, pp. 1-8, Mar. 1963.

[35] F. Tufvesson, and A.F. Molisch, “Ultra-Wideband Communication Using Hybrid Matched Filter Correlation Receivers,” *IEEE Semi-annual Vehicular Technology Conference (VTC)*, pp. 1290 – 1294, May 2004.

[36] J.J. van de Beek, M. Sandell and P.O. Borjesson, “ML Estimation of Time and Frequency Offset in OFDM Systems,” *IEEE Trans. Sig. Proc.*, vol. 45, pp. 1800-1805, Jul. 1997.

[37] D.E. Cartier, “Partial Correlation Properties of Pseudonoise (PN) Codes in Noncoeherent Synchrnoization / Detection Schemes,” *IEEE Trans*. *Commun*., vol. 24, no. 8, pp. 898–903, Aug. 1976.

[38] A.J. Viterbi, “CDMA, Principles of Spread Spectrum Communications,” *Addison-Wesley Wireless Communications Series*. Addison-Wesley Publishing Company, Apr 1995.

[39] R. De Gaudenzi, F. Giannetti, and M. Luise, “Signal Recognition and Signature Code Acquisition in CDMA Mobile Packet Communications,” *IEEE Trans*. *Veh*. *Technol*., pp. 196–208, Feb. 1998.

[40] A. Polydoras and C.Weber, "A unified approach to serial search spread-spectrum code acquisition - parts I and II," *IEEE Trans. Comm*, vol. 32, pp. 542–560, May. 1984.

[41] S. Vijayakumaran, and T. F. Wong, "A search strategy for ultra-wideband signal acquisition," *IEEE Trans. Comm*, vol. 53, No 12, pp. 2015 – 2019, Dec. 2005.

[42] S. Aedudodla, and S. Vijayakumaran, and T.F. Wong, "Timing acquisition for transmitted reference DS-UWB signals," *IEEE Military Communication conference*, vol. 5, pp. 3087-3093, Oct. 2005.

[43] L. Reggiani, and G. M. Maggio, "On the acquisition time for serial and parallel code search in UWB impulse radio," *IEEE Inter. Symp. On Circuit and Systems (ISCAS)*, vol. 1, pp. 53-55, May 2005.

[44] S. Gezici, F. Tufvesson, and A. F. Molisch, "On the performance of transmitted-reference impulse radio," *IEEE Global Telecommunication Conference (GLOBECOM)*, vol. 5, pp. 2874-2879, Dec. 2004.

[45] C. Carbonelli, and U. Mengli, "Timing recovery for UWB signals," *Global Telecommunication Conference (GLOBECOM)*, vol. 1, pp. 61 – 65, Dec.2004.